Cape Peninsula
University of Technology

A comparative study of the thermal conductivities of nanofluids measured via a modified guarded hot plate method.

by

Kalvin George Snyders

A thesis submitted in fulfilment of the requirements for the degree

Master of engineering: Mechanical Engineering

in the Faculty of Engineering and the Built Environment

at the Cape Peninsula University of Technology

Supervisor: Dr O. Nemoraoui
Co-supervisor: Dr F. Ismail

Bellville
November 2023

CPUT copyright information

The dissertation/thesis may not be published either in part (in scholarly, scientific, or technical journals) or as a whole (as a monograph) unless permission has been obtained from the University.

DECLARATION

I, Kalvin Snyders, declare that the contents of this dissertation/thesis represent my unaided work and that the dissertation/thesis has not previously been submitted for academic examination towards any qualification. Furthermore, it represents my own opinions and not necessarily those of the Cape Peninsula University of Technology.

24/10/2023

Signed **Date**

1 ABSTRACT

In the current debate surrounding nanofluids, more experimental studies are required for comparison to clarify much of the ambiguity surrounding the thermal conductivity of nanofluids. In recent years the development of nanofluids has come to a relatively slow crawl due to disagreements in results reported from different testing methods. The following study explores designing and constructing a guarded hot plate (GHP) apparatus. The apparatus was calibrated using deionized water. The GHP was then used to test the ethylene glycol and a Cobalt Oxide nanofluid's thermal conductivity, which was compared to existing reported results and numerical models of nanofluids. Ethylene glycol is a base fluid used for the nanofluids and will be used to establish a baseline.

A finite element analysis(FEA) analysis was performed to validate numerical models of the device and to guide engineering choices of the selection of components; The GHP uses Fourier's law of thermal conduction to extract the sample's thermal conductivity. The GHP uses an embedded system that replicates steady-state conditions. The thermal conductivity is computed using the temperature readings from the two parallel plates and the voltage drop and current measurements across the 120W resistive heat elements embedded in the hot plate. The embedded system uses a PI controller to maintain the cold plate temperature at 20˚C through a 154W Peltier element. The Guard heater will maintain parity between the hot plate and the guard heater to ensure heat flux through the sample. The system was designed for a temperature differential of 40˚C.

The research has led to the successful measurement of Cobalt Oxide nanofluids And their comparison to similar fluids and numerical models. The research endeavours to address if there is an increase in thermal conductivity using a methodology not frequently employed in the existing literature.

2 ACKNOWLEDGEMENTS

I wish to thank:

- My Loving parents, Janet and Francois Snyders, for their continued support of my dreams and aspirations.
- My supervisors, Dr Nemraoui and Dr Ismail, For providing me with technical insight and continued support of my academic endeavours.
- Dr Saleh, For introducing me to the fascinating topic of nanofluids.
- Matthew Schouw, Daniel Barnard and Deen Ebrahim for their assistance and motivation in completing this degree.

The financial assistance of the Cape Peninsula University of Technology towards this research is acknowledged. Opinions expressed in this thesis and the conclusions arrived at are those of the author, and are not necessarily to be attributed to the Cape Peninsula University of Technology.

3 TABLE OF CONTENTS

DECLARATION ..... **ii**
1 ABSTRACT iii
2 ACKNOWLEDGEMENTS iv
3 TABLE OF CONTENTS v
4 LIST OF FIGURES vii
5 LIST OF TABLES viii
1 CHAPTER ONE: Introduction 1
1.1 Problem statement 1
1.2 Aims and objectives 4
1.3 Constraints 4
1.4 Methodology 5
2 CHAPTER TWO: Literature review 6
2.1 Synthesis and preparation 8
2.1.1 Two-step methodology 8
2.1.2 One-step methodology 10
2.1.3 Preparation 11
2.2 Properties 13
2.2.1 Thermal conductivity 13
2.2.2 Viscosity 16
2.2.3 Density 17
2.2.4 Characterisation 18
3 CHAPTER THREE: Design and Fabrication 30
3.1 Design 30
3.1.1 Hot plate 36
3.1.2 Cold plate 39
3.1.3 Guard heater 41
3.1.4 Electronics 42
3.1.5 Breakout boards connected to controller board 43
3.1.6 External instrumentation for experimentation 45
3.2 Fabrication 46
3.3 Challenges 48
4 CHAPTER FOUR: Testing and commissioning 50
5 CHAPTER FIVE: Discussion of results 56
5.1 Experimental procedure 56
5.2 Results 57
5.2.1 Glycol 57
5.2.2 Cobalt oxide nanofluid 59
5.3 Discussion 62
5.3.1 Comparison to numerical models 63

5.3.2 Comparison to published literature 64
6 CHAPTER SIX: Conclusion and recommendations 66
6.1 Recommendations 67
APPENDIX A: Calculations 75
APPENDIX B: Specification sheets 79
APPENDIX C: Data 82
APPENDIX E: Drawings 96

4 LIST OF FIGURES

Figure 1.1: A schematic diagram illustrating the original design of the GHP apparatus (Thermtest Inc., 2015b) 2
Figure 1.2: Guarded hot plate apparatus schematic diagram (Wang & Xu, 1999) 3
Figure 2.1 Basic setup of the laser ablation process (Amendola & Meneghetti, 2009) 11
Figure 2.2: Schematic overview of a computerised THW setup (Choi, Li & Eastman, 1999) 19
Figure 2.3: Close up of hot disk design (Gustafsson, 1991) 21
Figure 2.4: 3D rendering of Lee's disk method (Thermtest INSTRUMENTS, n.d.) 23
Figure 2.5: GHP apparatus setup (Challoner & Powell, 1956) 24
Figure 2.6: GHP configurations (Linseis Inc., n.d.) 24
Figure 2.7: Cross section of the modified guarded hot plate (Smith, Hust & VanPoolen, 1982) 26
Figure 2.8: Cross section of GHP apparatus for fluids and solids 28
Figure 3.1: 3D rendering of apparatus 31
Figure 3.2: Thermal resistance circuit of stack assembly 32
Figure 3.3: Nodal temperatures of stack assembly 35
Figure 3.4: Heat flux analysis of stack assembly 36
Figure 3.5: Orthographic projections of the hot plate 37
Figure 3.6: 3D rendering of the hot plate 38
Figure 3.7: FEA analysis of hot plate 39
Figure 3.8: Orthographic projections of the cold plate 40
Figure 3.9: Schematic of the cold plate control scheme 41
Figure 3.10: Schematic of guard heater 42
Figure 3.11: K-type thermocouple sensor (botshop.co.za, 2020) 44
Figure 3.12: 5-Volt relay board 44
Figure 3.13: Agilent 34970A (Technologies, n.d.) 46
Figure 3.14: GW instek gps3033 (Good Will Instrument Co., n.d.) 46
Figure 3.15: Milling of the controller board PCB 48
Figure 3.16: Orientation of final GHP setup 49
Figure 4.1: Left: cold temperature calibration; Right: hot temperature calibration 51
Figure 4.2: A graph of the hot plate temperatures recorded 53
Figure 4.3: A graph of cold plate temperatures 54
Figure 5.1: Power and temperature differential of glycol test 1 58
Figure 5.2: Recorded results of glycol test 2 59
Figure 5.3: Recorded results of sample A3 60
Figure 5.4: Recorded results of sample B3 test 1 61
Figure 5.5: Recorded results of sample B3 test 2 62
Figure 5.6: Comparison of samples 63

5 LIST OF TABLES

Table 3-1: Material properties....33
Table 3-2: Stack assembly dimensions....34
Table 3-3: FEA query results....35
Table 4-1: Parameters used for water thermal conductivity....55
Table 5-1: Average values used glycol test 1 58
Table 5-2: Average values used glycol test 2 59
Table 5-3: Average values used for sample A3 60
Table 5-4: Average values used sample B3 test 1....61
Table 5-5: Average values used sample B3 test 2....62
Table 5-6: Comparison of test results to numerical models....64
Table C-1: Cold bath calibration. 82
Table C-2: Boiling water calibration: 82
Table C-3: Ethylene Glycol test 1 data. 83
Table C-4: Ethylene Glycol test 2 data. 84
Table C-5: Sample A3 test 1 data. 85
Table C-6: Sample B3 test 1 data. 86
Table C-7:Sample B3 test 2 data. 87

GLOSSARY

Acronyms/Abbreviations	Definition/Explanation
AIO	All In One
ASRE	American Society of refrigeration engineer
ASTM	American Society for Testing and Materials
BET	Brunauer–Emmett–Teller
BS	British Standard
CNC	Computer Numerical control
CRM	Chemical Reduction Method
DIN	Deutsches Institut für Normung
FEA	Finite element analysis
GHP	Guarded hot plate
LASiS	Laser Ablation Synthesis in Solution
MOSFET	Metal–oxide–semiconductor field-effect transistor
NBS	National Bureau of Standards
PCB	Printed circuit board
PID	Proportional integral derviative
PTFE	Polytetrafluoroethylene
PWM	Pulse width modulation
THW	Transient hot wire
TPS	Transient plane source

Symbols	
$\dot{Q}$=	Rate of heat conduction
k=	Thermal conductivity
A=	Area
$k_{eff} =$	Effective thermal conductivity.
$k_p =$	Particle thermal conductivity.
$k_f =$	Fluid thermal conductivity.
$\emptyset =$	Volume fraction.
α=	The ratio of particle to base fluid thermal conductivity.
β=	(α-1)/(α-2).
k_{nf}=	Thermal conductivity of nanofluid.
$k_f =$	Thermal conductivity of the base fluid.
$k_p =$	Thermal conductivity of nanoparticles.
$C_1 =$	Proportional constant (18x10^6).
$d_f =$	Diameter of fluid.
$d_{nano} =$	Diameter of the nanoparticle.
Re=	Reynolds number.
Pr=	Prandtl number.
$k_f =$	Thermal conductivity of the fluid.

$k_p =$	Thermal conductivity of nanoparticles.
$\omega =$	Correction factor.
$T =$	Temperature.
$T_0 =$	Reference temperature (293ºK).
τ=	Shear stress.
μ=	Absolute viscosity.
du=	Change in velocity.
dy=	Change in the distance between surfaces.
ρ=	density
m=	mass
V=	Volume
ρ_{nf}=	The density of the nanofluid
ρ_f=	The density of the base fluid
ρ_p=	The density of the nanoparticle
$R(t) =$	Resistance at a given time.
R_0=	Initial resistance
∝=	Temperature coefficient of resistance.
ΔT=	Change in temperature.
τ=	Time-dependent constant.
R=	Thermal resistance
∆x=	Thickness

Glossary of terms	
Agglomeration	A clump of multiple particles.
Analogue to digital	An integrated circuit used to convert analogue signals to digital signals.
Attritor	A grinding machine used to reduce the size of particles.
Chemical precursor	A chemical precursor is a chemical used to produce another chemical compound.
Convection	A movement within a fluid caused by density changes due to temperature differentials.
Crystalline	A highly ordered microstructure. A solid material is arranged into a lattice structure.
Density	A measure of the mass per unit volume of a substance.
Dispersants	Dispersants are an additive to a liquid or solid medium to progress the separation of particles.
Heat flux	Heat flux is the measurement of the amount of heat that is transmitted through a material.

Homogeneous	**A uniform mixture of two materials.**
Least squares method	**A numerical method for finding the best fitting curve/line for a data set.**
Nanoparticle	**A nanoparticle is a particle within the size range of 1 to 100 nm.**
Pulse width modulation	**A method for reducing the mean power supplied by varying the frequency of the power supplied.**
Prandtl number	**The ratio of momentum diffusivity and thermal diffusivity.**
Reducing agent	**A substance that tends to bring about reduction by being oxidized and losing electrons.**
Solvent	**A substance used to dissolve other materials to form a solution.**
Steady state	**A constant condition in a physical process. (one in which all variables are controlled.)**
Surfactant	**A surfactant is an agent that decreases the surface tension between two media.**
Suspension	**A suspension is a heterogeneous mixture of a fluid that contains solid particles sufficiently large for sedimentation.**
Thermal conductivity	**The ability of a material to transfer heat.**
Transient	**A momentary or rapid process.**
Viscosity	**A measure of a fluid's resistance to flow.**
Wheat stone bridge	**An electrical circuit used to determine an unknown resistance.**
Van Der Waals force	**weak, short-range electrostatic attractive forces between uncharged molecules, arising from the interaction of permanent or transient electric dipole moments.**
Zeta potential	**The electrical potential of the shear plane.**

1 CHAPTER ONE: Introduction

1.1 Problem statement

Many problems impede nanofluids' advancement, some of which are not directly linked to nanofluids. Suider *et al.* (2011) attribute these factors to the poor characterisation of suspensions of nanoparticles, the lack of agreement of results between researchers and a lack of understanding of the mechanisms behind the changing of properties between nanoparticles and the base fluid. Considering the lack of agreement with the reported increase in the thermal conductivity of nanofluids, there has been speculation about the accuracy of the results.

In this investigation, the basic concept of Fourier's Law of conduction will govern the thermodynamic analysis used for the nanofluids. Fourier's Law states that the rate of heat conduction is directly proportional to the temperature difference across a given area but inversely proportional to the thickness of the plane upon which the heat is conducted (Yunus & Afshin, 2015). The Law is represented by Equation (5.1); the coefficient of proportionality denoted as "k" is known as thermal conductivity. Yunus and Afshin (2015) define *thermal conductivity* as the measurement of the ability of a material to conduct heat.

$$\dot{\boldsymbol{Q}} = -\boldsymbol{kA}\frac{\boldsymbol{\Delta T}}{\boldsymbol{\Delta x}} \qquad \textbf{(5.1)}$$

Where:

$\dot{Q}$=	Rate of heat conduction
k=	Thermal conductivity
A=	Area
ΔT=	Change in temperature
Δx=	Thickness

A steady-state system is one in which the variables remain constant when analysing heat conduction as time progresses. The one-dimensional steady-state (Equation (5.**1**) forms the basis for the analysis of thermal systems in the

thermal analysis industry. A guarded hot plate apparatus (GHP) measures nanofluids' thermal conductivity. The GHP apparatus was developed simultaneously in the 19th century in America and Germany; however, the initial design was used to measure insulating materials' thermal conductivity (Thermtest Inc., 2015b). The GHP apparatus uses steady-state conditions and Fourier's Law of thermal conduction in its operation and is still in use to this day. A schematic of the original two specimen set up is presented in Figure 1.2.

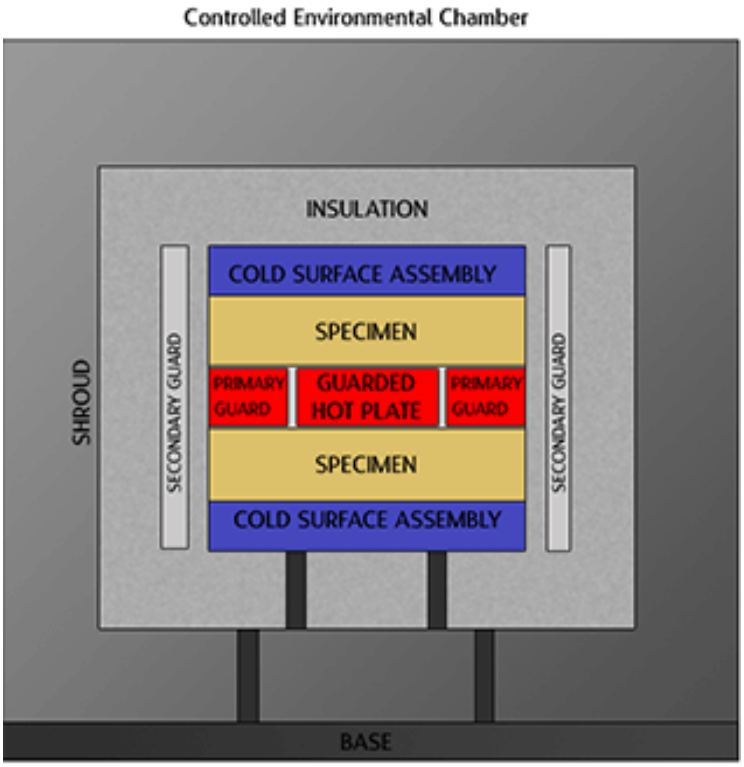

Figure 1.1: A schematic diagram illustrating the original design of the GHP apparatus (Thermtest Inc., 2015b)

The GHP design was modified by Channel and Powel in 1956 to measure the thermal conductivity of water but was further modified to measure the thermal conductivity of nanofluids by Wang and Xu in 1999 (Wang & Xu, 1999). The schematic of the apparatus used by Wang and Xu can be seen in **Figure 1.2.**

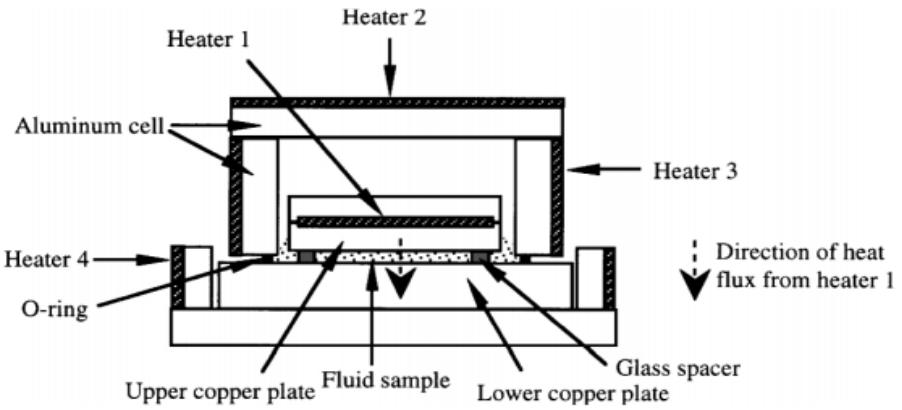

Figure 1.2: Guarded hot plate apparatus schematic diagram (Wang & Xu, 1999)

The fluid sample was placed between two parallel plates constructed of round copper. The copper plates are separated by a set of glass spacer rings which rest on the cold plate below. The fluid level is slightly above the base of the bottom of the upper plate; any excess fluid is forced out the side of the glass spacer rings, ensuring no air is in the system, which may skew the results and render them invalid. To control the temperature around the system, aluminium cells with heating elements are placed around the testing chamber and heated to match the surface temperature of the hot plate. The heat flux in the direction of the cold plate eliminates the convection and radiation losses from the upper copper plate. The control of the heat flux replicates the steady-state conditions (Wang & Xu, 1999).

Various factors have been reported to influence the thermal conductivity of nanofluids. According to a review on thermophysical properties of nanofluids and heat transfer applications by Gupta *et al.* (2017), the factors include the particle size, the particle shape, the material of the solid particle, the base fluid, the temperature, additives (specifically surfactants), the pH value of the nanofluid and clustering (Gupta *et al.,* 2017). Two primary mechanisms have been identified for the increased thermal conductivity, the Brownian motion of the nanoparticles and the interfacial layer. Kole and Dey (2011) have noted in their experimental study that the effects of Brownian motion are only prevalent for temperatures greater than 30 ˚C (Kole & Dey, 2011). Gupta *et al.* (2017) stated that the interfacial layer acts as a ‘thermal bridge’ between the solid

particles and base fluid. However, these factors have been overlooked during the test phase of the thermophysical properties of nanofluids.

1.2 Aims and objectives

The primary aims of this project are to design, fabricate and evaluate a GHP test apparatus to test nanofluid thermal conductivity. The following key objectives need to be implemented within the GHP apparatus.

- Design, computer-aided simulation

  The modelling of the apparatus during the design phase will provide insight into the performance of the selected components. This concept will evaluate the thermal conductivity of nanofluids in a controlled environment.

- Construction of a prototype

  The prototype will be constructed to verify the simulated models.

- Testing of the prototype

  The readings from the prototype will be compared to the published results of two controls: water and ethylene glycol. These results will prove whether the prototype is providing accurate and trustworthy results.

- Testing of a nanofluid

  A nanofluid will be tested and compared to existing reported results and predictive numerical models.

1.3 Constraints

The prototype will only measure thermal conductivity of nanofluids. Only a cobalt oxide nanofluid will be used for comparison.

1.4 Methodology

- *Phase 1: Literature review*

A literature review will provide relevant information on the nanofluids and the design of the apparatus to evaluate the thermal conductivity. The literature review will be presented in Chapter 2.

- *Phase 2: Design of the modified guarded hot plate apparatus*

The apparatus will be designed using Solidworks™ and optimised using Abaqus to ensure heat is evenly distributed throughout the system, thereby enabling a numerical value to compare the prototype. This phase is detailed in Chapter 3.

- *Phase 3: Construct and commission a modified guarded hot plate apparatus prototype*

The apparatus will then be constructed, commissioned using water, and used to record nanofluids' thermal conductivity, detailed in Chapter 4.

- *Phase 4: Analysis of results*

The results will then be analysed and compared to other publications of a similar nature and will also be compared to the predicted results of various numerical models that have been proposed over the years. This phase will be further detailed in Chapter 5.

2 CHAPTER TWO: Literature review

Stephen Choi first coined the term *nanofluid* in the 90s to describe the suspension of particles (<100 μm) within a base fluid. The idea of suspending a solid medium within a fluid is not new. Maxwell first theorised the concept in the 1800s; however, the Maxwell model is confined to micrometre and millimetre-sized particles (Choi & Eastman, 1995). it is worth noting that the Maxwell equation severely underpredicts the thermal conductivities of nanofluids at higher temperature differentials (Kole & Dey, 2011). Nanofluids are a class of fluids of their own, despite their similarity to slurries. The Maxwell equation established the foundation upon which the effective thermal conductivity of nanofluids was established, as given in Equation (2.1).

$$\boldsymbol{k_{eff} = \frac{k_p + 2k_f + 2(k_p - k_f)}{k_p + 2k_f - (k_p - k_f)\emptyset} k_f}$$

(2.1)

Where:

$k_{eff} =$	Effective thermal conductivity
$k_p =$	Particle thermal conductivity
$k_f =$	Fluid thermal conductivity
$\emptyset =$	Volume fraction

The discovery of nanofluids yielded new possibilities for heat transfer. In the heat transfer Equation (1.1), there are three ways of increasing heat conduction: increasing the area (A) of the contact area; increasing the temperature differential (ΔT); or increasing the heat transfer coefficient (k). The system may be constrained by space, making it unfeasible to manipulate the area. Temperature differences could be limited by process or material. The last parameter that can be manipulated is thermal conductivity. The increased heat transfer coefficient can be achieved by utilising more efficient methods or improving the heat transfer medium. In the case of fluids, nanoparticles are used (Saidur, Leong & Mohammad, 2011).

The properties of nanofluids are influenced by five parameters: particle characteristics, thermo-fluids, heat transfer, colloid, lubrication, viscosity, viscosity index, friction coefficient, wear rate and extreme pressure. The properties of a particle are its size, shape, BET (surface area analysis) and crystalline phase. Thermo fluid properties include temperature, viscosity, density, specific heat and enthalpy. Heat transfer properties include thermal conductivity, heat capacity, Prandtl number and pressure drop. Colloid properties are influenced the by suspension stability, zeta potential and pH value (Devendiran & Amirtham, 2016).

A review was undertaken by Saidur *et al.* (2011) who noted multiple uses of nanofluids. As of the article's publication, the following uses have been listed: cooling of electronics, solar water heating and thermal storage. These are just a few applications; however, renewable energy is of particular interest. It was reported in the study that the nanofluids increase the absorption of incident radiation by more than nine times when compared to plain water (although it was suggested that better-designed solar absorption systems might be able to outperform nanofluid-based solar collectors in certain conditions). The addition of nanofluids could significantly increase the performance; however, the next problem is the challenges of nanofluids (Saidur, Leong & Mohammad, 2011). These challenges include the long-term stability of nanoparticle dispersion, increased pressure drop, pumping power requirements, nanofluid thermal performance in turbulent flow and fully developed flow regions, higher viscosity, lower specific heat, thermal conductivity, high production cost, and the difficulties inherent with the production processes (Devendiran & Amirtham, 2016).

According to Saidur *et al.* (2011), research into nanofluids is hindered by a lack of consistency of results obtained by researchers, poor characterisation of the suspensions and a lack of theoretical understanding of the mechanisms responsible for changes in properties. The nanoparticle's stability inside the fluid is one of a nanofluid's fundamental requirements. The preparation of stable nanofluids through a homogenous suspension is a technical challenge because the nanoparticles tend to aggregate due to the strong van der Waal interactions. Physical or chemical treatments can be implemented to obtain stability. A direct correlation was noted between stability and thermal conductivity enhancement,

although with time, the stability of nanofluids changed, and the nanoparticles tended to settle. Thermal conductivity is highest when the nanofluid is freshly prepared, and there is a noticeable performance degradation over time. A challenge presented by nanofluids is increased pressure drop associated with the increasing viscosity over the base fluids' viscosity and lower specific heat capacity (Saidur, Leong & Mohammad, 2011).

2.1 Synthesis and preparation

Nanofluids' preparation phase requires a stable suspension, low agglomeration of nanoparticles and no chemical change to the fluids. The addition of surfactants or any agent that facilitates a nanoparticle's suspension will affect the nanofluid's thermophysical properties (Devendiran & Amirtham, 2016). Xuan and Li (2002) suggest three methods for stabilising the suspensions: surface activators and dispersants, changing the pH value of suspensions and ultrasonic vibration. These methods can change the surface properties of the suspended particles and can be used to suppress the tendency to agglomerate, increasing the stability of the suspension.

There are two methodologies for synthesising nanofluids: the one-step and the two-step method. It should be noted that the preparation methodology affects the stability of nanofluids. The synthesis of nanofluids has challenges such as thermal stability, dispersibility and chemical compatibility (Das *et al.*, 2007). "Thermal stability is defined as the ability of a fluid to resist breaking down under heat stress" (Spurlin.com). Dispersion stability refers to the ability of the nanoparticle to remain in a uniform distribution within the base fluid, not to be confused with solubility (Ha, Weitzmann & Beck, 2013). Lastly, chemical compatibility measures the stability of the nanoparticles within the solvent.

2.1.1 Two-step methodology

The two-step methodology involves dispersing a nanopowder into a solvent in two separate phases. Most nanofluids containing oxide nanoparticles and carbon nanotubes reported in academic studies are produced via this methodology (Das *et al.*, 2007). The nanopowders are obtained via chemical

reduction or mechanical crushing. Once the nanopowder is placed into the base fluid/solvent, it is magnetically stirred and then sonicated at various frequencies depending on the combination of nanopowder and base fluid (Devendiran & Amirtham, 2016). Nanofluids produced using the two-step method have been known to agglomerate before being dispersed. The lack of dispersion reduces the effective thermal conductivity of the nanofluid, and the agglomerated clusters tend to settle, further reducing the stability of the nanofluid.

There are two primary methods of fabricating nanoparticles, bottom-up and top-down methods. The top-down method involves breaking down bulk materials to the desired size. The bottom-up method involves constructing the nanoparticles from constituent atoms (Critchley, 2019).

Top-down approaches can produce copious quantities of nanopowders; however, this approach has no control over the shape and size distribution of the particles produced. The first variation of a top-down approach is that of mechanical attrition. As the name suggests, mechanical attrition involves the milling, shearing, cleaving or wearing down bulk material to the nano-size range (20nm-100nm) (Critchley, 2019). The attrition of materials is the backbone of many industries, including but not limited to the mineral industry, ceramics and powder metallurgy industries. Mechanical attrition is referred to as mechanical milling or a tumbler ball mill. The working principle behind mechanical milling is the transference of kinetic energy from the mechanical balls (usually tungsten carbide or hardened steel) to the material being broken down. The kinetic energy is a function of their mass and velocity; however, too dense a packing of these metallic balls reduces the free path of the ball's motion, thereby reducing the effect of collisions. The first mechanical milling method used is the high-energy ball mill, which John Benjamin first developed in the 1960s at the International Nickle Company. The primary objective of milling is particle size reduction, mixing and blending, particle shape changes and the synthesis of nanocomposites. The typical setup consists of a hollow cylinder rotating around its axis with metallic balls. The balls impact the bulk material as the mill rotates, breaking the material down into a fine powder. It should be noted that the tumbler ball mill is operated as close to the critical speed as possible to maximise the kinetic energy transfer to the balls. Speeds greater than the critical speed will cause the centrifugal forces to overcome the centripetal forces,

forcing the metallic balls to the outside of the shell and pinning them there. The attritor is a modification of the mechanical. Szegvari developed the attritor in 1922. This mill consists of a vertical cylindrical shell with a shaft running down the centre. On the shaft, there are horizontal arms that stir the metal balls. The rotation of the vertical shaft causes differential movement between the balls and the material being broken down. This method provides a more significant surface contact than the latter (Yadav, Yadav & Singh, 2012).

The chemical reduction method (CRM) is the most common two-step methodology. CRM is a simplistic, non-time-consuming methodology for producing nanoparticles. CRMs can be categorised into two subgroups: co-reduction and successive reduction. Co-reduction involves two different metal salts, and the second method is the successive reduction of two metal salts. CRM is considered a bottom-up method of producing nanoparticles as it relies heavily on three stages: organic synthesis, self-assembly and colloidal aggregation. It was noted by Manikim *et al.* that CRMs could produce finer nanoparticles than mechanical means. CRMs are not without their disadvantages, however, the most important of which is that the chemicals used in this method are harmful to the environment, particularly when scaled up for mass production. The chemical reduction method comprises three items: a precursor, a reducing agent and a stabiliser or protective agent. A catalyst may also be added to speed up the reaction rate (Manikam, Cheong & Razak, 2011). A chemical precursor is a chemical that is changed into another compound during a chemical reaction. Reducing agents are defined as compounds or elements that lose an electron during the chemical reaction (Purdue University, 2004), and a stabiliser is an agent that hinders further reactions and prevents degradation of the nanoparticles into clusters (Hawkins, 2014). The surfactant type and reducing agent influence particle size; more potent reducing agents generate narrower particles. These narrower particles avoid agglomeration better than others (Manikam, Cheong & Razak, 2011).

2.1.2 One-step methodology

As the name suggests, the one-step methodology combines the manufacturing and dispersion of a nanoparticle into a base fluid in one process (Das *et al.*,

2007). Nanofluids produced through this method have proven to be more stable than those produced through the latter.

LASiS is considered a one-step methodology and is free of the disadvantages presented by CRMs. In LASiS, nanoparticles are produced during the condensation of a plasma plume formed by the laser ablation of a metal specimen suspended within a liquid. Amendola and Meneghetti (2009) note that the process had been used successfully to create nanoparticles of gold, silver, platinum, copper and other materials in various solvents. It was pointed out that the poor control of NMNp size and size distribution can be controlled by laser irradiation, exploitation of plasmon absorption or interband transitions. Despite these perceived shortcomings, the most significant advantage is that NMNps can be obtained stable within solvents without stabilising agents (Amendola & Meneghetti, 2009).

The basic setup of the LASiS process consists of a pulsed laser, a set of focusing optics and a container with a metal plate suspended within a liquid. The metal, placed in the focal point of the laser, can be seen in **Figure 2.1**. The most critical parameters for the LASiS process are the time duration, wavelength and fluence of the laser pulses (Amendola & Meneghetti, 2009).

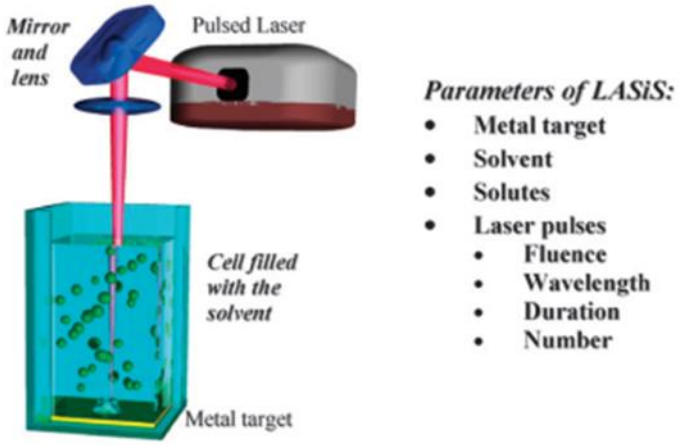

Figure 2.1 Basic setup of the laser ablation process (Amendola & Meneghetti, 2009)

2.1.3 Preparation

The stability of the fluid affects the performance of nanofluids. Agglomeration is a challenge faced by nanofluids. Nanofluids naturally tend to agglomerate, allowing the particle clusters to be overcome by gravitational effects. The deterioration of nanofluids manifests as an increase in unwanted thermophysical properties of nanofluids, such as viscosity. The increase of clustering within the fluid may also reduce the thermal conductivity of the nanofluid. To circumvent agglomeration in nanofluids, they are subjected to sonication to separate them. Sonication is not the only means of reducing the effects of agglomeration, as there are other alternatives such as magnetic stirring, surface charge and the addition of surfactants. There is a correlation between sonication time and nanofluid stability. Ultrasonication can be categorised into two categories: direct and indirect sonication. Direct sonication involves direct contact between the horn of the ultrasonic homogeniser and the sample. Indirect sonication involves an intermediary medium between the sample and the ultrasonic head. The most common indirect sonication method is the ultrasonic bath. The primary mechanism behind sonication is cavitation. The cavitation allows for nanoparticle dispersion and may even lead to smaller particles being formulated in the nanofluid.

It should be noted that direct sonication provides a more direct and focused ultrasonic effect on the fluid, whilst indirect ultrasonication provides a low-intensity and broad-spread effect. Two parameters of ultrasonication affect nanofluid the most: the power of sonication and the duration of the sonication (Asadi *et al.*, 2019). The sonication time and power positively affect the thermal conductivity of nanofluids. The thermal conductivity increases with sonication time until a critical point, after which there is a decrease in thermal conductivity. The typical sonication time for a nanofluid is approximately two hours at 500 W (Haddad *et al.*, 2014).

The addition of surfactants is another means of increasing the stability of nanofluids. The surfactants have a positive effect on stability but a negative effect on thermal conductivity. The surfactant modifies the surface properties of the particle. The selection of surfactants is crucial for the stability of nanofluids. Surfactants fall into three categories: cationic, anionic or non-ionic. The addition of surfactants affects the pH value of the nanofluid (Ilyas, Pendyala & Marneni, 2014).

2.2 Properties

2.2.1 Thermal conductivity

Thermal conductivity is the most crucial property responsible for the enhancement of the thermal performance of nanofluids (Devendiran & Amirtham, 2016). According to Cengal & Afshin (2015), thermal conductivity is "the rate of heat transfer through a unit thickness of the material per unit area per unit temperature difference" (Yunus & Afshin, 2015:18). The definition can be expressed mathematically in Equation (5.1). Devendiran and Amirtham (2016) note that the experimental results proved the thermal conductivity increased, and they disagreed with the numerical models for nanofluids. Numerical models often underpredict the thermal conductivity of nanofluids. Khedar *et al*. (2012) tested the effect of CuO nanoparticles in water and monoethylene glycol, and determined that for nanofluids comprising of water and CuO nanoparticles, there was a maximum increase of 21.26% in thermal conductivity over that of water. For monoethylene glycol nanofluids, there was a maximum increase of 32.25%, and both results were taken at a 7.5% volume fraction (Khedkar, Sonawane & Wasewar, 2012). Hu, Fei and Chen tested the performance of AlN nanoparticles in ethanol, recording a 20% increase in thermal conductivity over that of the base fluid with a 4% volume fraction (Hu, Fei & Chen, 2008). Saidur, Leong and Mohammad observed a lack of explicit agreement between reported results (Saidur, Leong & Mohammad, 2011).

Apart from experimental studies, various mathematical models have been proposed to predict the thermal conductivity of nanofluids. The Maxell model has already been discussed in Chapter 1 (5.1). The Jeffery model, as seen in Equation **(2.2**) was proposed by D. Jeffery in 1973 to approximate spherical particles suspended in a base fluid. The model assumes a homogeneous suspension of spherical particles within the fluid (Jeffrey, 1973).

$$\frac{k_e}{k_f} = 1 + 3\beta\emptyset + \emptyset^2(3\beta^2 + \frac{3\beta^2}{4} + \frac{9\beta^3}{16}\frac{\propto +2}{2\propto +3} + \frac{3\beta^4}{2^6} \ldots)$$

(2.2)

Where:

k_e =	Effective thermal conductivity
k_f =	Base fluid thermal conductivity
α=	Ratio of particle-to-base fluid thermal conductivity
β=	(α-1)/(α-2)
Ø=	Volume fraction

In 2004, Yu and Choi modified the Maxwell model to accommodate nanofluids. The model explicitly considers the collisions of the molecules, thermal diffusion, volume fraction, particle size and temperature. This modification was made after an initial model created by Jang and Choi in 2003; the model specifically considers the nanolayer effect. It should be noted that the model was restricted to water-based nanofluid in a rectangular cavity. The nanoparticles used were 6 nm copper and 2 nm diamond particles with a 0.5% to 2% volume fraction. In the study, they exclusively calculated the theoretical results of the nanofluids and concluded that there was an increase in thermal conductivity according to the model (Yu & Choi, 2004).

$$k_{nf} = k_f(1 - \emptyset) + k_p\emptyset + 3C_1\frac{d_f}{d_{nano}}k_f Re^2{}_{dnano} Pr\emptyset$$

(2.3)

Where:

k_{nf}=	Thermal conductivity of nanofluid
k_f =	Thermal conductivity of the base fluid

$\emptyset =$ Volume fraction

$k_p =$ Thermal conductivity of nanoparticles

$C_1 =$ Proportional constant (18x10^6)

$d_f =$ Diameter of fluid

$d_{nano} =$ Diameter of the nanoparticle

Re= Reynolds number

Pr= Prandtl number

A recent numerical model, developed by Garoosi in 2020, was based on various published experimental studies of metal oxide nanofluid. It compensates for volume fractions ranging from 0% to 12% and particle sizes ranging from 5 μm to 10 nm. It was found that older models, such as the Maxwell-Garnet model, underpredicted the thermal conductivity and were far too conservative. According to Garoosi, existing models show agreement between experimental and theoretical results but are limited to spherical nanoparticles. The model proposed in Equation **(2.4)** agreed with a larger pool of published data than its predecessors and is one of the most recent models to achieve this agreement. The proposed model was derived using the least-squares method; it has a 4.7% standard deviation from the 458 experimental data sets (Garoosi, 2020).

$$\frac{k_{nf}}{k_f} = \frac{k_p + 2k_f + 2(k_p - k_f)\emptyset}{k_p + 2k_f - (k_p - k_f)\omega\emptyset}$$
$$+ 3.762\left(\frac{T}{T_0}\right)^{8.661}\left(\frac{d_p}{d_f}\right)^{-0.4351}\left(\frac{k_p}{k_f}\right)^{0.08235}\emptyset^{0.64}e^{(-5.742\emptyset)} \quad \textbf{(2.4)}$$

Where:

$k_{nf=}$ Thermal conductivity of nanofluid

$k_f =$ Thermal conductivity of the fluid

$k_p =$ Thermal conductivity of nanoparticles

$\omega=$ Correction factor

$\emptyset =$ Volume fraction

$T =$ Temperature

$T_0 =$ Reference temperature (293 ºK)

$d_p =$ Diameter of the nanoparticle

$d_f =$ Diameter of the base fluid

2.2.2 Viscosity

Viscosity is best described as a fluid's internal resistance to motion/flow (Cengel & Cimbala, 2013). Mathematically the viscosity of a Newtonian fluid can be described by Equation (2.5) (Upadhyay, 2017). Equation **(2.5**) is known as Newton's Law of viscosity as follows:

$$\tau = \mu \frac{du}{dy} \quad \textbf{(2.5)}$$

Where:

τ= Shear stress

μ= Absolute viscosity

du= Change in velocity

dy= Change in the distance between surfaces

The viscosity of nanofluids relies on particle size, particle shape, particle size distribution, volume concentration, aggregation, temperature, pH value and dispersion method (Chandra & Sayantan, 2014). The base fluid on its own will usually exhibit Newtonian behaviour, but the addition of nanoparticles sometimes results in the fluid exhibiting non-Newtonian behaviour (Liu *et al.*, 2020). Nanofluids with even distributions of nanoparticles and a volume fraction less than or equal to 0.6% would display Newtonian behaviour. However, fluids with a volume fraction greater than 0.6% will begin to exhibit shear thinning and, as such, can no longer be considered Newtonian fluid (Li *et al.*, 2015). Multi-walled carbon nanotubes (MWCNT) in liquid paraffin are a recent development in nanomaterials. MWCNT nanofluids exhibit non-Newtonian behaviour, and the greater the volume fraction/temperature differential, the more significant the

deviation from Newtonian behaviour (Liu *et al.*, 2020). Fe-Si nanoparticles in water showed an almost sinusoidal curve of viscosity compared to concentration; in the study, the maximum viscosity was found at a volume fraction of 1.0% (Huminic, Huminic & Fleacă, 2020). There is an exponential relationship between the volume fraction and viscosity (Bao *et al.*, 2021).

2.2.3 Density

Density, traditionally defined as the mass per unit volume, is typically expressed by the following equation (Douglas *et al.*, 2005):

$$\rho = \frac{m}{V}$$

(2.6)

Where:

ρ=	Density
m=	Mass
V=	Volume

However, the formula does not consider that nanofluids contain both solids and liquids; therefore, the equation is insufficient to approximate the density of nanofluids. Equation **(2.7)** provides the density of the base fluid and the particle. The density is based on the volume fraction of nanoparticles added to the base fluid (Garoosi, 2020).

$$\rho_{nf} = (1 - \emptyset)\rho_f + \emptyset\rho_p$$

(2.7)

Where:

ρ_{nf}=	Density of the nanofluid
ρ_f=	Density of the base fluid
ρ_p=	Density of the nanoparticle
∅=	Volume fraction

2.2.4 Characterisation

There are multiple ways to evaluate the thermal conductivity of nanofluids, such as the transient hot wire (THW), hot disk technique, temperature oscillation technique and the guarded hot plate apparatus. Much of the disagreement of results stems from the various testing methodologies employed by various researchers. Zagabathuni, Ghosh and Pabi compared the results obtained from the laser flash method to those of the THW method and found that the laser flash method obtained results one order of magnitude lower than the THW methodology. The measurement of the thermal conductivity of nanofluids falls into one of two distinct categories: steady-state or transient. The steady-state was discussed in section 1.1; the transient state is one in which the heat transfer is rapid (Zagabathuni, Ghosh & Pabi, 2016).

A typical modern THW setup consists of the transient hot-wire apparatus, an analogue-to-digital converter and a computer or data logger (Loong & Salleh, 2017). The analogue-to-digital converter would not be necessary if the data logger is used. A schematic view is presented in **Figure 2.2**. The THW apparatus consists of a platinum hot wire with a diameter ranging from 12.7 μm to 50.8 μm (depending on commercial availability), a pressure cell/container and a wheat stone bridge. In more recent iterations of the THW apparatus, the platinum wire is coated in Teflon to circumvent the electrically conductive nature of metallic nanoparticles present in a nanofluid. As the name suggests, this method falls into the category of transient methods, as the heating and data collection takes place at a rapid pace. This method relies on Fourier's one-dimensional transient heat conduction in the cylindrical bodies' equation. The heat is applied via a platinum wire that passes through the core of the apparatus. The platinum wire is connected to a wheat stone bridge. The power supplied to the platinum wire is monitored and recorded, and the change in resistance of the platinum wire is monitored and used to calculate the thermal conductivity of the fluid sample. **Figure 2.2** displays the typical test setup of the THW.

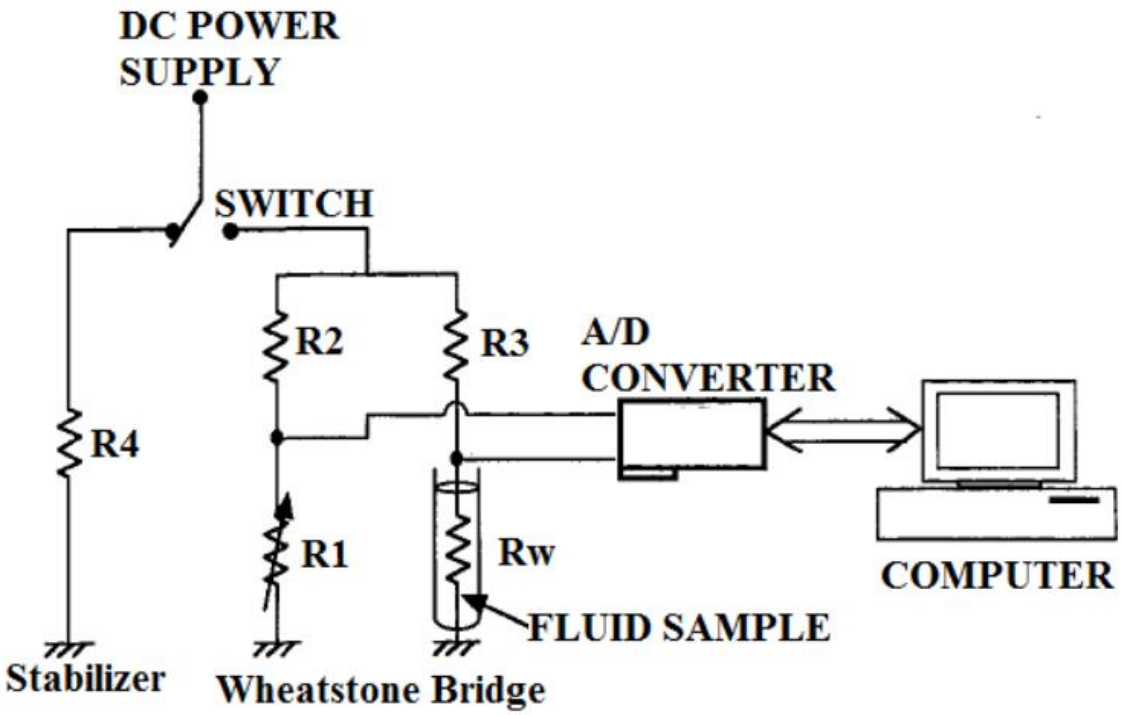

Figure 2.2: Schematic overview of a computerised THW setup (Choi, Li & Eastman, 1999)

Beyond the wheat stone bridge and platinum wire, the setup consists of a hot wire cell, whose sole purpose is to contain the fluid and to provide the relevant tension on the platinum wire.

The transient hot disk is commonly referred to as a transient plane source, thermal constant analyser or Gustafsson probe technique. The typical setup contains the Gustafsson probe, constant temperature bath, material sample and thermometer (Loong & Salleh, 2017). In conjunction with those mentioned earlier, it is used by a thermal analyser to determine the thermal conductivity of a test sample. The transient plane source (TPS) operates on a principle similar to that of the transient hot wire in which the heat source is also the sensor. The change in resistance is measured and used to calculate the thermal conductivity of the fluid (Buonomo *et al.*, 2014). The plane source is typically made of insulated copper or nickel of a double spiral construction, as seen in **Figure 2.3**. The probe itself can be shaped as required to fit the test sample. Custom TPS probes are made of a thin film of copper or nickel and then insulated with Kapton tape (Hu *et al.*, 2008). The working principle is like that of the THW apparatus, but the governing equation deviates from Fourier's Law of heat conduction in cylinders to that of Fourier's Law of heat conduction, as seen in Section (5.1).

The working principle of the TPS probe is that the voltage change across the element is recorded while a direct current pulse heats the element; the pulse is short enough so that the element is considered to be infinite or semi-infinite throughout the transient recording. By doing this, the outer boundaries of the test sample can be negated, and it can be assumed that no external factors are acting on the system other than the controlled variables. The governing equation for a TPS probe is shown in Equation **(2.8**) (Gustafsson, 1991):

$$R(t) = R_0(1 + \overline{\propto \Delta T(\tau)}) \qquad \textbf{(2.8)}$$

Where:

$R(t) =$	Resistance at a given time
R_0=	Initial resistance
$\propto$=	Temperature coefficient of resistance
ΔT=	Change in temperature
τ=	Time-dependent constant

Equation (2.8) is then substituted into Fourier's Law to calculate the thermal conductivity of a sample. The TPS system has gained market acceptance as a standard in many industries for the measurement of thermal conductivities, as evidenced by systems such as the TPS 2500 S. This model of apparatus has been used by Buonomo *et al.* (2014) and a self-manufactured variant was used by P. Hu *et al*. in their study of AlN-ethanol nanofluids (Hu, Fei & Chen, 2008; Buonomo *et al.*, 2014).

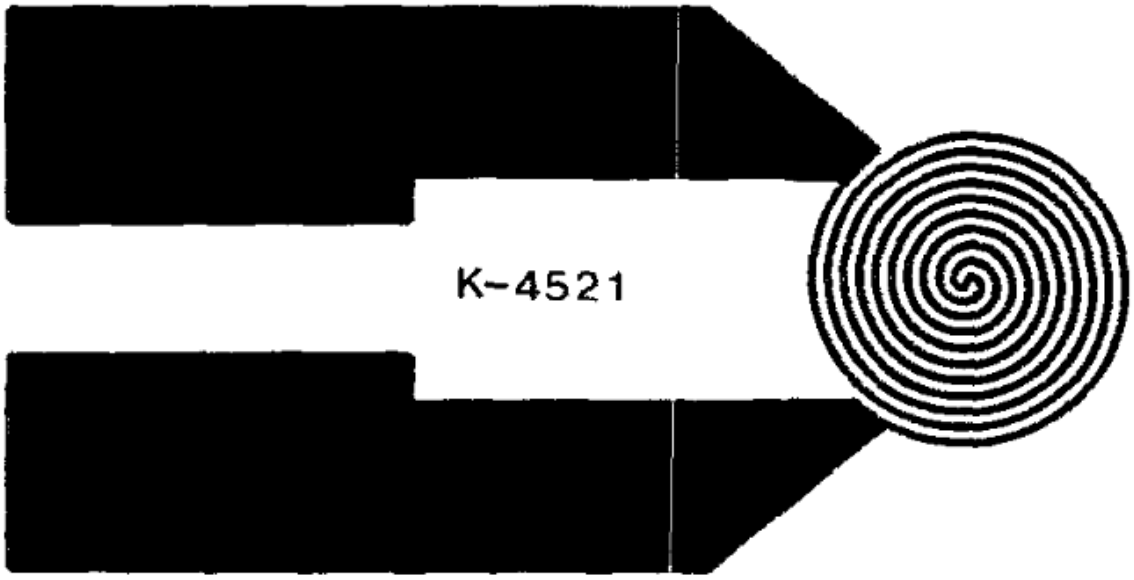

Figure 2.3: Close up of hot disk design (Gustafsson, 1991)

The TPS system is capable of measuring between 0.5 K to 2 K, and the sample is open to the atmosphere (Hu, Fei & Chen, 2008). Furthermore, the TPS system is suitable for measuring various materials, encompassing solids and fluids. Commercial models can detect thermal conductivities in the range of 0.005 W/m.K to 500 W/m.K with an uncertainty of 5% (Buonomo *et al.*, 2014). The TPS cannot measure the thermal conductivities of a fluid that undergoes the boiling process, but it does notify the end-user of the presence of natural convection that may skew the results (Loong & Salleh, 2017).

The temperature oscillation technique set-up consists of a cylindrical tube, two Peltier modules placed in series with each other at opposite ends, two end plates that act as heat spreaders and two heat exchangers to dissipate the heat generated by the thermoelectric coolers. The Peltiers are placed in series for a constant current across both Peltier modules, allowing for parity in the temperatures of the two units. The end plates seal the cylinder so the tested fluid cannot leak (Phelan, 2004). The working principle of such a device is based on the transient heat transfer equation. The amplitude attenuation, the phase shift and the amplitude of thermal diffusivity are measured, and the thermal conductivity can be calculated. One of the advantages of this method is its

similarity to that of the 3ω method; it was relatively simple in comparison to other measurement methods (Badarlis *et al.*, 2020). Czarnetizki and Roetzel (1995) also contend that the method combines the advantages of steady-state measurement with the ability to measure properties that describe non-steady-state conditions (Czarnetzki & Roetzel, 1995). Concerning disadvantages, the lack of literature available was the most likely reason for the lack of adoption amongst many research groups. There is no guidance for the configuration of the experimental setup and what amplitudes and temperature frequency to use (Bhattacharya *et al.*, 2006). The final disadvantage is that the relatively low-temperature ranges that were measured are only within 2.5 °C (Czarnetzki & Roetzel, 1995).

The guarded hot plate apparatus, initially developed in the early 1900s, was based on Lee's disk method (Thermtest Inc., 2015a). The Lee's disk method consisted of a steam chamber, a cast iron upper disk, a slab of a specimen, a cast-iron lower disk and a series of thermometers. The working principle of such an apparatus was that steam was generated, which flowed into the steam chamber. This would in turn heat the upper cast iron disk in direct contact with the specimen slab. Once the system has reached a steady-state, the steam supply and upper cast iron disk is removed whilst the specimen slab and lower cast iron disk remain. The lower disk is then heated to 10 degrees above the steady-state temperature, and readings are then taken every 5 minutes till the lower disk has cooled. Based on these readings, it would be possible to calculate the thermal conductivity of the specimen. A 3D rendering of the setup can be seen in **Figure 2.4**; it should be noted that the steam chamber is in grey, the upper and lower disks are in yellow, and the specimen is in red. The upper and lower disks are of a known mass (Alam *et al.*, 2012).

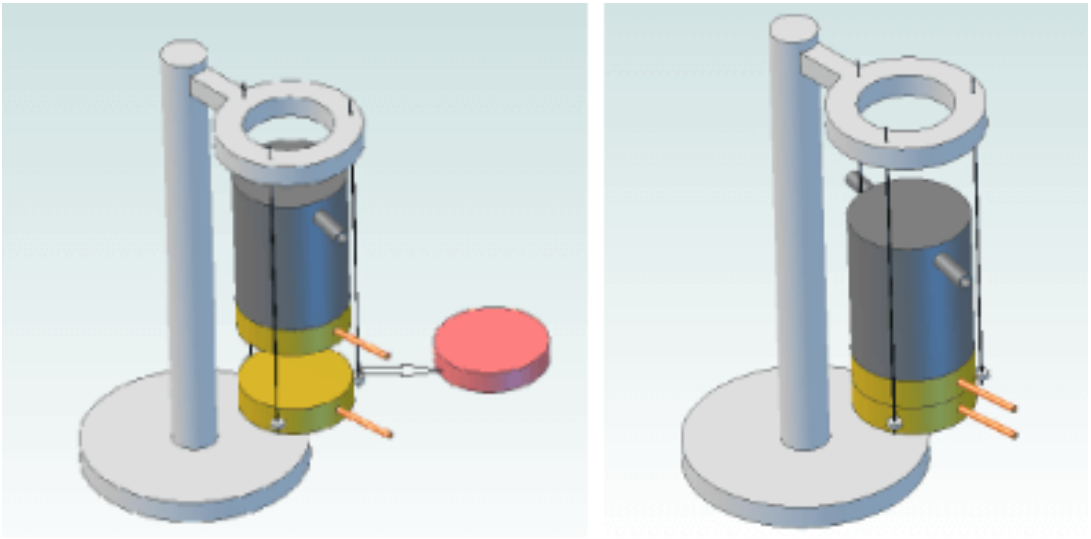

Figure 2.4: 3D rendering of Lee's disk method (Thermtest INSTRUMENTS, n.d.)

In the early 1900s, the guarded hot plate apparatus was developed concurrently in both the United States and Germany. In the United States, the American Society of Refrigeration Engineers (ASRE) requested the National Bureau of Standards (NBS) to develop a means of testing insulation materials. This request is what set the development of the GHP in motion. At the same time as the request from the ASRE, Richard Poensgen of Germany was developing a similar device for the same reason: there has been no standard method of precisely measuring the heat transmission in insulating materials. The two constructed devices had similar experimental setups and operated on the same working principle. Poensgen's device was released first in 1910, and two years later, in 1912, the NBS machine was released. Since then, the GHP apparatus has been an industry standard across fields such as refrigeration and insulation (Thermtest Inc., 2015b).

Two norms govern the GHP apparatus: ASTM C177 and ISO 8302 (Linseis Inc., n.d.). According to Challoner and Powell (1956), they designed a completely enclosed GHP for the explicit purpose of testing liquids, a cross-section of which is presented in **Figure 2.5**. Their device was similar in construction to that of the NBS in that it consisted of the typical cold plate, hot plate and guard heater. This arrangement is typical of GHP setups and typically contains a thermocouple on the respective elements of the setup. In Challoner and Powell's setup, the heat was supplied via resistive heating elements in the guard and hot plate, whilst

the cold plate was kept cool via a water cooling loop that maintained the temperature at ±0.01 ˚C (Challoner & Powell, 1956).

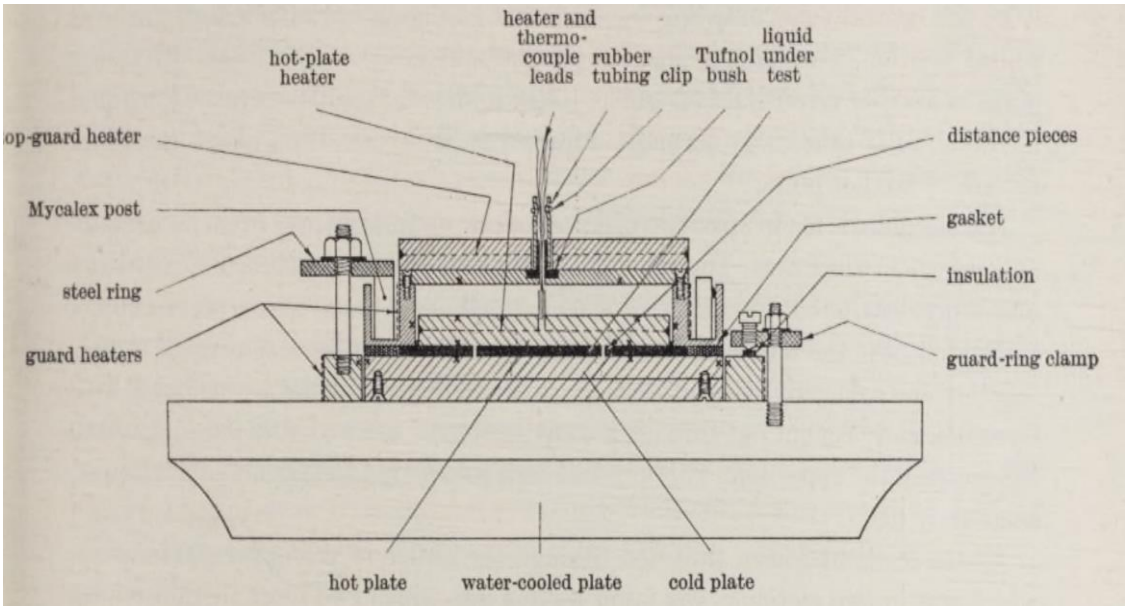

Figure 2.5: GHP apparatus setup (Challoner & Powell, 1956)

The basic working principle of a GHP setup is based on Fourier's Law of conduction which was briefly touched on in section 1.1. As previously stated, the typical setup for all GHP setups consists of a guard to prevent heat losses from the hot plate; this is achieved by having a guard temperature that matches that of the hot plate, a hot plate that provides the source of heat to the sample and a cold plate that removes the heat from the sample. Across the sample, a temperature difference will need to be measured, along with the power supplied.

There are two possible configurations for a GHP, the one-plate method and the two-plate method. In the one-plate method, the heat flows in a single direction, and in the two-plate method, the heat flows in two directions. These configurations are illustrated in **Figure 2.6**.

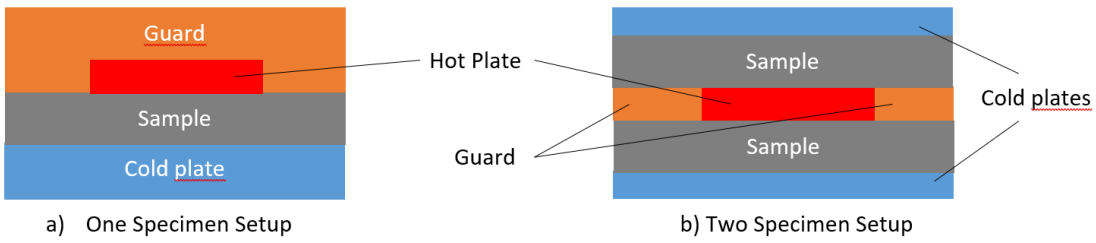

Figure 2.6: GHP configurations (Linseis Inc., n.d.)

In 1982 Smith, Hust and VanPoolen (1982) obtained a commercial GHP apparatus from the Langley Research Centre. The group working for the NBS found through experimental means that the device had uncertainty of measurements of glass fibre board of ±2% at ambient temperatures and ±5% at sub-ambient temperatures. These results were obtained using the supplied water-cooling loop and then via a modified LN2 loop. The results were deemed out of spec, and the authors noted that this was not representative of all machines supplied by the Langley Research Centre; furthermore, the apparatus was designed to comply with the ASTM C-177 standards. The device was a two-specimen setup consisting of two cold plates, a main heater, an inner guard heater, an outer guard heater, auxiliary cooling plates and an environmental chamber. Altogether, the cold, hot and guards make up the stack. As per **Figure 2.7**, it can be seen that the specimens are placed on either side of the main heater via glass or stainless-steel tubes stuffed with glass fibre. Around the guard heater is the inner guard heater; on the outer sides of the specimens are the cold plates; and around the cold plates are the auxiliary cold plates. Around this stack are the outer guard heater and environmental chamber, which contains a cooling shroud. The cold plates and heaters were constructed out of anodised aluminium, which was done to promote conductive and radiative heat transfer. The group modified the cooling system to run an inter-connected cooling loop as opposed to the independent systems with which the system came packaged. Differential thermocouples are connected to each plate, and the guards measure each plate's temperature. The temperature data was used to calculate the thermal conductivity along with the control circuitry. Lastly, the auxiliary heaters, guards and environmental chamber were implemented strictly to prevent radial heat flow and external influences on the system (Smith, Hust & VanPoolen, 1982). It should be noted that this device pertains to insulation materials and not fluids.

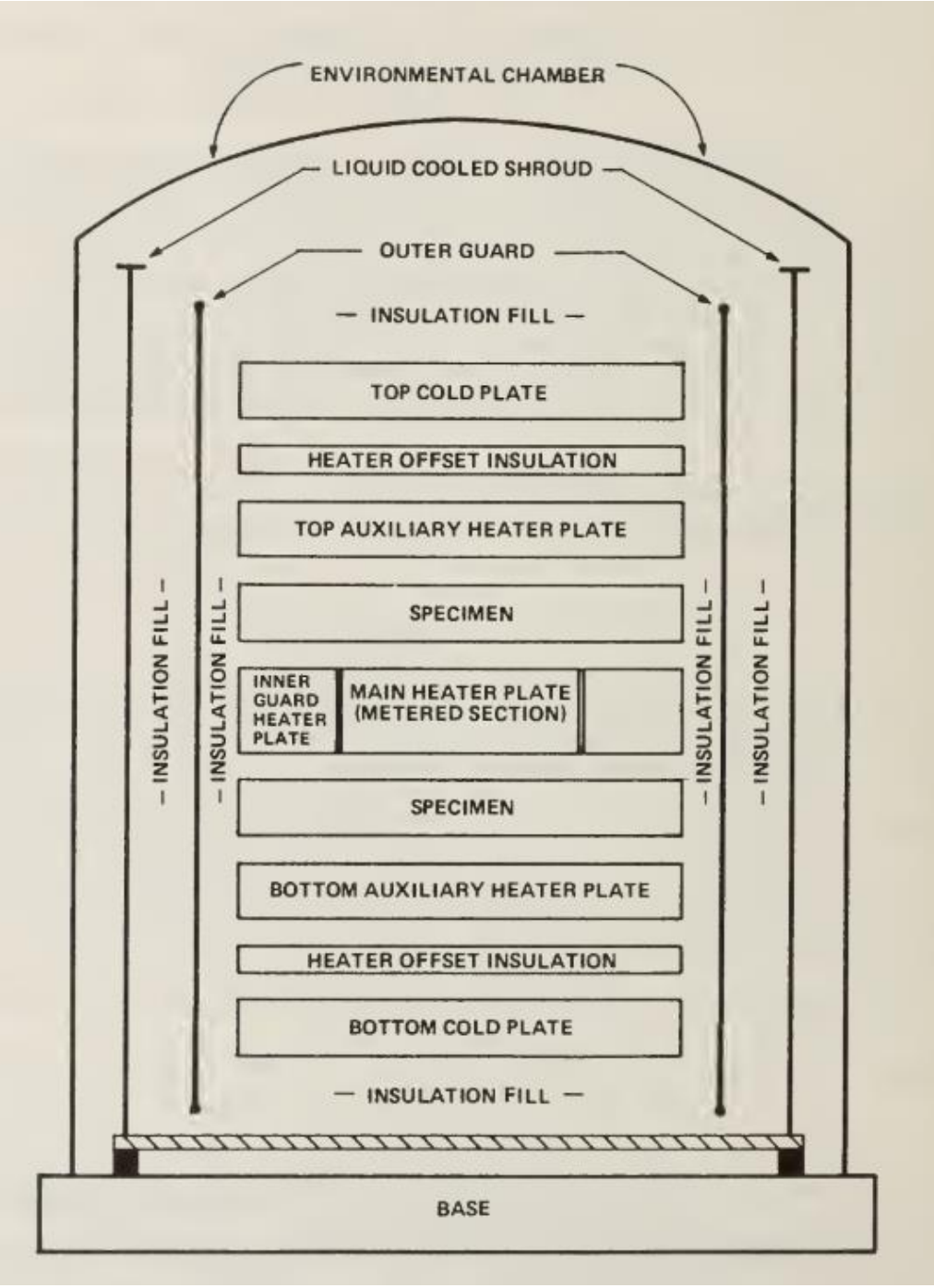

Figure 2.7: Cross section of the modified guarded hot plate (Smith, Hust & VanPoolen, 1982)

In recent developments, Choi and Eastman used a GHP apparatus when they discovered nanofluids in 1990. The machine was based on Challoner and Powell's device (Choi & Eastman, 1995). In 2013 Raush *et al.* (2013) attempted to create a GHP capable of measuring the thermal conductivity of gases, liquids and solids. The device had a similar setup as that of Choi and Eastman in that the device consisted of a cold plate, hot plate and guard plate. The plate also

included a Peltier element for cooling and micrometre screws for adjustment. A cross-section of the device is presented in **Figure 2.8**. The cold plate is connected to the Peltier for cooling, and the hot face is connected to a set of fins for cooling. A two-part guard system ensures heat flow through the sample area. The top guard plate is heated to the same temperature as the hotplate to ensure no bi-directional heat flow through the sample and a guard ring around the entire setup. The guard ring comprises an inner guard ring and an outer guard ring, both in place to mitigate the effects of ambient conditions. Heating to the system is provided by a constant current source to the system via a resistive heating element embedded in the hot plate and cold plate. The authors noted that the hot plate was intentionally placed above the cold plate to mitigate the likelihood of convection in fluid samples.

The top assembly (hot plate, guard and micrometre screws) can be removed to clean the system between tests quite easily. The entire system is then placed within an environmental chamber for sub-ambient tests. A custom-made programme was generated to control the system through PID control schemes for cooling, heating and the guard heater to ensure steady-state conditions. The PID is fed information from the DC power supply, thermostats and a digital multimeter. With this setup, the authors could achieve a 5% deviation from reference data for water, Toluene, air and polytetrafluoroethylene (PTFE). The authors note that although the GHP could not achieve uncertainties similar to that of transient methods, its ease of use and accuracy make it a viable testing methodology for various materials (Rausch *et al.*, 2013).

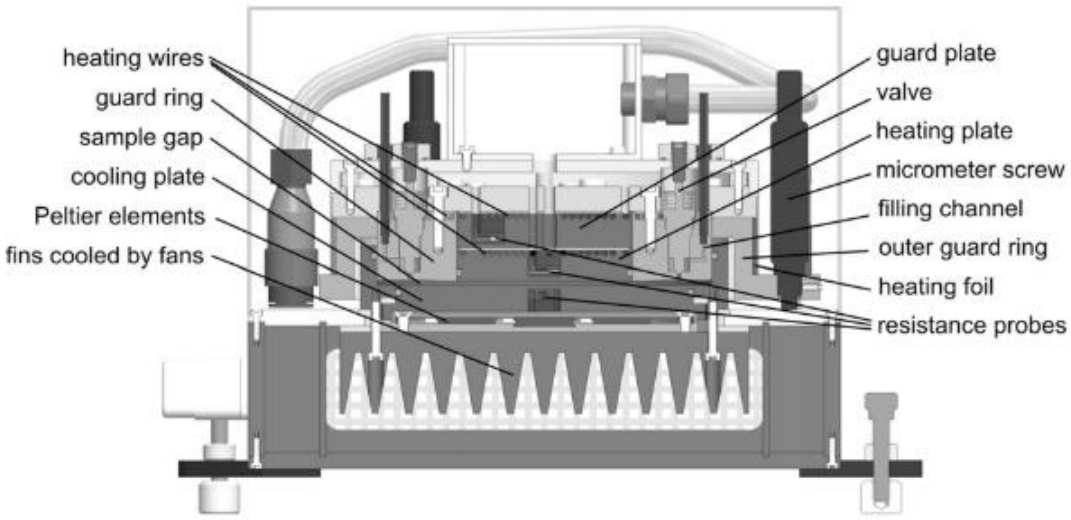

Figure 2.8: Cross section of GHP apparatus for fluids and solids (Rausch *et al.*, 2013)

The guarded hot plate is one of the most commonly employed methods of testing in various fields due to its simplicity and the fact that it is considered an absolute method because the thermal conductivity is measured directly from the value obtained from the device (Yüksel, 2016). The uncertainty of the measurements of the GHP is approximately 2% at low temperatures; beyond this, the heat losses to the environment become greater when compared to other means of measurement, such as the thermal comparator (tec-science, 2020). A further advantage of the GHP is the standardisation in countries such as the US (ASTM C 177-63), Britain (B.S 874:1965) and Germany (DIN 52612) (Yüksel, 2016).

The primary disadvantage of the GHP is the long testing times, as it takes a relatively long time for the system to attain a steady state; however, this statement is true for all steady-state techniques. Another disadvantage is that the contact resistance between the thermocouples is a potential source of error in readings. The final disadvantage is that the recorded results of approximately 20 GHPs diverged significantly from reference values ranging from 13 to 16% (Yüksel, 2016).

In conclusion, the GHP is primarily used for the testing of the insulation; however, it is just as capable of measuring the thermal conductivity of other substances. Furthermore, due to the GHP being an absolute method that

significantly reduces computation, it is relatively simple to fabricate and operate. It is also evident that there are myriad contributing factors to the thermal conductivity enhancement of nanofluids. Some of these can be controlled, such as the manufacturing method and combination of surfactant, base fluid and nanoparticle employed. There are also inherent challenges in the means of testing that need to be overcome, such as gravitational effects, whether a testing method is considered obtrusive or not, and the onset of natural convection within the testing chamber. These challenges need to be accommodated in the design, and uncertainty in the results must be minimised.

3 CHAPTER THREE: Design and Fabrication

The proceeding chapter will delve into further depth of the design and fabrication of the guarded hot plate apparatus. The design will be based upon that of Challoner and Powell, as described in the literature review, and will include modifications such as those made by Rausch to make additional observations.

3.1 Design

The present design is similar to that of Challoner and Powell; however, Stephen Choi provided brief dimensions for the apparatus used in the initial study of nanofluids. According to Wang, Xu and Choi (2008), the GHP setup consisted of copper plates with a surface area of 9.552 cm^2, which equates to a diameter of 34.874 mm. Three glass spacer rings separate these with a thickness of 0.9652 mm. These spacer rings make Δx equate to 2.8956 mm. The guard is constructed of aluminium and heated electrically via a resistance heater. Both copper plates have holes of 0.89 mm in diameter drilled into them to accommodate E-type thermocouples; it is not stipulated how deep these holes are drilled. In total, 14 thermocouples were used to measure the temperature differences. The researchers noted that their primary goal was to minimise the temperature difference between thermocouples on each plate. The present, depicted in Figure 3.1, consists of the GHP apparatus, a GW Instek gps 3303 power supply and the Agilent 34970A data logger. The GHP apparatus consists of a frame, cold plate, hot plate, guard heater, water cooling loop and Arduino microcontroller-controlled PID circuit. Each will be discussed in greater detail in subsequent sections.

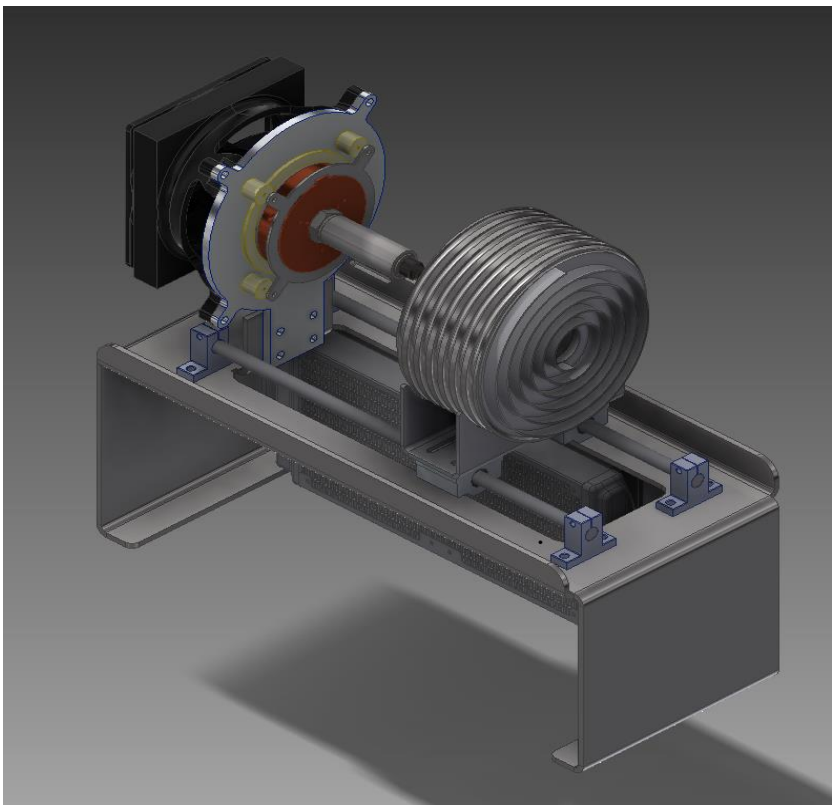

Figure 3.1: 3D rendering of apparatus

The apparatus overall consists of a frame, aluminium backplate, the core/stack assembly, rails, guard heater, fan cowling and water-cooling loop. The core assembly is mounted to the aluminium backplate via a stainless-steel retention plate, which also serves to align the thermocouples on the hot plate with their corresponding mate on the cold plate. The retention plates are bolted to nylon spacers. The bolts are long enough to hold the spacer plates but short enough that the bolts do not come into contact; this is done to prevent conductive heat transfer from the hot plate to the cold plate. On the face of the aluminium back plate, fibreglass insulation is placed to prevent heat from seeping through the sides of the cold plate. In the centre of the aluminium plate, a nylon spacer ring isolates the copper from the aluminium and creates a small air pocket to further insulate the cold plate. The aluminium back plate is bolted to the stainless-steel frame via a section of equal leg right angle ss304. On the frame are a series of slotted holes that allow for minor adjustments of the rails and aluminium back plate.

Additionally, a mounting plate is bolted to the frame's rear to accommodate the water-cooling loop's radiators. A vesconite ring separates the hot and cold plates. The vesconite ring has grooves machined into it to accommodate a nitrile cord; this acts as a means of sealing the testing cavity and preventing leakage of the fluid samples. The bulk of the apparatus was fabricated from SS304. This material was selected for its anti-corrosive properties.

For the current setup, the volume inside the vesconite ring amounts to 7.5 ml of fluid. This equates to an Δx of 5.68 mm. It was possible to create a simplified thermal circuit base formulated from the geometry of the stack assembly, which can be seen in Figure:

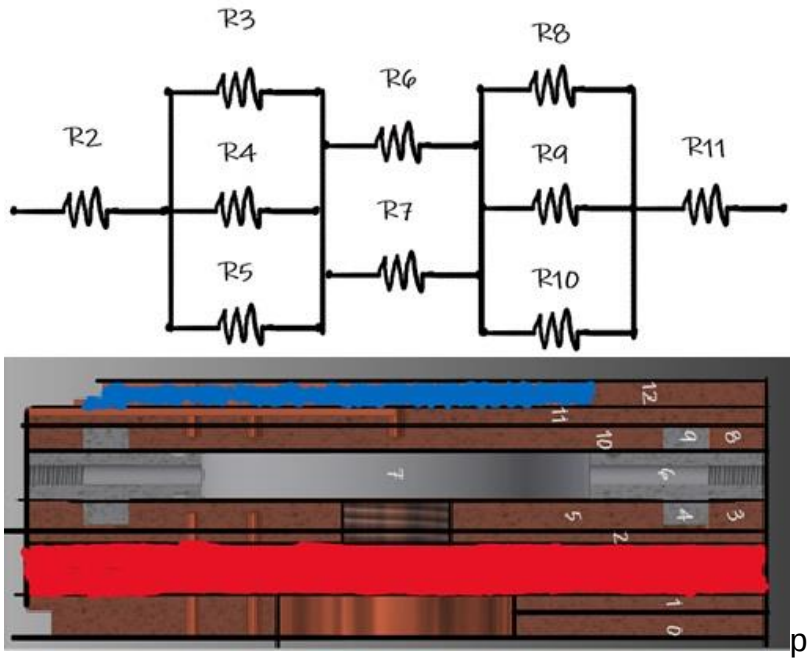

p

Figure 3.2: Thermal resistance circuit of stack assembly

The thermal resistance was calculated for each section using the following formula:

$$R = \frac{\Delta x}{kA}$$

(3.1)

Where:

R= Thermal resistance

∆x=	Thickness
k=	Thermal conductivity
A=	Area

Based on Equation (3.1), each value can be calculated individually. Due to the circuit having parallel and series resistive elements, the total resistance can be calculated using the following formula:

$$R_T = R_2 + (\frac{1}{R_3} + \frac{1}{R_4} + \frac{1}{R_5})^{-1} + (\frac{1}{R_6} + \frac{1}{R_7})^{-1} + (\frac{1}{R_8} + \frac{1}{R_9} + \frac{1}{R_{10}})^{-1} + R_{11}$$

(3.2)

Next, the temperature differential can be calculated based on the power input into the system using the following formula:

$$\Delta T = R_T Q$$

(3.3)

Analysing the ideal system will make it possible to determine the losses from the system during testing and commissioning. For the analysis, it was assumed that the contact resistance would be negligible, that there was no heat loss radially and that there was no fluctuation in the supplied power to the hot plate. The thermal conductivity for each material can be found in **Table 3-1**:

Table 3-1: Material properties

Material	Thermal conductivity	Reference
Copper	385	(Thermtest Inc., 2022)
Water	0.65	(Thermtest Inc., 2021)
Vesconite	0.25	(Vesconite, 2019)

Table 3-2 includes all details of the system. The dimensions and areas were extracted from the 3D model generated within the Solidworks draughting package.

Table 3-2: Stack assembly dimensions

Part	Section	Area (mm²)	Thickness (mm)
Hot plate	2	4656	2
Hot plate	3	1297	3
Vesconite ring	4	967	3
Hot plate	5	2391	3
Vesconite ring	6	3458	5.68
Water sample	7	1320	5.68
Cold plate	8	1297	3
Vesconite ring	9	967	3
Cold plate	10	2513	3
Cold plate	11	4599	2

From these dimensions, it was calculated that the system has a total thermal resistance of 3.4 K/W, which means a temperature differential of 3.3 K between the resistive heater and the cold plate. The numerical calculations were compared to an FEA analysis of the core assembly.

The model was exported from Solidworks to Abaqus. The properties in Table 3-1 were assigned to the relevant parts. Next, the assembly was constrained so that the contact solver could be used to determine the relevant interactions. A mean contact resistance of 1 was used throughout all interactions. In the initial step, a temperature of 20 ˚C was applied. Two boundary conditions were inserted, one on the interface of the cold plate to the Peltier element of 20 ˚C and one on the interface of 23.5 ˚C on the interface of the hot plate and the cartridge heaters. The temperature of 23.5 ˚C was selected based on the calculations in the previous section. A load of 1 W was applied to the interface of the heat cartridges and the hot plate. The simulation was then run.

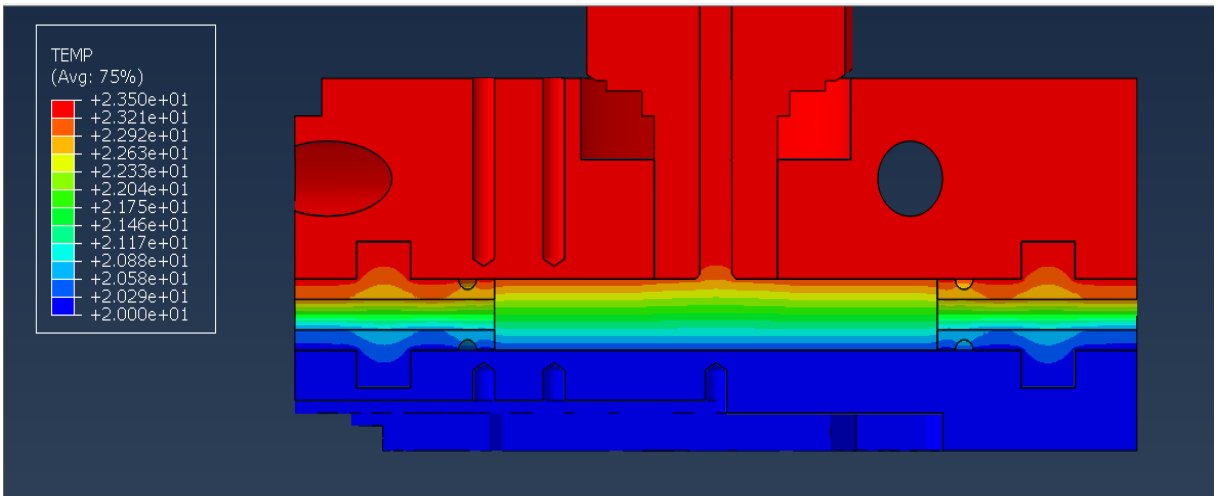

Figure 3.3: Nodal temperatures of stack assembly

Figure 3.3 shows the nodal temperatures through the core assembly. It should be noted that this analysis included the pressure transducer to prove that there would be little parasitic drain through the pressure transducer to the surrounding. It is observed that the hot plate achieves a uniform temperature, along with the cold plate achieving a uniform temperature. To verify the uniformity of the temperature distribution, nodal temperatures were observed via the query tool in Abaqus at the point at which the thermocouple interfaces with the hotplate and cold plate and the surface temperature of the hot plate and cold plate. These results are presented in **Table 3-3**.

Table 3-3: FEA query results

Part Instance	Node ID	Orig. Coordinates			Nodal temp
		x	y	z	
Hot plate	21	23.3	50.5	73.9	23.5
Water sample	64287	23.3	49.5	73.7	23.2
Cold plate	289117	23.1	43.8	73.8	20
Cold plate	3	23.3	42.8	73.9	20
Cold plate	99102	23.3	39.8	70.9	20

The heat flux can be observed in **Figure 3.4**: the bulk of the heat flux flows through the sample; however, it should be noted that this may vary according to the medium placed within the sample area. The difference in the temperature that

the thermocouples and the actual temperature will record will be 0.3035 ˚C which, given the accuracy of the K-type thermocouples, is virtually negligible. The same can be said for the cold plate.

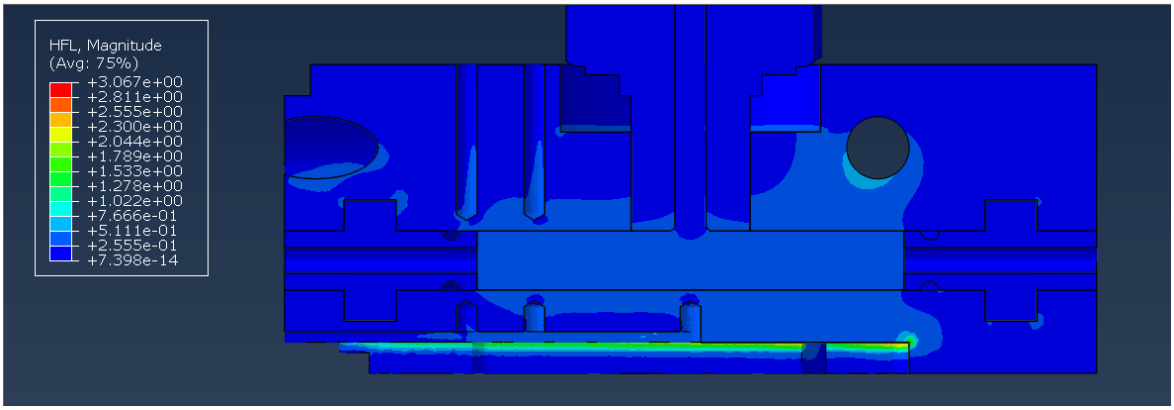

Figure 3.4: Heat flux analysis of stack assembly

It is clear that there is an agreement between the FEA analysis and the thermal circuit generated by a numerical method.

3.1.1 Hot plate

The hot plate consists of a copper block with seats drilled for the thermocouples, a tapped hole for the pressure transducer, holes drilled at 60-degree angles to accommodate three heating cartridges, a groove for the O-ring and a groove for the separation ring. Copper was selected as the material of choice due to its relatively high thermal conductivity. Due to the complexity of the shape, there is no shape factor for the hot plate; as such, the approach taken was that of an FEA analysis, which was validated via a simplified heat resistance circuit. The thermal resistance circuit is a truncated version of the circuit created in section

3.1. A graphical representation of what has been described is presented in **Figure 3.5**, and a 3D rendering in Figure 3.6.

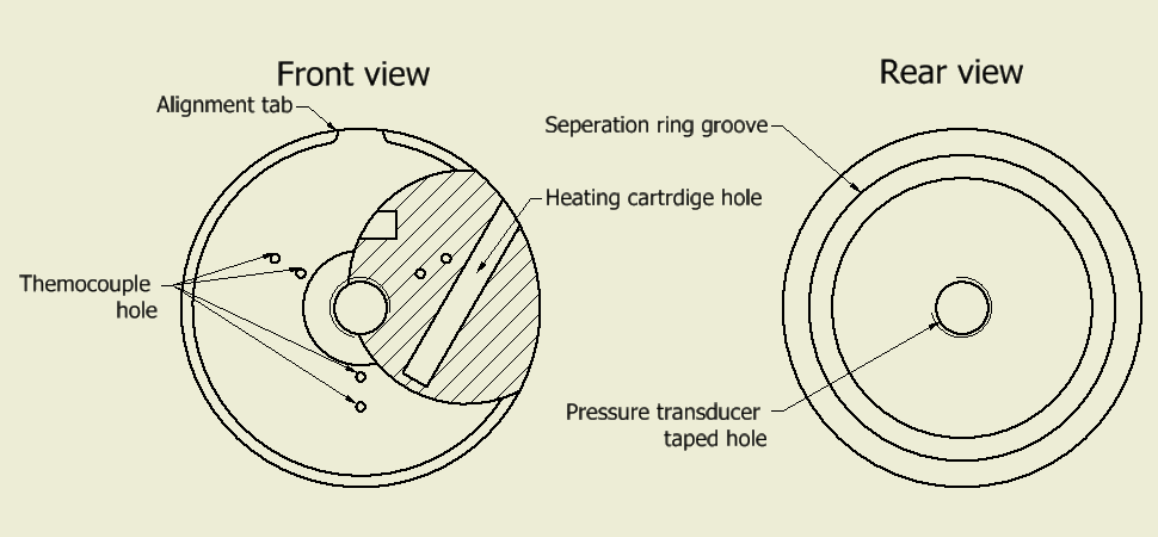

Figure 3.5: Orthographic projections of the hot plate

A preliminary analysis of the hot plate alone, of mass 0.566 kg, shows that raising the temperature of the hot plate (by a single degree kelvin) would require 214 W; however, given the fact that each heating cartridge can produce 40 W and a total of 120 W altogether, the total time to achieve this temperature change would be 1.78 seconds. Because of the limitations of the GW instek power supply, a constant 1 W will be supplied, which means heating the hot

plate from an ambient temperature of 20 ˚C to 23.5 ˚C would take 12 minutes and 29 seconds.

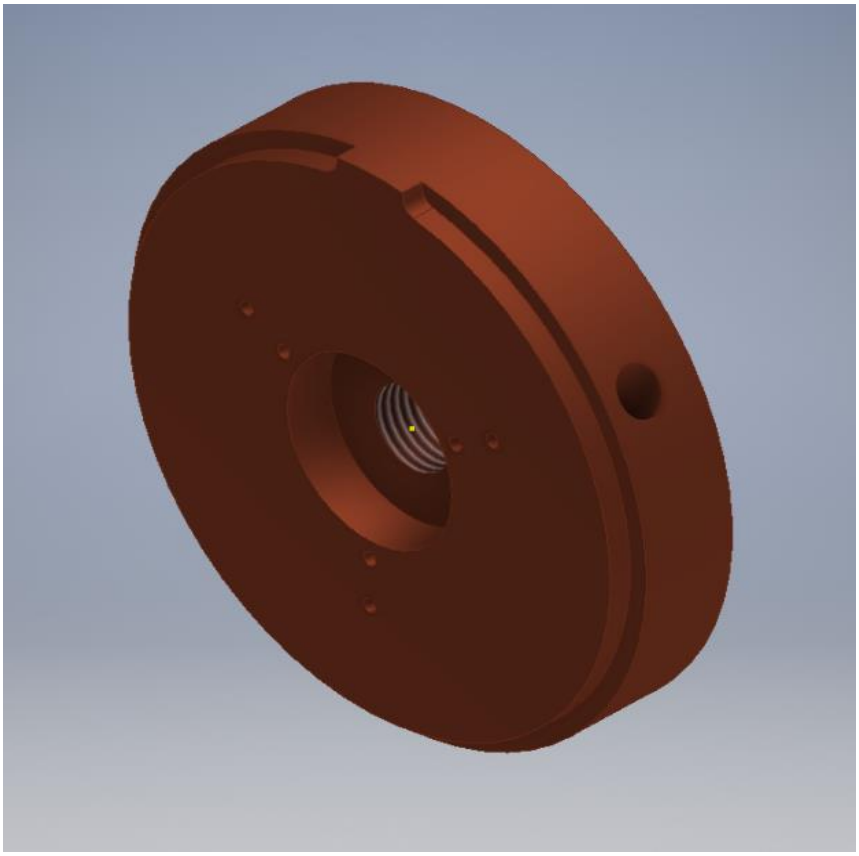

Figure 3.6: 3D rendering of the hot plate

The material selected for the hot plate was copper due to the high thermal conductivity of copper. The hot plate allows for the heat supplied to be evenly distributed throughout the hot plate; this was confirmed in the FEA analysis and through testing. The FEA analysis was conducted using Abaqus. The initial boundary conditions were set as follows: the surface of the interface between the heating cartridges and hot plate temperature was set at 20 ˚C; and the heat flux was set at 1 W at the surface of the holes drilled for the heating cartridges. The initial temperature was set at 20 ˚C, considered ambient temperature, and 120 W was the sum of the heat applied via the three 40-watt heating cartridges. Note should be taken that the FEA analysis neglects the PID control implemented to maintain the temperatures of the plates. As seen from the snapshot in **Figure 3.7**, temperatures rise substantially above the heating cartridges, and the heat is then dissipated radially throughout the hot plate. These localised hot spots dissipate, and the whole plate reaches a normalised temperature. Further assumptions made during the FEA analysis were that

there was no heat loss to ambient; this assumption was made due to the guard heater being set at the same temperature as the hot plate, which would eliminate radiative heat transfer between the two. The thermal conductivity was maintained constant as the hot plate's temperature would be close to ambient due to limitations imposed by the power supply.

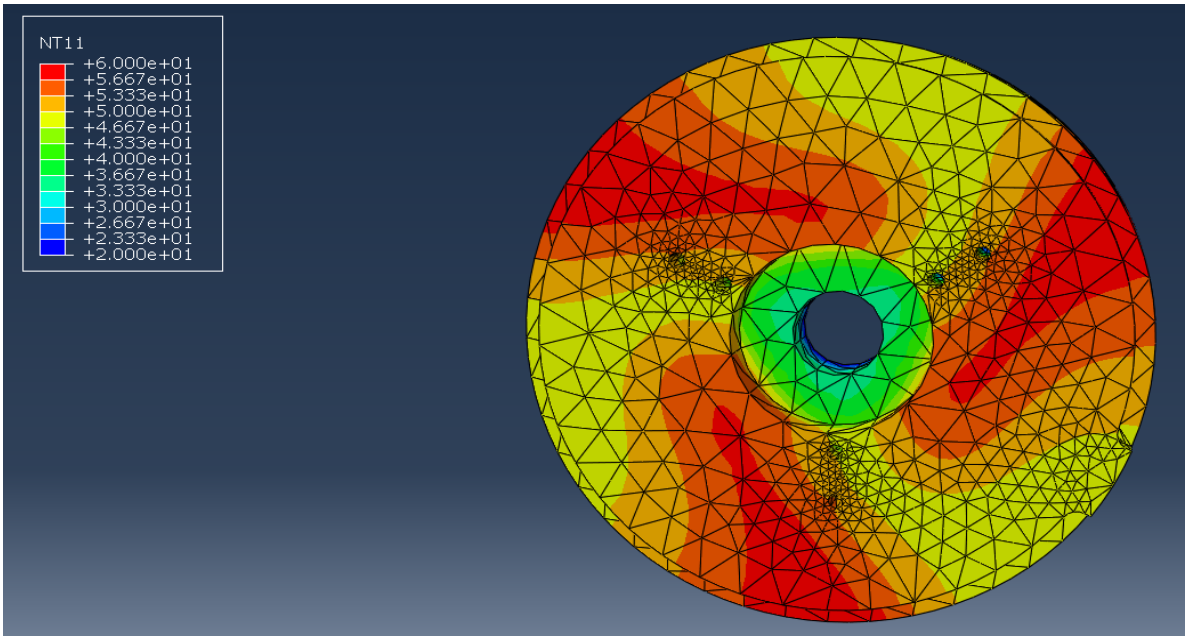

Figure 3.7: FEA analysis of hot plate

The device was then tested with similar conditions. These results were compared to a thermal circuit constructed per **Figure 3.2**.

Using the thermal resistance formula, which is just the reciprocal of the thermal conductivity formula, it was possible to ascertain the temperature drop across the copper hot plate to the surface, which was determined at 0.003 K.

3.1.2 Cold plate

The cold plate was similar in design to that of the hot plate, the only significant differences were that there was no pressure measurement from the plate, and the heating cartridges were substituted for that of a Peltier module which acts as the heat pump. Furthermore, the copper plate was made smaller to reduce the effects of the heat capacity of the cold plate. Otherwise, the cold plate maintains a grove for the separation ring, a grove for the O-ring and a network of holes drilled for the thermocouples.

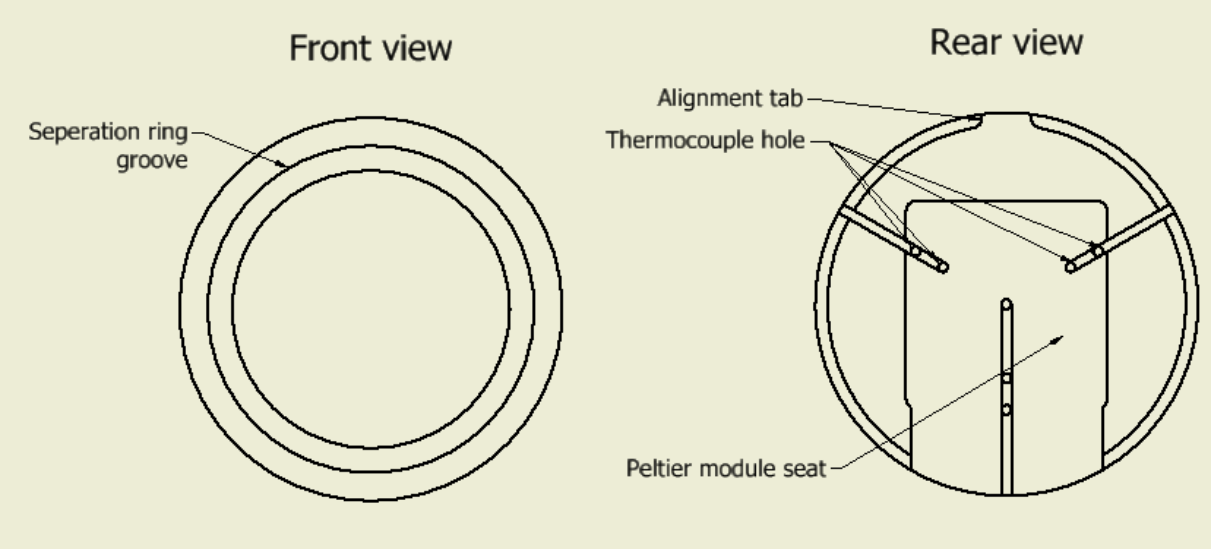

Figure 3.8: Orthographic projections of the cold plate

The cold plate has a mass of 0.226 kg; performing the same preliminary analysis as the hot plate, to drop the temperature of the cold plate by 1 degree requires the removal of 92.8 W from the cold plate, as per the calculations in Appendix A, given that the system would be in a temperature-controlled environment that would be maintained at approximately 20 ˚C. The FEA analysis of the cold plate was forgone as the analysis conducted on the core assembly was deemed sufficient. A closed-loop all-in-one (AIO) cooler was selected to remove the heat from the hot side of the Peltier element. This was done for two reasons, the first being that the water-cooling loop would facilitate more stable temperatures and the low maintenance requirement of the device. The liquid cooling loop inherently contains a radiator, pump and reservoir. The water-cooling loop would run continuously; however, the cold plate would be controlled via a PI control scheme integrated into the Arduino code. The temperature would be taken from the cold plate via a Max 6675 break-outboard and used as input for the PI controller. The PI controller would then generate a value that controlled the IRL520n MOSFET. The result of this loop would be an appropriate response to fluctuations in the temperature of the cold plate. The primary objective of the cold plate was to maintain a set temperature. A schematic of the cooling circuit is presented Figure 3.9.

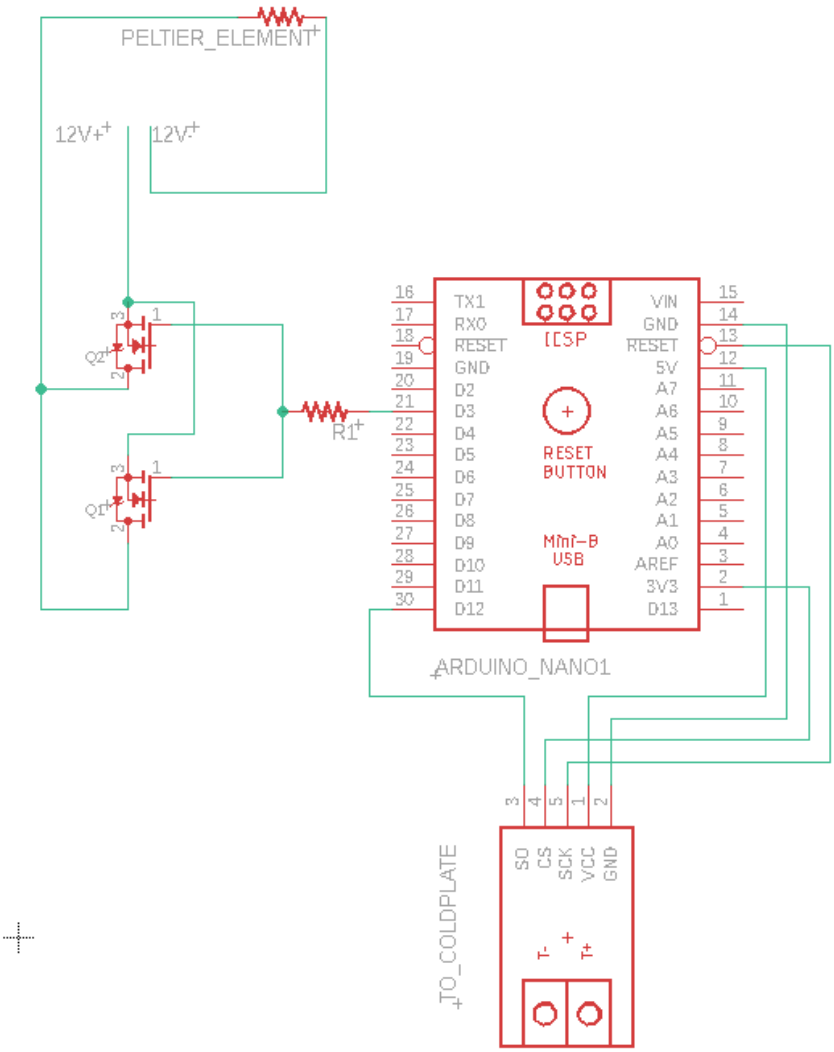

Figure 3.9: Schematic of the cold plate control scheme

3.1.3 Guard heater

The guard heater is particularly important as it fundamentally differentiates the guarded hot plate from the Lee disk method. Where the Lee disk method leaves the sample open to the atmosphere, the guard prevents heat loss from the hot plate to the surrounding. The guard is set to match the temperature of the hot plate to prevent radiative heat loss and heat loss through conduction or convection. The design was similar to that of the parallel plates; consequently, the total heat capacity was considered. For the guard, it was decided to use steel instead of aluminium because a larger mass would be required. The larger mass made the guard less prone to minor fluctuations allowing for a more consistent temperature. Helical grooves were machined into the guard heater to facilitate a nichrome wire that would be wound around it. On the base of the

guard heater, a mounting bracket was mounted to allow the attachment of two linear bearings. The linear bearings would then glide along two adjustable rails attached to the frame. The linear bearings would ensure the alignment of the guard heater around the stack assembly.

The nichrome wire would act as a resistive heater. The guard heater was controlled by a bang-bang controller, which was integrated into the Arduino microcontroller's code. The Arduino would take temperature measurements via two max 6675s. The temperature would then be used in a conditional 'if statement' within the Arduino code, which would control a relay that would allow the current to flow through the resistive element. A schematic diagram can be seen in **Figure 3.10** of the guard heater circuit.

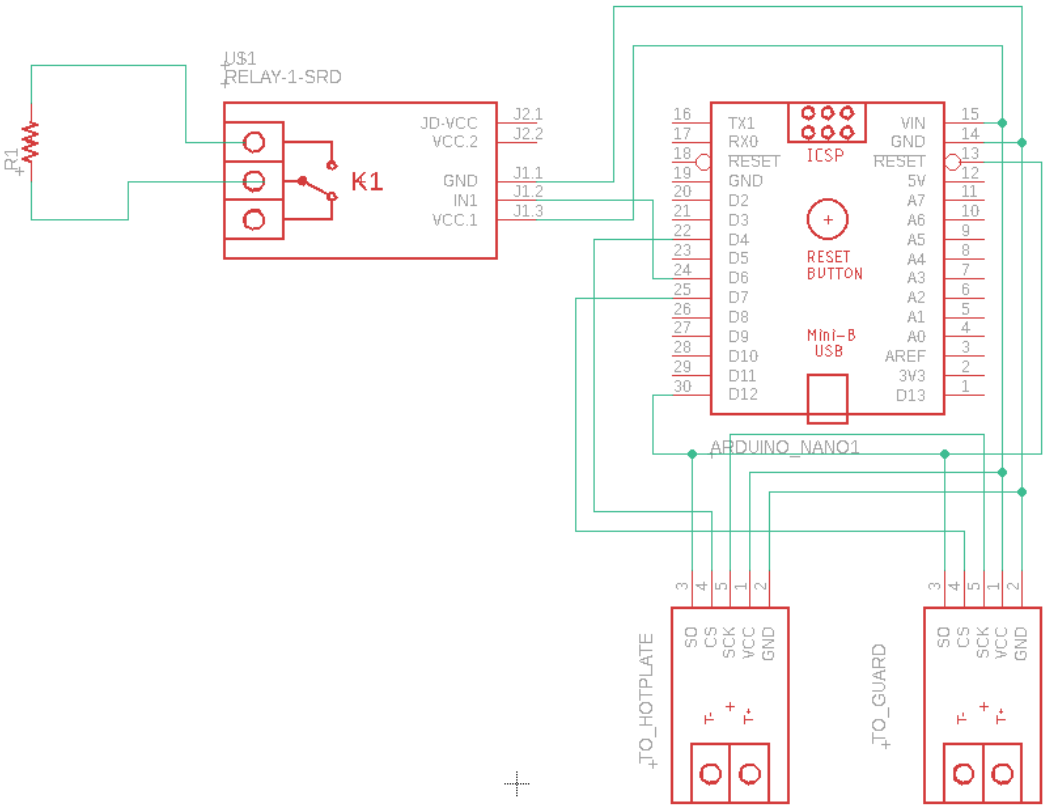

Figure 3.10: Schematic of guard heater

3.1.4 Electronics

Aside from the laboratory power supply and data logger, ancillary electronics are embedded in the system to replicate steady-state conditions. Most of these

electronics have been briefly discussed in previous sections. Here further details will be provided. The complete schematic can be found In Appendix B, and the code can be found in Appendix E. The board design was based upon a design found on electronoobs.com; however, the PID controller was deemed insufficient. Instead, a custom auto-tuning PI controller was implemented as the derivative function was subtractive and would result in a less responsive controller. The max 6675 temperature sensor was selected as the input for the PI controller and had a resolution of 0.25 ˚C. The Arduino nano was selected as the microcontroller due to its relative simplicity and small form factor. The IRL520n was selected due to its current limit and the fact that it is a logic-level transistor, which allowed the Arduino nano to control it via a PWM signal. As mentioned previously, a pair of MOSFETs and a relay controlled the cold plate and guard heater, respectively. The spec sheets for all components mentioned here are found in Appendix C. A circuit board was designed in KiCAD. Additionally, screw terminals were placed on the board to interface the circuit board and the external electronics to maintain the modular design.

3.1.5 Breakout boards connected to controller board

The following section will discuss the breakout boards connected to the controller board. Breakout boards were selected as they would reduce the complexity of the PCB design and directly interface with the Arduino microcontroller with no further modifications required.

- *Max 6675 K-type thermocouple sensor*

Three Max 6675 were used on the main controller board, one for each of the temperatures found throughout the GHP. The Max 6675 has an on-board cold junction compensation and a resolution of 0.25 ˚C. The unit has a temperature range from 0 ˚C to 1024 ˚C (Maxim, 2002).The Max 6675 connected to the cold plate is the input to the PI controller that governs the cold plate temperatures. The Max 6675 connected to the hot plate and guard controls the on-off controller of the guard heater. The hot plate temperature is used as a set point and the guard heater temperature is established for comparison.

Figure 3.11: K-type thermocouple sensor (botshop.co.za, 2020)

- *Relay board*

  The relay board was a 5-V breakout board used to implement the on-off controller. The board was selected to isolate the 5-V circuit from the high current 12-V circuit and prevent damage to the Arduino nano board.

Figure 3.12: 5-Volt relay board

- *Peltier element*

  The Peltier element selected was a TEC12715. This element was selected due to its 154 W cooling capabilities.

- *AIO liquid cooling loop*

  The liquid cooling loop is a generic all-in-one package with a dual-fan radiator.

- *Current shunt*

  The current shunt was constructed of three 1 Ω resistors.

- *K-type thermocouples*

  The thermocouples used to measure the temperatures were K-type thermocouples. The K-type thermocouple is constructed from nickel-chromium and nickel-alumel. They have a temperature range of -270 ˚C to 1260 ˚C. While the standard error for these thermocouples are +/- 1.1 ˚C, this can be reduced through calibration (REOTEMP Instrument Corporation, 2011).

3.1.6 External instrumentation for experimentation

The GHP was used in conjunction with two external systems: the Agilent 34970A and the GW instek gps3303.

- *Agilent 34970A*

  The Agilent 34970A is a data logger with a 6.5-digit display (22-bit resolution). The unit is coupled with a 20-channel multiplexer that uses reed switches. The multiplexer is capable of measuring 60 channels per second. The unit has a built-in cold junction compensation and an accuracy of 1.5 ˚C for K-type thermocouples. The accuracy at 1 V is 0.004 V. It should be noted that the thermocouple accuracy is in line with the standard measurement error of K-type thermocouples (Agilent, 2012). The data logger was used for all measurements from the GHP. All thermocouples were connected to channels 1 through 11 of the data logger. Channels 12 and 16 were used for voltage measurements across the current shunt and heating cartridges.

Figure 3.13: Agilent 34970A (Technologies, n.d.)

- *GW instek gps3303*

The GW instek gps3303 is a laboratory power supply. The power supply, with two channels, is capable of 0 to 30 V and 0-3 A. The unit has a ripple of 1 mVrms and a 3 mArms in a constant current configuration (GW instek, 2018). The power supply was selected due to the low noise on its output. Due to the device's limitations, it applied a limit on the power that could be applied to the heating cartridges.

Figure 3.14: GW instek gps3033 (Good Will Instrument Co., n.d.)

3.2 Fabrication

For fabrication, the cold and hot plates were sent for CNC machining through Gullwing engineering and all sheet metal parts were sent to SPP laser for CNC laser cutting and bending. The sheet metal parts include the frame, aluminium

back plate, radiator mount and mounting plates. The separation ring was machined from vesconite, and the guard heater was sent for turning once the parts were laser-cut and welded together. The parts sent for machining and laser cutting was manufactured as per the drawings in Appendix B. The apparatus was designed so that the entire assembly could be bolted together. This was done for modularity so that parts could be removed or adjusted during the prototyping phase. The electronics were all consolidated onto a single board and machined via a CNC router. The schematic generated in KiCad was used to create a DXF file that could be imported into a post-processing software. The post-processing software generated a g-code to plot the tool path of the CNC router. The holes were first peck drilled with a 0.8 mm bit, and then the traces were routed with a 1 mm milling bit.

Figure 3.15: Milling of the controller board PCB

3.3 Challenges

Throughout the project, various technical challenges were faced. The first challenge encountered was that of galvanic corrosion. The corrosion occurred at the interface between the cold plate and the copper cold plate. To circumvent the corrosive effects, a nylon ring was placed between the interface of the two materials to mitigate direct contact between the two. Initially, the hot plate's current was similarly controlled via the Arduino microcontroller to that of the cold plate; however, this was later substituted for GW instek gps3033 due to the fluctuation in output from the IRL520n MOSFET. This resulted in a constant misreading of the current, which is vital for calculating the power input into the heaters.

The 1 mm milling bit used to machine the PCB could not route the pins for the Arduino nano. Thus all the traces to the pins of the Arduino were connected. An engraving bit was used to separate the pins to remedy this fault. The vias for the board were soldered into place to ensure the connection between the top and bottom traces.

Natural convection is where the denser parts of the fluid are overcome by gravity, and a convective flow develops within the fluid, and natural circulation takes place, affecting the fluid's thermal conductivity readings. Natural convection became apparent only through testing, whereby the thermal limits of the cold plate were reached much faster than anticipated. To circumvent the formation of natural convection, the entire test apparatus was positioned so that the cold plate was at the bottom and the hot plate was at the top.

Figure 3.16: Orientation of final GHP setup

The guard heater acted as an inductor due to the nichrome wire used as a heat source coiled around the guard. This, in turn, acted as an inductor. The ground wire was coiled reverse to the initial coil to circumvent this inductance.

4 CHAPTER FOUR: Testing and commissioning

For the commissioning and testing of the experimental setup, each component was tested individually and then assembled. There are two methods for the calibration of thermometers: fixed point and comparison calibration. Fixed point calibration entails a point bath or furnace. Fixed point calibration is primarily used for temperature measurements through secondary measurement devices such as thermometers. The advantage of fixed-point calibration is that it produces low uncertainties but is not sufficient for an ISO9000 certification. Comparison calibration entails the comparison of one measurement method to a second means of measurement. Comparison calibration is the most frequently employed method for ISO9000 certification (de Silva, 2002).

Before testing could be conducted, it was necessary to calibrate the thermocouples. To do this, crushed ice was placed in a container and filled with water; the container was left to stand in ambient conditions for 10 minutes to allow this ice to melt, which is precisely 0 ˚C. The water was then drained, leaving the ice wet. The thermocouples were then placed into the container, and readings were taken every 10 seconds for five minutes (see **Figure 4.1**). Next, the thermocouples were placed into a boiling kettle to verify the accuracy of the thermocouples. It was determined that the error recorded per thermocouple was within the specified tolerance. The calculated error was within 1.5%. The aforementioned methodology is in line with those outlined for ISO9000 certification. All results were compared to those of an RTD and mercury thermometer.

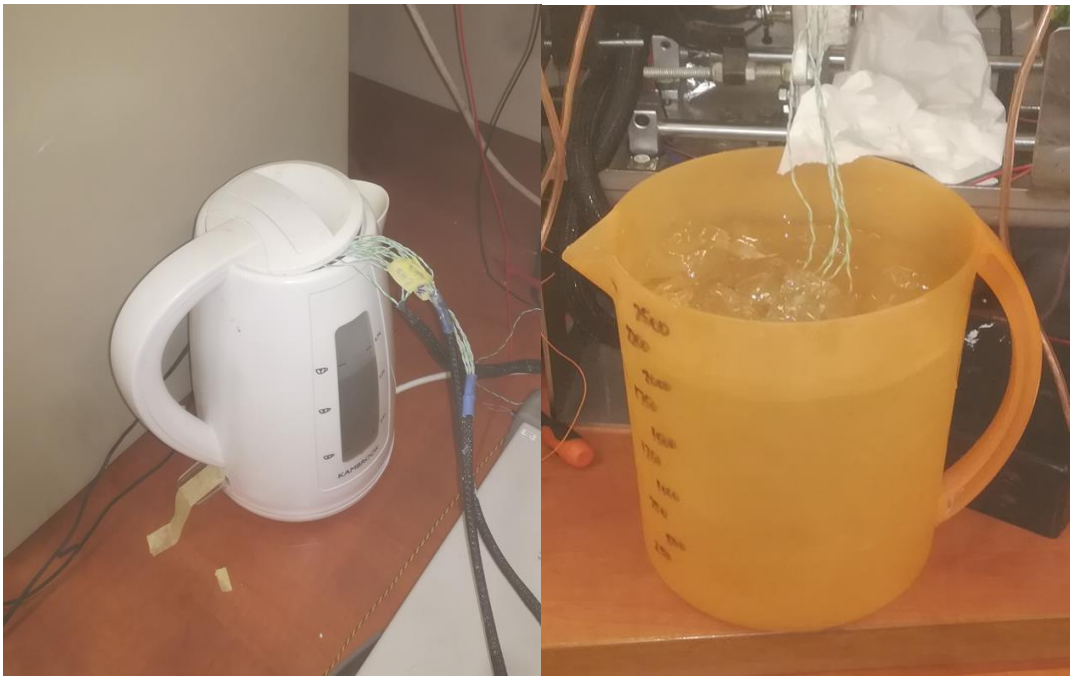

Figure 4.1: Left: cold temperature calibration; Right: hot temperature calibration

The results of the cold bath test can be seen in Table C-7. It was found that there was an average standard deviation of 0.022126 ˚C and an average temperature reading of -0.10313 ˚C. The median was -0.10557 ˚C. The mercury thermometer had a reading of 0 ˚C and the RTD registered a value of -0.1 ˚C The results of the hot bath test are presented in Table C-8 in the appendix. A standard deviation of 0.039719 ˚C and a median of 98.91497 ˚C were observed. The average boiling water temperature was found to be 97.91771 ˚C. The mercury thermometer had a reading of approximately 99 ˚C and the RTD registered a value of 98.9. Based on this, the calibration of the thermocouples were deemed acceptable. It was noted that the Max 6675 had an error in measurement of approximately 1 ˚C and as such, the code was compensated to account for this error.

The current shunt was configured into a 4-wire output mode. The wires of the current shunt were connected to the data logger and the resistance was measured. The resistance value was found to be 0.00758 Ω This value remained constant for the duration of the test. The resistance of the of the current shunt will be used to calculate the power input on using Equation (4.1) where the current is equal to the voltage difference across the current shunt

divided by the resistance value. The current is then multiplied by the voltage drop across the heating cartridges.

$$P = I.V \tag{4.1}$$

The first component tested was that of the hot plate. The hot plate was encased in Styrofoam, and controlled power was supplied. The hot plate was left for one hour under these conditions before temperature readings were taken via the Agilent data logger. These results were compared to the results from the FEA analysis, as discussed in the preceding section 3.1.1. The cold plate was placed into similar conditions; however, this test was conducted to begin tuning the PI controller. Once an appropriate proportional response was tuned, the hot plate was then placed in direct contact with the cold plate to begin further tuning. The PI controller was tuned by applying sufficient power to generate a hot plate temperature of at least 10 degrees higher than that of the cold plate. The cold plate was given a set point of 20 ˚C. The relevant proportional and integral values were adjusted incrementally; between adjustments, the system would be given 40 minutes to equalise before values were adjusted until a desirable control was found. The next component tested was the guard heater. The guard heater was left open to ambient conditions; the set point was then set and allowed to heat up until the desired temperature. The test found that the set point of the guard plate needed to be offset to compensate for the thermal lag that would cause the guard heater to overheat.

Once each component had been tested in isolation, the system was brought together. The PI controller was fine-tuned with a water sample in the test cavity. This was done to smooth out temperature fluctuations that would throw the system out of a steady state. With the water sample in the system, a continuous 1 watt of power was provided to the heater. The system was left to run for one hour to ensure a steady state condition. The temperatures were then taken via the data logger every minute for 15 minutes. Once the test was complete, the system was turned off and allowed to return to ambient conditions. The water was then replaced with a fresh sample, and the test was then run again with this procedure a total of five times. These results were then analysed and compared to the ideal model used in Chapter 3.1. To calculate the losses, the power

supplied to the heating cartridges was recorded and the temperatures were recorded. The temperature differential was used to calculate the actual heat flux through the sample based on Equation **(3.3)**. The measured power could then be calculated based on Equation (4.1). The actual was subtracted from the measured to obtain a correction factor. A 17.5% loss in the system was determined and a correction factor would need to be applied to compensate for these losses. The calculations can be found in Appendix A: Calibration Calculations.

Figure 4.2 presents a graph depicting the hot temperatures recorded for each test run. From this, it was determined that temperatures tended to fluctuate within an allowable limit of ~0.25 ˚C for the system. The rest of the fluctuations could be due to noise, and a similar noise was present when doing the calibration tests for each thermocouple.

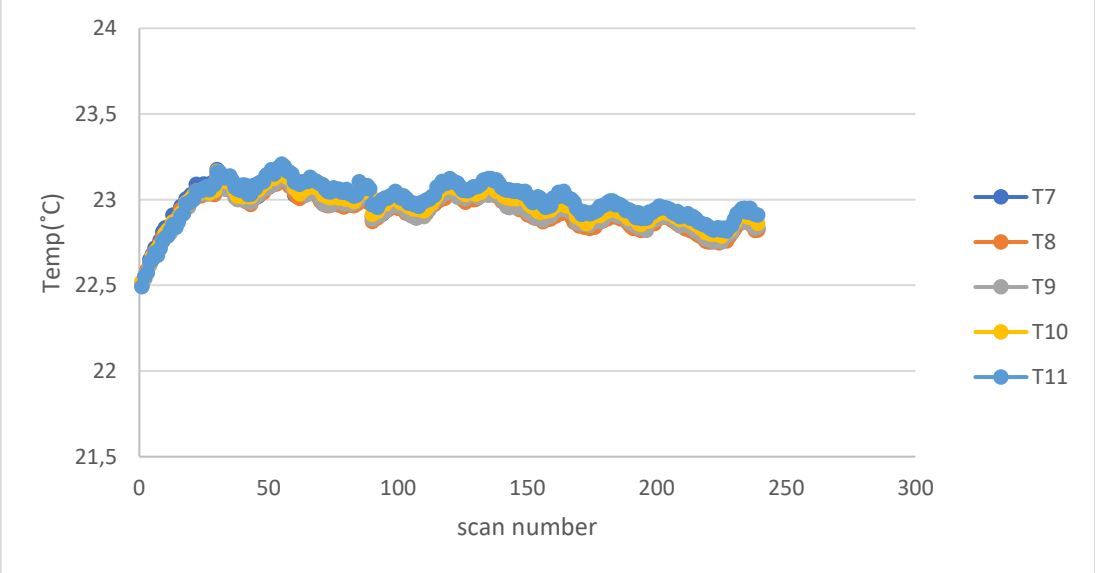

Figure 4.2: A graph of the hot plate temperatures recorded

From the cold temperatures, we can see far more significant fluctuations; this is due to the resolution of the Max 6675 that provides the temperature data to the PI controller. It should be noted that this does indeed influence the calculated thermal conductivity.

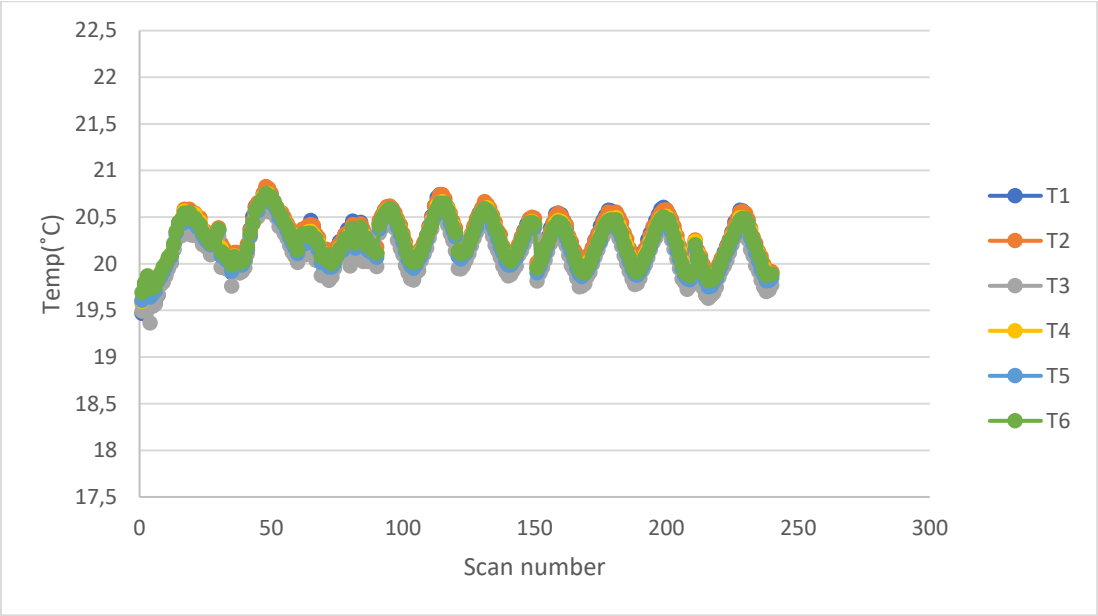

Figure 4.3: A graph of cold plate temperatures

An additional test was conducted on a water sample. The test yielded a mean thermal conductivity of 0.612 W/mK at a mean temperature differential of 2.722 ˚C. The test was based upon the averages of the power and temperature differentials to eliminate the variance between the samples of results. The averages can be seen in **Table 4-1**. The test was started prematurely to identify if there were any external influences on the system; it was found that there is a spike in the calculated thermal conductivity, which appears to correlate with a spike in the ambient air temperatures. This could result from the back plate being open to the environment, thus making the system susceptible to external influence. In addition, there is a rise in the calculated thermal conductivity when the cold plate heats up prior to the PI controller compensating for the temperature rise. Despite this, the mean thermal conductivity is within range of the reported results. There was a 2.3% difference between the reported thermal conductivity and the measured thermal conductivity. Thus the accuracy of the GHP is far greater than that reported by Yüksel.

Table 4-1: Parameters used for water thermal conductivity

Parameter	Value
$\Delta T_{=}$	2.722 ˚C
P=	0.881 W
R_{water}=	7.19 W/mK
ΔL=	5.68 mm
A_f=	0.001 m^2

Furthermore, the results from the water calibration test were compared to the results of the FEA analysis. There was a difference of 0.372 ˚C between the calculated temperature difference. This was a variance 11.9% and can be compensated for by the power loss to the GHP's surroundings.

5 CHAPTER FIVE: Discussion of results

For testing, the GHP was compared to the reported results of ethylene glycol and then a nanofluid, i.e., cobalt oxide (Co_3O_4) nanoparticle suspended in ethylene glycol. The experimental procedure employed for each experiment will be outlined and discussed.

5.1 Experimental procedure

Prior to testing and filling the fluid cavity, the guard heater was rolled back, which was then removed via the four bolts compressing the stack/core assembly. The vesconite ring could then be removed and thoroughly cleaned in deionised water, and the same would be done for the hot and cold plates. The part would then be allowed to dry before reassembly of the stack assembly by reversing the previous steps. Once assembled, the M3 bolt at the top would be removed, and the sample material would be injected into the testing chamber. The thread tape on the M3 bolt would be replaced; this occurs between each test to prevent cross contamination of samples. The system is left to attain thermal equilibrium before the power supply is turned on, along with the Meanwell 12 V power supply. The system was left for approximately one hour to attain steady state conditions before the Agilent 34970A is manually turned on, and readings would be taken every 30 seconds for 15 minutes. When testing was completed, all power supplies would be turned off, and the system would be allowed to cool. At this point, the sample could be removed, or subsequent tests could be conducted following the previous steps. To remove the sample from the testing area, the top M3 bolt would be left in whilst the bottom M3 screw would be removed; the vacuum within the testing area would hold the fluid in place whilst a container is placed underneath the opening in the vesconite ring. The top bolt was then removed, and the fluid flows, as there would no longer be a vacuum. For all tests, constant power of 1 watt was applied due to the limitations of the equipment.

5.2 Results

The procedure above was followed for the ethylene glycol samples; however, additional steps were taken for the nanofluids to stabilise the suspended nanoparticles. For testing purposes, two samples of cobalt oxide nanofluids were procured from the chemical department of CPUT. The nanoparticles were manufactured through a CRM method to produce a nanopowder. The nanopowder was then placed into the ethylene glycol and sonicated for approximately one hour. Two samples were produced. The first marked A3 contained nanoparticles with a volume fraction of 0.5%. The second marked B3 contained nanoparticles with a volume fraction of 1%. It should be noted that these are comparatively high-volume fractions.

5.2.1 Glycol

The glycol sample was taken from the same batch as the one used to produce the nanofluid. **Figure 5.1** shows the temperature differentials and power plotted. It can be seen that the system has attained steady state conditions as of scan 10. Thus the averages of the recorded results will be calculated from that point forward. The averages can be seen in Table 5-1. Two separate tests, conducted with different samples, established a baseline with which the nanofluid could be compared to see if there would be an increase in thermal conductivity. In the first test, presented in Figure 5.1, it can be observed that the mean temperature differential between the two plates is 4.46 ˚C. This equates to a mean thermal conductivity of 0.247 W/mK.

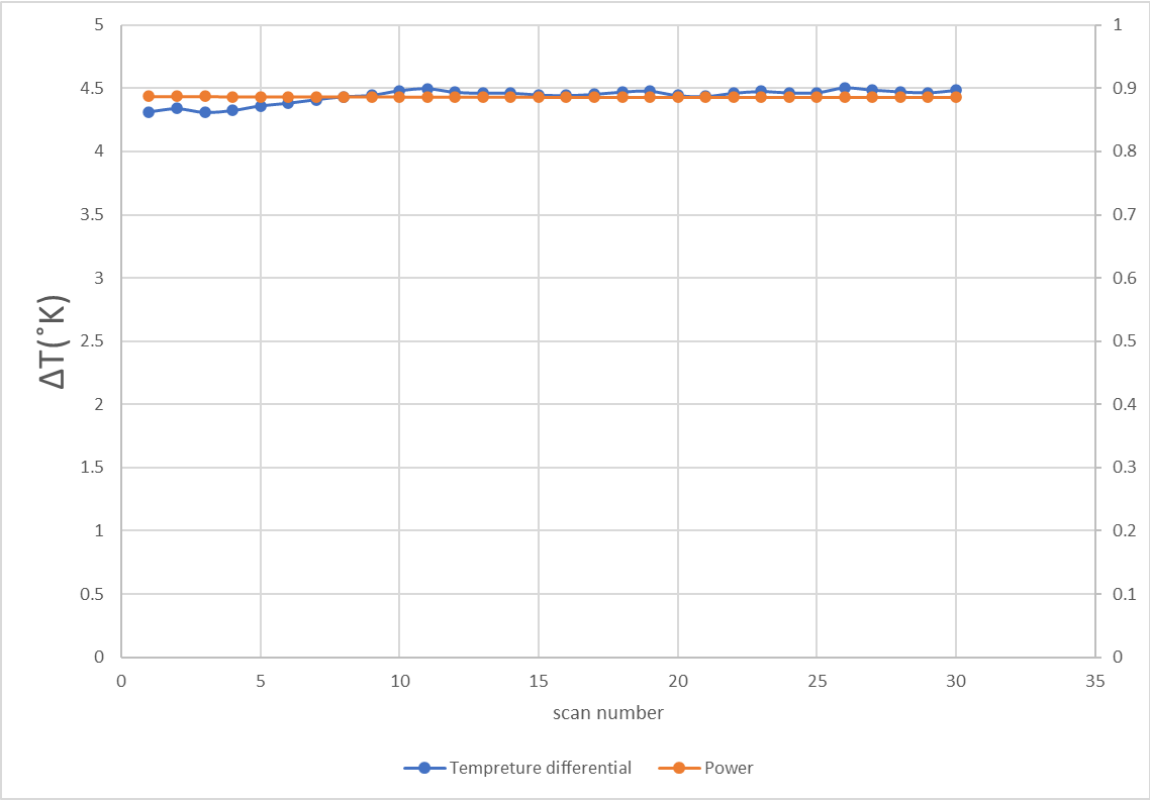

Figure 5.1: Power and temperature differential of glycol test 1

Table 5-1: Average values used glycol test 1

Parameter	Value
ΔT=	4.468 ˚C
V=	1.077 V
I=	0.997 A

In the second graph, similar results to that of the first are evident; however, two minor disturbances can be seen in the graph due to the response of the PI controller. This sample reached a mean temperature differential of 4.65 ˚C, and a mean thermal conductivity of 0.208 W/mK was calculated as per the values of Table 5-2.

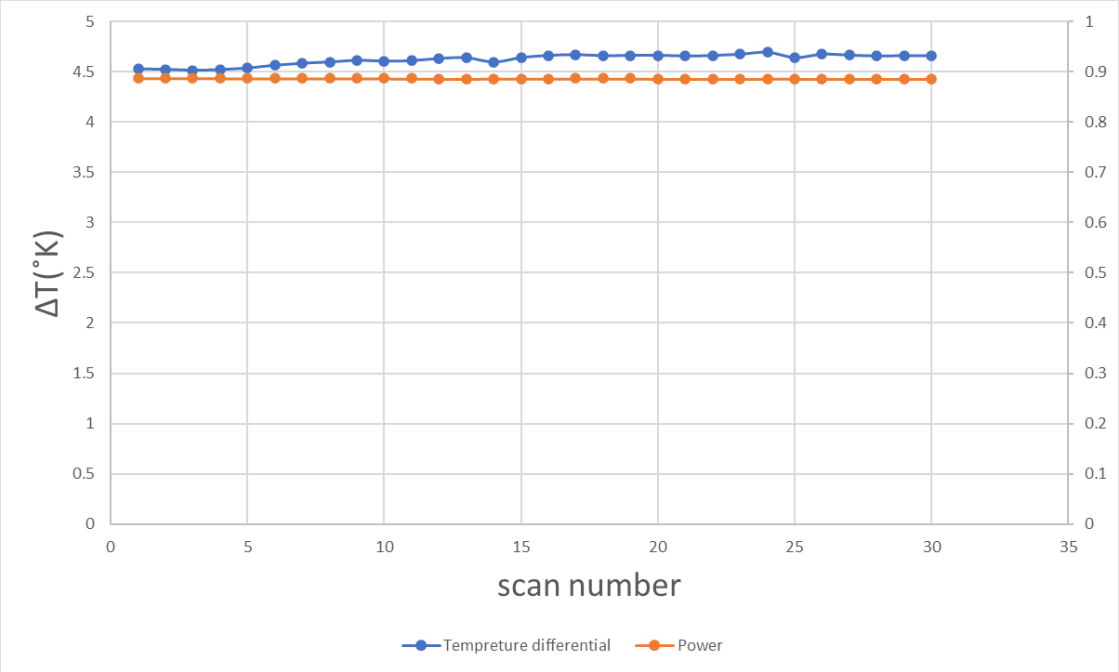

Figure 5.2: Recorded results of glycol test 2

Table 5-2: Average values used glycol test 2

Parameter	Value
ΔT=	4.650 ˚C
V=	1.077 V
I=	0.997 A

Compared to the reported results of 0.254 W/mK, there is a 10.5% deviation from the results recorded during testing. These results will be used as a baseline moving forward for the comparison of the cobalt oxide nanoparticles.

5.2.2 Cobalt oxide nanofluid

The first sample tested was the sample with the lower volume concentration. It should be noted that only a single test was run as subsequent tests yielded near identical results to that of ethylene glycol. This is most likely due to the lack of surfactants present in the nanofluid to act as a suspending agent. Furthermore, there appears to be very little particle size control in the sample, and gravitational effects overcame the particles. The gravitational effects caused agglomeration and forced the particles to settle on the surface of the cold plate, leaving nothing but ethylene glycol as the heat transfer medium. Figure 5.3 data

show that the temperature differential begins to rise towards the end of the test, and the thermal conductivity drops. As previously stated, this is most likely due to the gravitational effects. For this test, there was a mean temperature differential of 4.45 ˚C, and the mean thermal conductivity was calculated at 0.255 W/mK.

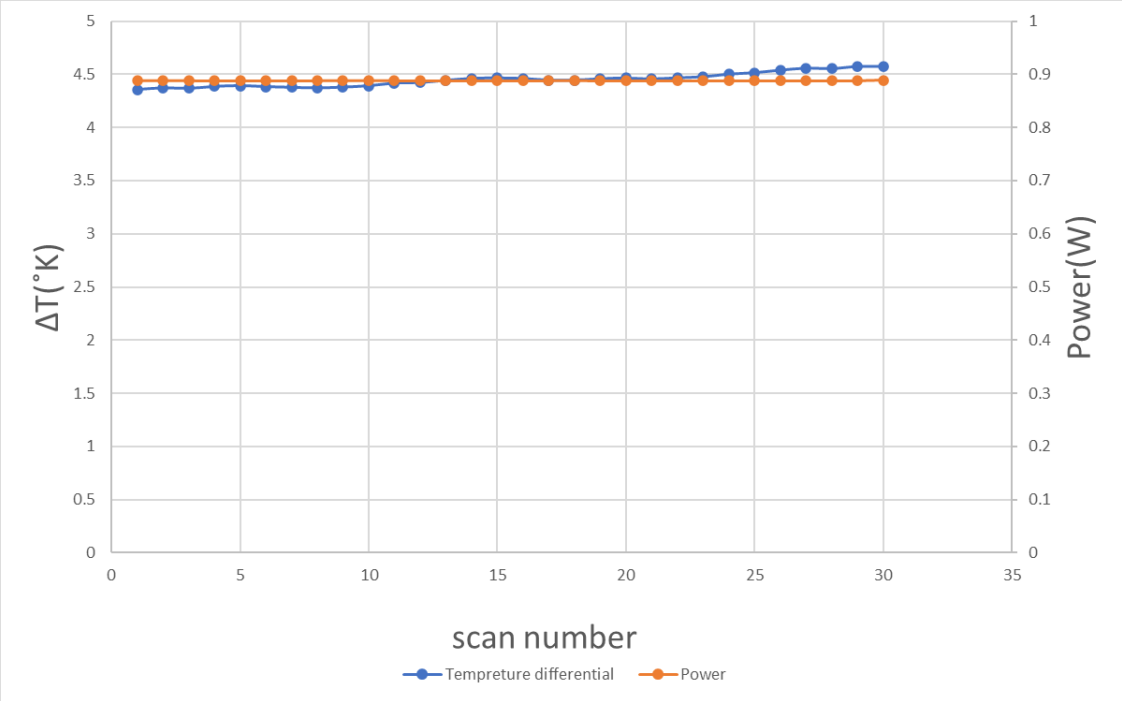

Figure 5.3: Recorded results of sample A3

Table 5-3: Average values used for sample A3

Parameter	Value
ΔT=	4.44 ˚C
V=	1.08 V
I=	0.996 A

The following sample tested was the sample with a higher volume concentration factor. The sample appeared more stable than its predecessor, and the mean temperature differential was calculated at 3.72 K while the mean thermal conductivity was calculated at 0.454 W/mK. Toward the end of the test, the thermal conductivity began to drop due to agglomeration.

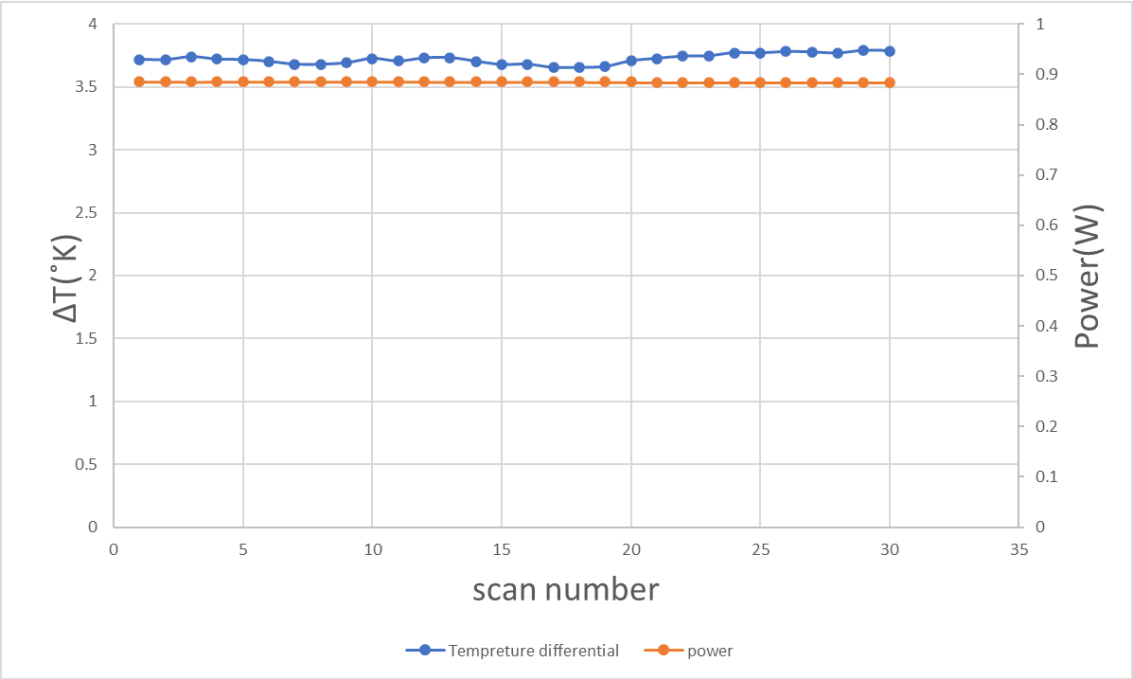

Figure 5.4: Recorded results of sample B3 test 1

Table 5-4: Average values used sample B3 test 1

Parameter	Value
ΔT=	3.722 ˚C
V=	1.077 V
I=	0.996 A

The second test of the same sample yielded similar results, albeit marginally higher. The mean temperature differential was found to be 3.68 ˚C, and the mean thermal conductivity was calculated as 0.467 W/mK. It should be noted that a slight fluctuation in temperature is noticed after 15 minutes. The calculated thermal conductivity began to drop again due to the settling of the nanoparticles.

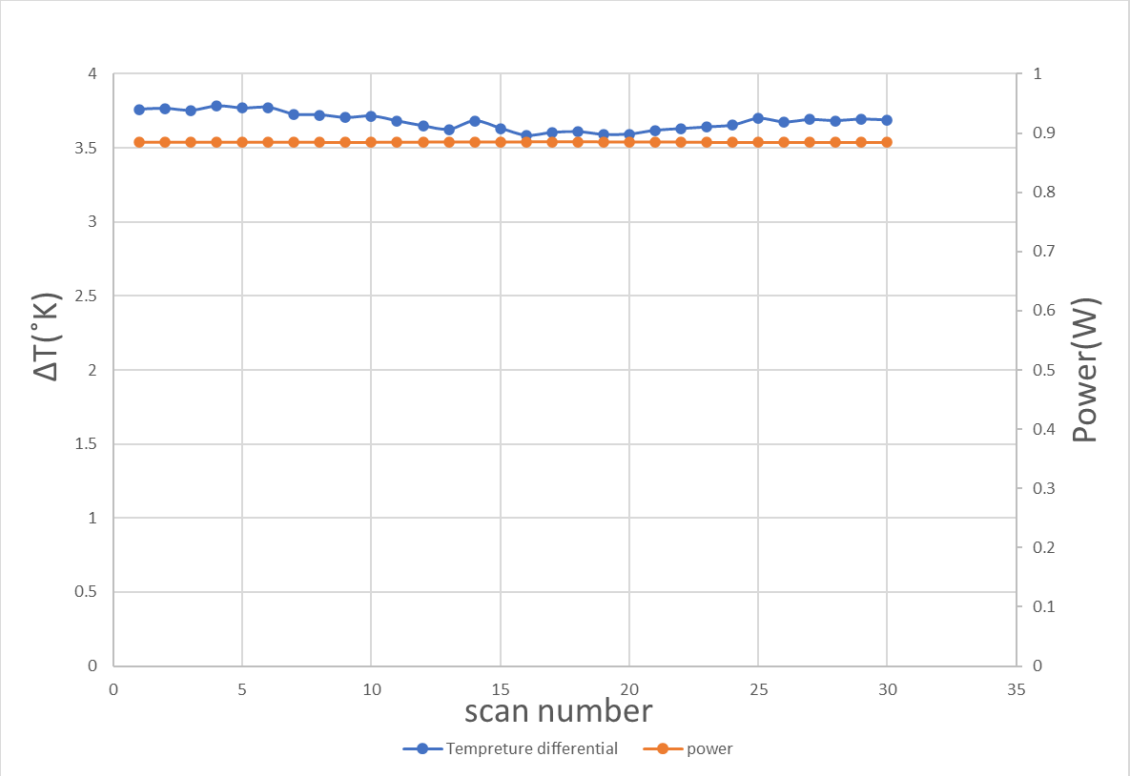

Figure 5.5: Recorded results of sample B3 test 2

Table 5-5: Average values used sample B3 test 2

Parameter	Value
ΔT=	3.679 ˚C
V=	1.076 V
I=	0.995 A

5.3 Discussion

As seen in the results, the addition of nanoparticles yields a higher thermal conductivity. However, it should be noted that nanoparticles produced through CRMs typically tend to be less stable than those produced from optical methods such as laser ablation. The particles may tend to agglomerate, and the smaller particles remain suspended. This may have been the case for sample B3. The settling of the nanoparticles could be further agitated by the long testing times and the time taken for the system to obtain steady-state conditions.

Another observation made during testing was the rapid decay of the samples provided. **Figure 5.6** shows a comparison of the sample directly after sonication (on the right) and after approximately four hours (on the left). Sample B3 remains slightly opaque; it is evident that gravitational effects have taken effect.

As for sample A3, the nanofluid has become very clear. This settling could explain why sample A3 degraded in the test cavity. It should also be noted that during cleaning, a layer of cobalt oxide was present on the cold plate as well, as such precautions were taken to prevent skin contact. As stated in the literature review, the addition of surfactants may have a negative impact on the thermal performance of the nanofluid; as such, the results collected are not skewed by the additional chemicals.

Figure 5.6: Comparison of samples

5.3.1 Comparison to numerical models

Of the numerical models presented in the literature review, only three will be used for comparative purposes, the Maxwell model, the Jeffery model and the Garoosi model. The modified Maxwell model was excluded due to the incorporation of the convective heat transfer. As the average size of nanoparticles produced at an industrial scale is 48 nm, this value will be used in the computation of the thermal conductivities of nanofluids (nanografi, n.d.). The diameter of a water molecule was found to be 2.8 angstrom which equates to 2.8 nm (D'Arrigo, 1978). The thermal conductivity of the nanoparticles was found to be 16.8 W/mK (Mariano *et al.*, 2015). **Table 5-6** shows the comparison of the recorded results to that of the numerical models. The Maxwell and Garoosi models severely over predict the thermal conductivity, whilst the Jeffery model closely approximates the value of sample A3 but not B3. The Maxwell model performance is to be expected as it assumes that the suspension is stable and does not account for the interfacial layer nor the low volume fraction. The Maxwell model is also the oldest model in use. The Garoosi model, based upon multiple data sets, attempts to fit a trend line to the results. All results consulted

for the Garoosi model had volume fractions less than 1%. The Garoosi model does not account for surfactants or the interactions between the base fluid and nanoparticles. The Jeffery model closely approximated sample A3 but could not do the same for sample B3. This is most likely due to the assumption that all particles are spherical in the model. It also does not account for the interactions between the base fluid and nanoparticle.

Table 5-6: Comparison of test results to numerical models

	Measured value	Maxwell model	Jeffery model	Garoosi model
Sample A3	0.255 W/mK	0.747 W/mK	0.262 W/mK	0.769 W/mK
Sample B3 test 1	0.454 W/mK	0.743 W/mK	0.258 W/mK	0.758 W/mK
Sample B3 test 2	0.467 W/mK			

It should be reiterated that the nanofluids tested had far higher volume fractions than most reported literature. Despite this, they yielded higher thermal conductivities but displayed lower stability.

5.3.2 Comparison to published literature

The measured results are compared to existing results for cobalt oxide nanofluid thermal conductivity. In comparison to results collected by Mariano *et al.,* they had found a mean thermal conductivity of 0.284 W/mK across volume fractions of 0.09% to 0.56% (Mariano *et al.*, 2015). The thermal conductivity of sample A3 was similar to those recorded with a deviation based upon the volume fraction. Sample B3, however, exhibited far higher thermal conductivities than those reported by Mariano *et el.* In fact, Alsboul *et el.* found thermal conductivities far higher than those recorded by the GHP, ranging from 0.260 W/mK to 0.296 W/mK. It should be noted that a KD 2 sensor was used, which is a Gustafsson probe. The volume fractions used ranged from 0.025 to 0.4% (Alsboul *et al.*, 2022). No surfactants were mentioned in the study. Based upon these comparisons, it is evident that sample A3 yielded similar results to those reported by these two groups who used ethylene glycol and cobalt oxide. Both studies did not make use of surfactants, so as such, the comparison is more valid as it proves the results obtained by the GHP. The higher-than-average thermal conductivity measured in sample B3 could be attributed to

agglomeration. It should again be reiterated that the volume fractions of the samples measured were far higher than those used in the studies for comparison.

6 CHAPTER SIX: Conclusion and recommendations

In conclusion, a GHP apparatus was designed and tested for the explicit purpose of testing fluids. The design relied primarily on the initial work of S. Choi and included modifications similar to that of Rausch. Due to the modular design, the apparatus is flexible and can be used for solids and liquids. It was noted that the device was susceptible to fluctuation in ambient conditions.

The GHP consisted of a core assembly, frame assembly and supporting electronics. The core was fabricated of two copper plates, A vesconite separation ring and two stainless steel retention plates. The fluid was held in the testing cavity by O-rings and two stainless steel M3 bolts. The frame assembly was constructed of stainless steel and aluminium. The core assembly was connected to the frame assembly using four nylon nuts and the bolt holes on the stainless steel retention rings. The supporting electronics were made into an embedded system designed around the Arduino nano microcontroller. An on-off controller and a PI controller controlled the guard heater and cold plate. An Agilent 34970A was used for data collection, and a GW instek GPS-3303 was used as the primary power supply to the heating cartridges.

Measurements were taken from the thermocouples placed through-ou the hot and cold plates, the voltage drop across the heating cartridges and a current shunt placed across the wires connected to the heating cartridges to measure the power supplied.

The apparatus was calibrated using water and then used to test the thermal conductivity of a base fluid and then a nanofluid. From the tests, it appears that the device operates as intended. The device could accurately predict water and ethylene glycol thermal conductivity. Additionally, it was noted during the testing of the nanofluids that there was a distinct increase in the thermal conductivity of the base fluid through the addition of nanoparticles. Based upon the calibration, it was determined that there was a deviation of 2% from the reported literature; however, the ethylene glycol results were within 10% of the reported results.

In comparison to the performance of the testing devices used by Mariano *et al.* and Alsboul *et al.,* the GHP was capable of measuring within the range of the two despite the higher-than-typical volume fractions.

Furthermore, it was found that the addition of nanoparticles yielded a higher thermal conductivity. However, gravitational effects did take over and cause the nanofluids to become unstable. The instability resulted in errors in the readings and caused the nanoparticles to agglomerate.

6.1 Recommendations

First and foremost, the cooling system should be replaced with a water-cooling loop maintained at the desired temperatures. This would alleviate the temperature fluctuations in the results because the PI controller only has a resolution of 0.25 ˚C. Furthermore, the guard heater should instead be relegated to an auxiliary guard heater, and a primary guard heater should then be designed in direct contact with the hot plate. Additionally, an environmental chamber capable of withstanding a vacuum should be incorporated into the design to alleviate the effects of ambient temperature fluctuations in the system. These aforementioned changes would minimise many of the losses found in the system.

Next, the control scheme should be redesigned to minimise noise and create an all-in-one system that does not rely on external power supplies or systems to function as intended. Other systems should also be incorporated into future builds to minimise the effects of handling the fluid sample; this could be done by incorporating a sonication system that would ensure the nanofluid sample is free of agglomeration. Additionally, the hot and cold plates could be coated in a thin film of diamond to prevent adverse reactions or interactions between the copper plates and the metallic particles in nanofluids. Additionally, an alternative material should be considered for the sample ring should higher testing temperatures be required for testing.

The present work has the potential for further exploration as the pressure transducer could be incorporated into the design, allowing for further insight into the nature of nanofluids and their properties.

APPENDIX/APPENDICES

References

Agilent (2012) ‘Agilent 34970A Data Acquisition / Switch Unit Family’, *Documentation*, 90012(34970), pp. 1–28. Available at: www.agilent.com.

Alam, M. *et al.* (2012) ‘Lee’s and Charlton’s Method for Investigation of Thermal Conductivity of Insulating Materials’, *IOSR Journal of Mechanical and Civil Engineering*, 3(1), pp. 53–60. doi: 10.9790/1684-0315360.

Alsboul, M. *et al.* (2022) ‘Experimental and Theoretical Investigation of the Thermophysical Properties of Cobalt Oxide (Co3O4) in Distilled Water (DW), Ethylene Glycol (EG), and DW–EG Mixture Nanofluids’, *Nanomaterials*, 12(16). doi: 10.3390/nano12162779.

Amendola, V. and Meneghetti, M. (2009) ‘Laser ablation synthesis in solution and size manipulation of noble metal nanoparticles’, *Physical Chemistry Chemical Physics*, 11(20), pp. 3805–3821. doi: 10.1039/b900654k.

Asadi, A. *et al.* (2019) ‘Effect of sonication characteristics on stability, thermophysical properties, and heat transfer of nanofluids: A comprehensive review’, *Ultrasonics Sonochemistry*, 58(July). doi: 10.1016/j.ultsonch.2019.104701.

Badarlis, A. *et al.* (2020) ‘D2.2 - Thermal Property Determination of Gases Based on Temperature Oscillating Technique. An Investigation’, pp. 495–500. doi: 10.5162/sensor2013/d2.2.

Bao, Z. *et al.* (2021) ‘Ti3C2Tx MXene contained nanofluids with high thermal conductivity, super colloidal stability and low viscosity’, *Chemical Engineering Journal*, 406, p. 126390. doi: 10.1016/j.cej.2020.126390.

Bhattacharya, P. *et al.* (2006) ‘Characterization of the temperature oscillation technique to measure the thermal conductivity of fluids’, *International Journal of Heat and Mass Transfer*, 49(17–18), pp. 2950–2956. doi: 10.1016/j.ijheatmasstransfer.2006.02.023.

botshop.co.za (2020) *MAX6675 Type K Thermocouple Temperature Sensor*. Available at: https://botshop.co.za/products/max6675-type-k-thermocouple-temperature-se?currency=ZAR&utm_medium=cpc&utm_source=google&utm_campaign=Google Shopping&gclid=CjwKCAiA68ebBhB-EiwALVC-Ni4Ti4KFYZWeeUhOxNIS-imNuVW0VwyCqvrG34WdNZ35-fW-fIpCjhoCIMYQAvD_BwE (Accessed: 20 June 2019).

Buonomo, B. *et al.* (2014) ‘A comparison of nanofluid thermal conductivity measurements by flash and hot disk techniques’, *Journal of Physics: Conference Series*, 547(1). doi: 10.1088/1742-6596/547/1/012046.

Cengel, Y. A. and Cimbala, J. (2013) *Fluid Mechanics Fundamentals and Applications*. third edit. McGraw-Hill.

Challoner, A. R. and Powell, R. W. (1956) ‘Thermal conductivities of liquids: new determinations for seven liquids and appraisal of existing values.’, (1939), pp. 90–106. doi: 10.1098/rspa.1956.0205.

Chandra, P. and Sayantan, M. (2014) ‘A brief review on viscosity of nanofluids’, pp. 109–120. doi: 10.1007/s40089-014-0126-3.

Choi, S. U. . and Eastman, J. A. (1995) ‘Enhancing thermal conductivity of fluids with nanoparticles’, (March).

Critchley, L. (2019) *Nanoparticle Manufacture - What Methods Are There?*

Czarnetzki, W. and Roetzel, W. (1995) ‘Temperature oscillation techniques for simultaneous measurement of thermal diffusivity and conductivity’, *International Journal of Thermophysics*, 16(2), pp. 413–422. doi: 10.1007/BF01441907.

D’Arrigo, J. S. (1978) ‘Screening of membrane surface charges by divalent cations: An atomic representation’, *American Journal of Physiology - Cell Physiology*, 4(2), pp. 9–17. doi: 10.1152/ajpcell.1978.235.3.c109.

Das, S. K. *et al.* (2007) *Nanofluids science and technology.* John wiley and sons,Inc.

Devendiran, D. K. and Amirtham, V. A. (2016) ‘A review on preparation, characterization, properties and applications of nanofluids’, *Renewable and Sustainable Energy Reviews*, 60, pp. 21–40. doi: 10.1016/j.rser.2016.01.055.

Douglas, J. F. *et al.* (2005) *FLUID MECHANICS*. 5th edn. pearsons.

Garoosi, F. (2020) ‘Presenting two new empirical models for calculating the effective dynamic viscosity and thermal conductivity of nanofluids’, *Powder Technology*, 366, pp. 788–820. doi: 10.1016/j.powtec.2020.03.032.

Good Will Instrument Co., L. (no date) *GPS-x303 Series Multiple Output Linear D.C. Power Supply*. Available at: https://www.gwinstek.com/en-GB/products/detail/GPS-x303 (Accessed: 2 January 2022).

Gupta, M. *et al.* (2017) ‘A review on thermophysical properties of nanofluids and heat transfer applications’, *Renewable and Sustainable Energy Reviews*, 74(February), pp. 638–670. doi: 10.1016/j.rser.2017.02.073.

Gustafsson, S. E. (1991) ‘Transient plane source techniques for thermal conductivity and thermal diffusivity measurements of solid materials’, *Review of Scientific Instruments*, 62(3), pp. 797–804. doi: 10.1063/1.1142087.

GW instek (2018) ‘GPS-2303/3303/4251/4303’, *Documentation*. Available at: https://medium.com/@arifwicaksanaa/pengertian-use-case-a7e576e1b6bf.

Ha, S., Weitzmann, M. N. and Beck, G. R. (2013) *Chapter 4. Dental and Skeletal Applications of Silica-Based Nanomaterials*, *Nanobiomaterials in Clinical Dentistry*. Elsevier Inc. doi: 10.1016/B978-1-4557-3127-5.00004-0.

Haddad, Z. *et al.* (2014) ‘A review on how the researchers prepare their nanofluids’, *International Journal of Thermal Sciences*, 76, pp. 168–189. doi: 10.1016/j.ijthermalsci.2013.08.010.

Hawkins, W. L. (2014) *Stabilizer (chemistry)*. doi: https://doi.org/10.1036/1097-8542.650250.

Hu, P. *et al.* (2008) 'Thermal conductivity of AlN-ethanol nanofluids', *International Journal of Thermophysics*, 29(6), pp. 1968–1973. doi: 10.1007/s10765-008-0529-3.

Hu, P., Fei, W. S. and Chen, Z. (2008) 'Thermal Conductivity of AlN – Ethanol Nanofluids', pp. 1968–1973. doi: 10.1007/s10765-008-0529-3.

Huminic, G., Huminic, A. and Fleacă, C. (2020) 'Experimental study on viscosity of water based Fe-Si hybrid nanofluids', *Journal of Molecular Liquids*, p. 114938. doi: 10.1016/j.molliq.2020.114938.

Ilyas, S. U., Pendyala, R. and Marneni, N. (2014) 'Preparation, sedimentation, and agglomeration of nanofluids', *Chemical Engineering and Technology*, 37(12), pp. 2011–2021. doi: 10.1002/ceat.201400268.

Jeffrey, D. J. (1973) 'Conduction Through a Random Suspension of Spheres', pp. 355–367. doi: 10.1098/rspa.1973.0130.

Khedkar, R. S., Sonawane, S. S. and Wasewar, K. L. (2012) 'Influence of CuO nanoparticles in enhancing the thermal conductivity of water and monoethylene glycol based nanofluids', *International Communications in Heat and Mass Transfer*, 39(5), pp. 665–669. doi: 10.1016/j.icheatmasstransfer.2012.03.012.

Kole, M. and Dey, T. K. (2011) 'Role of interfacial layer and clustering on the effective thermal conductivity of CuO – gear oil nanofluids', *Experimental Thermal and Fluid Science*, 35(7), pp. 1490–1495. doi: 10.1016/j.expthermflusci.2011.06.010.

Li, X. *et al.* (2015) 'International Journal of Heat and Mass Transfer Rheological behavior of ethylene glycol-based SiC nanofluids', *HEAT AND MASS TRANSFER*, 84, pp. 925–930. doi: 10.1016/j.ijheatmasstransfer.2015.01.104.

Linseis Inc. (no date) *https://www.linseis.com/en/methods/guarded-hot-plate-ghp/*. Available at: https://www.linseis.com/en/methods/guarded-hot-plate-ghp/.

Liu, X. *et al.* (2020) 'An experimental investigation on the rheological behavior of nano fl uids made by suspending multi-walled carbon nanotubes in liquid paraf fi n', *Journal of Molecular Liquids*, 300, p. 112269. doi: 10.1016/j.molliq.2019.112269.

Loong, T. T. and Salleh, H. (2017) 'A review on measurement techniques of apparent thermal conductivity of nanofluids', *IOP Conference Series: Materials Science and Engineering*, 226(1). doi: 10.1088/1757-899X/226/1/012146.

Manikam, V. R., Cheong, K. Y. and Razak, K. A. (2011) 'Chemical reduction methods for synthesizing Ag and Al nanoparticles and their respective nanoalloys', *Materials Science & Engineering B*, 176(3), pp. 187–203. doi: 10.1016/j.mseb.2010.11.006.

Mariano, A. *et al.* (2015) 'Co3O4 ethylene glycol-based nanofluids: Thermal conductivity, viscosity and high pressure density', *International Journal of Heat and Mass Transfer*, 85, pp. 54–60. doi: 10.1016/j.ijheatmasstransfer.2015.01.061.

MAXIM (2002) 'MAX6675 - Cold junction compensated K-Thermocouple to digital converter', *Maxim Dallas*, p. 8.

nanografi (no date) *Cobalt Oxide (Co3O4) Nanopowder/Nanoparticles, Purity: 99.75%, Size: 48 nm*. Available at: https://nanografi.com/nanoparticles/cobalt-oxide-

co3o4-nanopowder-nanoparticles-purity-99-75-size-48-nm/ (Accessed: 5 June 2022).

Phelan, P. E. (2004) ‘Thermal Conductivity of Aluminum Oxide – Water Nanofluid’, pp. 1–6.

Purdue University (2004) *Oxidizing and Reducing Agents*. Available at: https://chemed.chem.purdue.edu/genchem/topicreview/bp/ch9/redox.php (Accessed: 5 April 2021).

Rausch, M. H. *et al.* (2013) ‘A new guarded parallel-plate instrument for the measurement of the thermal conductivity of fluids and solids’, *International Journal of Heat and Mass Transfer*, 58(1–2), pp. 610–618. doi: 10.1016/j.ijheatmasstransfer.2012.11.069.

REOTEMP Instrument Corporation (2011) *Type K Thermocouple*. Available at: https://www.thermocoupleinfo.com/type-k-thermocouple.htm (Accessed: 2 February 2022).

Saidur, R., Leong, K. Y. and Mohammad, H. A. (2011) ‘A review on applications and challenges of nanofluids’, *Renewable and Sustainable Energy Reviews*, 15(3), pp. 1646–1668. doi: 10.1016/j.rser.2010.11.035.

de Silva, G. M. S. (2002) *Basic Metrology for ISO 9000 Certification*. 1 st. Great Britain: Butterworth-Heinemann.

Smith, D. R., Hust, J. G. and VanPoolen, L. J. (1982) ‘A guarded-hot-plate apparatus for measuring effective thermal conductivity of insulations between 80 K and 360 K’, (January). Available at: https://nvlpubs.nist.gov/nistpubs/Legacy/IR/nbsir81-1657.pdf.

Spurlin, M. (2000) *Defining Thermal Stability*. Available at: https://www.process-heating.com/articles/86924-defining-thermal-stability (Accessed: 5 March 2020).

tec-science (2020) *Guarded-Hot-Plate method for determining thermal conductivity (GHP)*. Available at: https://www.tec-science.com/thermodynamics/heat/guarded-hot-plate-method-for-determining-thermal-conductivity-ghp/#Design_of_a_Guarded-Hot-Plate_apparatus (Accessed: 20 March 2021).

Technologies, K. (no date) *34970A Data Acquisition / Data Logger Switch Unit*. Available at: https://www.keysight.com/zz/en/product/34970A/34970a-data-acquisition-control-mainframe-modules.html (Accessed: 2 January 2022).

Thermtest Inc. (2015a) *History.2 – The Guarded Hot Plate Method*, *thermtest.com*. Available at: https://thermtest.com/history-2-the-guarded-hot-plate-method (Accessed: 5 May 2021).

Thermtest Inc. (2015b) *HISTORY.2 – THE GUARDED HOT PLATE METHOD*.

Thermtest Inc. (2021) *Thermal Conductivity of Water*. Available at: https://thermtest.se/thermal-conductivity-of-water#:~:text=According to literature1 the,K at 20 °C. (Accessed: 2 February 2022).

Thermtest Inc. (2022) *Top 10 Thermally Conductive Materials*. Available at: https://thermtest.com/thermal-resources/top-10-resources/top-10-thermally-conductive-materials#:~:text=Copper – 398 W%2Fm•K (Accessed: 2 February 2022).

Thermtest INSTRUMENTS (no date) *Lee's Disc Method - Build Your Own Thermal Conductivity Meter*. Available at: https://thermtest.com/thermal-resources/build-your-own/lees-disc (Accessed: 5 May 2021).

Upadhyay, A. . (2017) *Fluid Mechaincs(Hydraulics)*. first edit. New Dheli: S.K. Kataria And Sons.

Vesconite (2019) *Vesconite - Typical Properties*. Available at: https://www.vesconite.com/wp-content/uploads/2019/11/VESCONITE-PROPERTIES-2019.pdf (Accessed: 10 November 2022).

Wang, X. and Xu, X. (1999) 'Thermal Conductivity of Nanoparticle – Fluid Mixture', 13(4).

Yadav, T. P., Yadav, R. M. and Singh, D. P. (2012) 'Mechanical Milling : a Top Down Approach for the Synthesis of Nanomaterials and Nanocomposites', 2(3), pp. 22–48. doi: 10.5923/j.nn.20120203.01.

Yu, W. and Choi, S. U. S. (2004) 'The role of interfacial layers in the enhanced thermal conductivity of nanofluids : A renovated Hamilton – Crosser model', pp. 355–361.

Yüksel, N. (2016) 'The Review of Some Commonly Used Methods and Techniques to Measure the Thermal Conductivity of Insulation Materials', *Insulation Materials in Context of Sustainability*. doi: 10.5772/64157.

Yunus A, C. and Afshin J, G. (2015) *Heat and mass transfer:fundamentals and applications*. 5th edn. Mcgraw Hill.

Zagabathuni, A., Ghosh, S. and Pabi, S. K. (2016) 'The difference in the thermal conductivity of nanofluids measured by different methods and its rationalization', *Beilstein Journal of Nanotechnology*, 7(1), pp. 2037–2044. doi: 10.3762/BJNANO.7.194.

APPENDIX A: Calculations

Assumptions:

m_h =0.566 kg

m_c =0.266 kg

ΔT = 1 K

C_p=385 J/kg*K

$$Q = m_h * c_P * \Delta T$$

$$Q = 217.91\ J$$

$$Q = m_c * c_P * \Delta T$$

$$Q = 102.41\ J$$

Dimensions as per **Table 3-2: Stack assembly dimensions**

Hot plate analysis:

$$R_2 = \frac{L_2}{k_{copper} * A_2} = 0.001\ K/W$$

$$R_3 = \frac{L_3}{k_{copper} * A_3} = 0.006\ K/W$$

$$R_4 = \frac{L_4}{k_{vesconite} * A_4} = 10.341\ K/W$$

$$R_5 = \frac{L_5}{k_{copper} * A_5} = 0.003\ K/W$$

$$R_{Parallel1} = (\frac{1}{R_3} + \frac{1}{R_4} + \frac{1}{R_5})^{-1} = 0.002\ K/W$$

$$R_{hot\ plate} = R_2 + R_{parallel1} = 0.003\ K/W$$

Testing area analysis:

$$R_6 = \frac{L_6}{k_{vesconite} * A_6} = 5.475\ K/W$$

$$R_7 = \frac{L_7}{k_{water} * A_7} = 7.194\ K/W$$

$$R_{Parallel2} = (\frac{1}{R_6} + \frac{1}{R_7})^{-1} = 7.194\ K/W$$

Cold plate analysis

$$R_8 = \frac{L_8}{k_{copper} * A_8} = 0.006\ K/W$$

$$R_9 = \frac{L_9}{k_{vesconite} * A_9} = 10.341\ K/W$$

$$R_{10} = \frac{L_{10}}{k_{copper} * A_{10}} = 0.003\ K/W$$

$$R_{11} = \frac{L_{11}}{k_{copper} * A_{11}} = 0.001\frac{K}{W}$$

$$R_{Parallel3} = (\frac{1}{R_8} + \frac{1}{R_9} + \frac{1}{R_{10}})^{-1} = 0.002\ K/W$$

$$R_{cold\ plate} = R_{11} + R_{parallel3} = 0.003\ K/W$$

Total:

$$R_{total} = R_{hot\ plate} + R_{parallel2} + R_{cold\ plate} = 3.115\ K/W$$

Power loss calculation:

$$P_{measured} = I.V = 1.065\ W$$

$$Q_{actual} = \frac{\Delta T}{R_{parallel2}} = 0.878\ W$$

$$Q_{lost} = P_{measured} - Q_{actual} = 0.175\ w$$

Therefore:

$$Cf = 1 - Q_{lost} = 0.825$$

Water thermal conductivity:

$$k_{water} = \frac{\Delta L}{R_w * Af} = 0.612\ W/mK$$

Glycol Thermal conductivity:

$$K_{sample} = \frac{V_1.V_2.C_f.\Delta L - \Delta T.R.K_v.A_1}{\Delta T.R.A_2} = 0.247\ W/mK$$

$$K_{sample} = \frac{V_1.V_2.C_f.\Delta L - \Delta T.R.K_v.A_1}{\Delta T.R.A_2} = 0.208\ W/mK$$

Sample A1 thermal conductivity test 1:

$$K_{sample} = \frac{V_1.V_2.C_f.\Delta L - \Delta T.R.K_v.A_1}{\Delta T.R.A_2} = 0.255\ W/mK$$

Sample B1 thermal conductivity test 1:

$$K_{sample} = \frac{V_1.V_2.C_f.\Delta L - \Delta T.R.K_v.A_1}{\Delta T.R.A_2} = 0.454\ W/mK$$

Sample B1 thermal conductivity test 2:

$$K_{sample} = \frac{V_1.V_2.C_f.\Delta L - \Delta T.R.K_v.A_1}{\Delta T.R.A_2} = 0.467\ W/mK$$

Numerical models:

Density of nanofluids:

$$\rho_{A3} = \left((1-\varphi_{A3}).\rho_f\right) + \left(\varphi_{A3}.\rho_p\right) = 1.163\ x10^3 kg/m^3$$

$$\rho_{B3} = \left((1-\varphi_{B3}).\rho_f\right) + \left(\varphi_{B3}.\rho_p\right) = 1.137\ x10^3 kg/m^3$$

Maxwell model:

$$k_{sample} = \frac{k_p + 2k_f + 2(k_p - k_f)}{k_p + 2k_f - (k_p - k_f)\varphi_{A3}} = 0.747\ W/mK$$

$$k_{sample} = \frac{k_p + 2k_f + 2(k_p - k_f)}{k_p + 2k_f - (k_p - k_f)\varphi_{B3}} = 0.743\ W/mK$$

Jeffery model.

$$k_e = k_f\left(1 + 3\beta\emptyset_{A3} + {\emptyset_{A3}}^2\left(3\beta^2 + \frac{3\beta^2}{4} + \frac{9\beta^3}{16}\frac{\propto +2}{2\propto +3} + \frac{3\beta^4}{2^6}\right)\right) = 0.262\ W/mK$$

$$k_e = k_f\left(1 + 3\beta\emptyset_{B3} + {\emptyset_{B3}}^2\left(3\beta^2 + \frac{3\beta^2}{4} + \frac{9\beta^3}{16}\frac{\propto +2}{2\propto +3} + \frac{3\beta^4}{2^6}\right)\right) = 0.258\ W/mK$$

Garoosi model:

$$k_e = k_f\left(\frac{k_p + 2k_f + 2\left(k_p - k_f\right)\emptyset}{k_p + 2k_f - \left(k_p - k_f\right)\omega\emptyset} + 3.762\left(\frac{T}{T_0}\right)^{8.661}\left(\frac{d_p}{d_f}\right)^{-0.4351}\left(\frac{k_p}{k_f}\right)^{0.08235}\emptyset^{0.64}e^{(-5.742\emptyset)}\right) = 0.796\ W/mK$$

$$k_e = k_f\left(\frac{k_p + 2k_f + 2\left(k_p - k_f\right)\emptyset}{k_p + 2k_f - \left(k_p - k_f\right)\omega\emptyset} + 3.762\left(\frac{T}{T_0}\right)^{8.661}\left(\frac{d_p}{d_f}\right)^{-0.4351}\left(\frac{k_p}{k_f}\right)^{0.08235}\emptyset^{0.64}e^{(-5.742\emptyset)}\right) = 0.758\ W/mK$$

APPENDIX B: Specification sheets

34970A/34972A accuracy specifications ± (% of reading + % of range) [1]

Includes measurement error, switching error, and transducer conversion error

	Range [3]	Frequency, etc.	24 hour [2] 23 ± 1 °C	90 Day 23 ± 5 °C	1 Year 23 ± 5 °C	Temperature coefficient 0 – 18 °C, 28 - 55 °C
DC voltage						
	100.0000 mV		0.0030 + 0.0035	0.0040 + 0.0040	0.0050 + 0.0040	0.0005 + 0.0005
	1.000000 V		0.0020 + 0.0006	0.0030 + 0.0007	0.0040 + 0.0007	0.0005 + 0.0001
	10.00000 V		0.0015 + 0.0004	0.0020 + 0.0005	0.0035 + 0.0005	0.0005 + 0.0001
	100.0000 V		0.0020 + 0.0006	0.0035 + 0.0006	0.0045 + 0.0006	0.0005 + 0.0001
	300.000 V		0.0020 + 0.0020	0.0035 + 0.0030	0.0045 + 0.0030	0.0005 + 0.0003
True RMS AC voltage [4]						
	All ranges from 100.0000 mV to 100.0000 V	3 Hz – 5 Hz	1.00 + 0.03	1.00 + 0.04	1.00 + 0.04	0.100 + 0.004
		5 Hz – 10 Hz	0.35 + 0.03	0.35 + 0.04	0.35 + 0.04	0.035 + 0.004
		10 Hz – 20 kHz	0.04 + 0.03	0.05 + 0.04	0.06 + 0.04	0.005 + 0.004
		20 kHz – 50 kHz	0.10 + 0.05	0.11 + 0.05	0.12 + 0.05	0.011 + 0.005
		50 kHz – 100 kHz	0.55 + 0.08	0.60 + 0.08	0.60 + 0.08	0.060 + 0.008
		100 kHz – 300 kHz [5]	4.00 + 0.50	4.00 + 0.50	4.00 + 0.50	0.20 + 0.02
	300.0000 V	3 Hz – 5 Hz	1.00 + 0.05	1.00 + 0.08	1.00 + 0.08	0.100 + 0.008
		5 Hz – 10 Hz	0.35 + 0.05	0.35 + 0.08	0.35 + 0.08	0.035 + 0.008
		10 Hz – 20 kHz	0.04 + 0.05	0.05 + 0.08	0.06 + 0.08	0.005 + 0.008
		20 kHz – 50 kHz	0.10 + 0.10	0.11 + 0.12	0.12 + 0.12	0.011 + 0.012
		50 kHz – 100 kHz	0.55 + 0.20	0.60 + 0.20	0.60 + 0.20	0.060 + 0.020
		100 kHz – 300 kHz [5]	4.00 + 1.25	4.00 + 1.25	4.00 + 1.25	0.20 + 0.05
Resistance [6]						
	100.0000 Ω	1 mA current source	0.0030 + 0.0035	0.008 + 0.004	0.010 + 0.004	0.0006 + 0.0005
	1.000000 kΩ	1 mA	0.0020 + 0.0006	0.008 + 0.001	0.010 + 0.001	0.0006 + 0.0001
	10.00000 kΩ	100 µA	0.0020 + 0.0005	0.008 + 0.001	0.010 + 0.001	0.0006 + 0.0001
	100.0000 kΩ	10 µA	0.0020 + 0.0005	0.008 + 0.001	0.010 + 0.001	0.0006 + 0.0001
	1.000000 MΩ	5.0 µA	0.002 + 0.001	0.008 + 0.001	0.010 + 0.001	0.0010 + 0.0002
	10.00000 MΩ	500 nA	0.015 + 0.001	0.020 + 0.001	0.040 + 0.001	0.0030 + 0.0004
	100.0000 MΩ	500 nA ‖ 10 MΩ	0.300 + 0.010	0.800 + 0.010	0.800 + 0.010	0.1500 + 0.0002
Frequency and period [7]						
	100 mV to 300V	3 Hz – 5 Hz	0.10	0.10	0.10	0.005
		5 Hz – 10 Hz	0.05	0.05	0.05	0.005
		10 Hz – 40 Hz	0.03	0.03	0.03	0.001
		40 Hz – 300 kHz	0.006	0.01	0.01	0.001
DC current (34901A only)						
	10.00000 mA	< 0.1 V burden	0.005 + 0.010	0.030 + 0.020	0.050 + 0.020	0.002 + 0.0020
	100.0000 mA	< 0.6 V	0.010 + 0.004	0.030 + 0.005	0.050 + 0.005	0.002 + 0.0005
	1.000000 A	< 2 V	0.050 + 0.006	0.080 + 0.010	0.100 + 0.010	0.005 + 0.0010
True RMS AC current (34901A only)						
	10.00000 mA and [4] 1.000000 A	3 Hz – 5 Hz	1.00 + 0.04	1.00 + 0.04	1.00 + 0.04	0.100 + 0.006
		5 Hz – 10 Hz	0.30 + 0.04	0.30 + 0.04	0.30 + 0.04	0.035 + 0.006
		10 Hz – 5 kHz	0.10 + 0.04	0.10 + 0.04	0.10 + 0.04	0.015 + 0.006
	100.0000 mA [8]	3 Hz – 5 Hz	1.00 + 0.5	1.00 + 0.5	1.00 + 0.5	0.100 + 0.06
		5 Hz – 10 Hz	0.30 + 0.5	0.30 + 0.5	0.30 + 0.5	0.035 + 0.06
		10 Hz – 5 kHz	0.10 + 0.5	0.10 + 0.5	0.10 + 0.5	0.015 + 0.06
Temperature	**Type**	**1-year accuracy [9]**		**Extended range 1-year accuracy [9]**		**Temp coefficient/°C**
Thermocouple [10]	B	1100 to 1820 °C	1.2 °C	400 to 1100 °C	1.8 °C	0.03 °C
	E	–150 to 1000 °C	1.0 °C	–200 to -150 °C	1.5 °C	
	J	–150 to 1200 °C	1.0 °C	–210 to -150 °C	1.2 °C	
	K	–100 to 1200 °C	1.0 °C	–200 to -100 °C	1.5 °C	
	N	–100 to 1300 °C	1.0 °C	–200 to -100 °C	1.5 °C	
	R	300 to 1760 °C	1.2 °C	–50 to 300 °C	1.8 °C	
	S	400 to 1760 °C	1.2 °C	–50 to 400 °C	1.8 °C	
	T	–100 to 400 °C	1.0 °C	–200 to -100 °C	1.5 °C	
RTD	R0 from 49 Ω to 2.1 kΩ	–200 to 600 °C	0.06 °C			0.003 °C
Thermistor	2.2 k, 5 k, 10 k	–80 to 150 °C	0.08 °C			0.002 °C

SPECIFICATIONS

		GPS-4303				GPS-4251				GPS-3303			GPS-2303	
OUTPUT MODE		CH1	CH2	CH3	CH4	CH1	CH2	CH3	CH4	CH1	CH2	CH3	CH1	CH2
	Voltage	0 ~ 30V		2.2 ~ 5.2V	8 ~ 15V	0 ~ 25V		3 ~ 6V	8 ~ 15V	0 ~ 30V		5V Fixed	0 ~ 30V	
	Current	0 ~ 3A		1A Max.	1A Max.	0 ~ 0.5A		2.5A Max.	1A Max.	0 ~ 3A		3A Max.	0 ~ 3A	
	Tracking Series Voltage	0 ~ 60V		----		0 ~ 50V		----		0 ~ 60V		----	0 ~ 60V	
	Tracking Parallel Current	0 ~ 6A				0 ~ 1A				0 ~ 6A			0 ~ 6A	
CONSTANT VOLTAGE OPERATION (CH1, CH2)	**Line Regulation**	≤ 0.01% + 3mV												
	Load Regulation	≤ 0.01% + 3mV (rating current ≤ 3A) ≤ 0.02% + 5mV (rating current > 3A)												
	Ripple & Noise	≤ 1mVrms , 5Hz ~ 1MHz												
	Recovery Time	≤ 100 μS (50% Load change, Minimum load 0.5A)												
CONSTANT CURRENT OPERATION (CH1, CH2)	**Line Regulation**	≤ 0.2% + 3mA												
	Load Regulation	≤ 0.2% + 3mA												
	Ripple & Noise	≤ 3mArms												
TRACKING OPERATION (CH1, CH2)	**Tracking Error**	≤ 0.5% + 10mV of the CH1												
	Series Regulation	≤ 300mV												
	Load Regulation	≤ 0.01% + 3mV												
	Ripple & Noise	≤ 2mVrms , 5Hz ~ 1MHz												
GPS-4303 2.2V ~ 5.2V OUTPUT (CH3) GPS-3303 5V FIX OUTPUT (CH3) GPS-4251 3V~6V OUTPUT(CH3)	**Line Regulation**	≤ 5mV												
	Load Regulation	≤ 15mV												
	Ripple & Noise	≤ 2mVrms, 5Hz ~ 1MHz												
	Current Output	GPS-4303: 1A, GPS-3303: 3A, GPS-4251: 2.5A												
GPS-4303 8V ~ 15V OUTPUT (CH4) GPS-4251 8V~15V OUTPUT (CH4)	**Line Regulation**	≤ 5mV												
	Load Regulation	≤ 10mV												
	Ripple & Noise	≤ 2mVrms, 5Hz ~ 1MHz												
	Current Output	1A												
METER	**Digital**	3 digits 0.5" LED display GPS-4303/4251/3303 Out ON Accuracy ± (0.5% rdg + 2 digits) GPS-4303/3303 Out OFF Accuracy ± (0.5% rdg + 8 digits) GPS-2303 Accuracy ± (0.5% rdg + 2 digits)												
INSULATION	**Chassis and Terminal**	≥ DC 500V / 20MΩ												
	Chassis and AC Cord	≥ DC 500V / 30MΩ												
POWER SOURCE	AC 100V/120V/220V(±10%)/230V(+10%~-6%), 50/60Hz													
ACCESSORIES	Power cord x 1, Instruction manual x 1 GPS-4303 : Test lead GTL-104 x 2, GTL-105 x 2 or GTL-203 x 2, GTL-204 x 2 GPS-4251 : Test lead GTL-105 x 4 or GTL-203 x 4 GPS-3303 : Test lead GTL-104 x 2, GTL-105 x 1 or GTL-203 x 1, GTL-204 x 2 GPS-2303 : Test lead GTL-104 x 2 or GTL-204 x 2													
DIMENSIONS & WEIGHT	255(W) x 145(H) x 265(D) mm, Approx. 7 kg (GPS-4303/3303/2303) ; Approx. 6.3kg (GPS-4251)													

Specifications subject to change without notice.

Vesconite - Typical Properties

		METRIC	IMPERIAL
Density (Specific Gravity)		1.38	1.38
Melting point		260°C	500°F
Hardness - Shore D (ASTM D2240)		83	83
Compressive Properties (ASTM D695 - 15)	**Compressive Strength @ Yield**	93 MPa	13,489 psi
	Modulus of Elasticity	2.3 GPa	333,590 psi
Tensile Properties (ASTM D695 - 15)	**Tensile Strength @ Yield**	66 MPa	9,573 psi
	Tensile Strength @ Break	63 MPa	9,137 psi
Tangent modulus of elasticity (ASTM D-790)		3,726 MPa	540,410 psi
Water swell - Mass change (ASTM D570)	**After 24 hours**	0.11%	
	After 28 days	0.12%	
Oil swell - Mass change (ASTM D570)	**After 24 hours**	0.077%	
	After 28 days	0.092%	
Shear strength (ASTM D732 -17)		49.1MPa	7,121 psi
Flexural yield strength		120 MPa	17,400 psi
Deflection temperature at 1.85MPa / 268 psi		93°C	200°F
Notched impact strength - Charpy (ISO 179)		245 kJ/m^2	0.49 $ft\text{-}lb/in^2$
Notched impact strength IZOD		30 J/m	0.56 ft-lb/in
Heat conductivity		0.3 w/m.K	2 $Btu\text{-}in/ft^2.hr.°F$
Coefficient of linear thermal expansion		$6x10^{-5}mm/mm.°C$	$3.3x10^{-5}$ in/in.°F
Dynamic friction coefficient on polished steel (no lubrication)		0.13 - 0.18	0.13 - 0.18
Dielectric strength		14kV/mm	360kV/in
Gamma ray resistance 50% loss of properties		100 Mrads	100 Mrads

The above data should be taken for indicative purposes. Physical properties may be altered to some extent by processing conditions.

APPENDIX C: Data

Table C-7: Cold bath calibration.

Scan	101 (C)	102 (C)	103 (C)	104 (C)	105 (C)	106 (C)	107 (C)	108 (C)	109 (C)	110 (C)	111 (C)	115 (C)	116 (C)	117 (C)
1	-0.212	-0.182	-0.14	-0.093	-0.087	-0.133	-0.078	-0.074	-0.025	-0.042	-0.042	-0.074	-0.517	0
2	-0.223	-0.196	-0.153	-0.101	-0.127	-0.131	-0.081	-0.087	-0.012	-0.055	-0.06	-0.074	-0.54	-0.01
3	-0.191	-0.17	-0.132	-0.093	-0.073	-0.112	-0.07	-0.062	-0.033	-0.059	-0.06	-0.078	-0.531	-0.009
4	-0.116	-0.103	-0.076	-0.044	-0.066	-0.085	-0.052	-0.058	-0.005	-0.051	-0.044	-0.081	-0.537	-0.025
5	-0.095	-0.095	-0.051	-0.04	-0.051	-0.077	-0.057	-0.073	0.002	-0.05	-0.05	-0.081	-0.555	-0.018
6	-0.106	-0.095	-0.089	-0.017	-0.055	-0.077	-0.054	-0.069	-0.021	-0.035	-0.047	-0.078	-0.539	-0.02
7	-0.127	-0.112	-0.081	-0.042	-0.08	-0.088	-0.053	-0.053	0.014	-0.052	-0.012	-0.055	-0.513	0.011
8	-0.159	-0.149	-0.104	-0.044	-0.087	-0.093	-0.042	-0.043	0.011	-0.019	-0.033	-0.05	-0.487	0.038
9	-0.167	-0.158	-0.118	-0.069	-0.092	-0.114	-0.052	-0.055	0.012	-0.028	-0.02	-0.047	-0.485	0.032
10	-0.183	-0.158	-0.129	-0.066	-0.103	-0.104	-0.052	-0.071	-0.001	-0.042	-0.031	-0.023	-0.49	0.038
STD dev	0.042819	0.035636	0.030887	0.026557	0.021557	0.019653	0.012112	0.012102	0.015664	0.012083	0.015109	0.018485	0.0238	0.023294
median	-0.163	-0.1535	-0.111	-0.055	-0.0835	-0.0985	-0.0535	-0.0655	-0.003	-0.046	-0.043	-0.074	-0.524	-0.0045
average	-0.1579	-0.1418	-0.1073	-0.0609	-0.0821	-0.1014	-0.0591	-0.0645	-0.0058	-0.0433	-0.0399	-0.0641	-0.5194	0.0037

Table C-8: Boiling water calibration:

Scan	101 (C)	102 (C)	103 (C)	104 (C)	105 (C)	106 (C)	107 (C)	108 (C)	109 (C)	110 (C)	111 (C)	114 (C)	115 (C)	116 (C)	117 (C)
1	98.805	98.854	98.776	98.823	98.893	98.927	98.847	98.857	98.795	98.895	98.863	99.088	98.848	99.049	98.593
2	98.96	98.956	98.824	98.807	98.941	98.955	98.853	98.879	98.821	98.923	98.922	99.027	98.858	99.101	98.595
3	99.073	99.023	98.892	98.95	98.917	99.027	98.881	98.916	98.832	98.913	98.918	99.126	98.85	99.073	98.592
4	99.152	99.107	98.896	98.956	98.997	99.042	98.942	98.88	98.818	98.952	98.937	99.124	98.845	99.01	98.578
5	99.037	99.056	98.924	98.913	98.972	98.999	98.935	98.957	98.83	98.964	98.933	99.139	98.792	98.959	98.556
6	98.958	98.945	98.899	98.829	98.932	98.938	98.939	98.977	98.863	98.965	98.958	99.127	98.896	99.056	98.602
7	98.976	98.931	98.884	98.911	98.951	98.94	98.87	98.919	98.835	98.935	98.918	99.119	98.838	99.071	98.6
8	98.983	98.937	98.901	98.844	98.923	98.994	98.885	98.952	98.839	98.966	98.922	99.137	98.848	99.133	98.622
9	99.001	98.947	98.894	98.822	98.958	98.94	98.869	98.938	98.825	98.965	98.948	99.137	98.886	99.093	98.614
10	98.945	98.956	98.87	98.835	98.894	98.951	98.937	99.01	98.839	98.968	98.949	99.089	98.871	99.088	98.629
STD dev	0.085949	0.068243	0.041523	0.054203	0.031429	0.038849	0.036287	0.045399	0.016595	0.025073	0.025159	0.033043	0.027121	0.0468	0.020117
median	98.9795	98.9515	98.893	98.8395	98.9365	98.953	98.883	98.9285	98.831	98.958	98.9275	99.125	98.849	99.072	98.5975
average	98.989	98.9712	98.876	98.869	98.9378	98.9713	98.8958	98.9285	98.8297	98.9446	98.9268	99.1113	98.8532	99.0633	98.5981

Table C-9: Ethylene Glycol test 1 data.

	glycol test 1																			
	101 (C)	102 (C)	103 (C)	104 (C)	105 (C)	106 (C)	107 (C)	108 (C)	109 (C)	110 (C)	111 (C)	112 (VDC)	current	113 (C)	114 (C)	115 (C)	116 (VDC)	DT	P	k
1	19.836	19.846	19.667	19.786	19.756	19.794	24.084	24.067	24.083	24.096	24.145	0.00756	0.99731	24.129	24.091	20.069	1.078461	4.314167	0.887337	0.286
2	19.82	19.82	19.658	19.781	19.73	19.773	24.109	24.076	24.082	24.105	24.143	0.007559	0.997271	24.096	24.101	20.021	1.078307	4.339333	0.887176	0.28
3	19.87	19.839	19.687	19.809	19.74	19.797	24.082	24.084	24.086	24.11	24.137	0.007559	0.997252	24.047	24.026	19.963	1.078308	4.309467	0.887159	0.287
4	19.807	19.862	19.673	19.806	19.735	19.8	24.102	24.074	24.104	24.102	24.143	0.007558	0.99711	24.029	23.979	19.918	1.078228	4.3245	0.886968	0.283
5	19.823	19.841	19.652	19.772	19.725	19.752	24.118	24.11	24.101	24.123	24.161	0.007558	0.99716	24.011	23.946	19.934	1.078184	4.361767	0.886976	0.275
6	19.817	19.836	19.637	19.793	19.696	19.75	24.133	24.108	24.132	24.141	24.174	0.007558	0.99716	23.966	23.925	19.934	1.078184	4.382767	0.886976	0.27
7	19.82	19.797	19.616	19.756	19.678	19.731	24.133	24.126	24.137	24.154	24.169	0.007558	0.997052	23.909	23.902	19.955	1.078101	4.4108	0.886811	0.263
8	19.765	19.799	19.605	19.748	19.667	19.713	24.141	24.133	24.148	24.162	24.169	0.007557	0.997008	23.886	23.868	19.942	1.078104	4.434433	0.886774	0.257
9	19.786	19.783	19.621	19.746	19.691	19.721	24.162	24.157	24.153	24.178	24.2	0.007558	0.997058	23.865	23.871	19.961	1.078057	4.445333	0.88678	0.255
10	19.726	19.752	19.562	19.713	19.646	19.702	24.141	24.145	24.155	24.189	24.2	0.007557	0.996998	23.937	23.902	19.897	1.078021	4.4825	0.886697	0.245
11	19.678	19.712	19.525	19.665	19.617	19.652	24.115	24.096	24.15	24.158	24.181	0.007557	0.99701	23.988	23.995	19.919	1.077912	4.4985	0.886619	0.242
12	19.744	19.723	19.561	19.706	19.638	19.671	24.146	24.128	24.129	24.146	24.166	0.007557	0.996911	24.106	24.054	19.918	1.077923	4.469167	0.886539	0.249
13	19.736	19.736	19.576	19.69	19.635	19.705	24.136	24.115	24.14	24.149	24.171	0.007556	0.996807	24.163	24.14	19.888	1.077877	4.462533	0.886409	0.249
14	19.762	19.754	19.605	19.722	19.664	19.687	24.151	24.128	24.153	24.172	24.205	0.007556	0.9969	24.179	24.143	19.898	1.077859	4.4628	0.886477	0.241
15	19.786	19.778	19.623	19.74	19.685	19.729	24.172	24.138	24.168	24.188	24.192	0.007556	0.996841	24.181	24.156	19.906	1.077858	4.4481	0.886424	0.253
16	19.799	19.802	19.634	19.766	19.685	19.763	24.177	24.167	24.173	24.188	24.218	0.007555	0.99673	24.148	24.13	19.912	1.077792	4.4431	0.886271	0.253
17	19.804	19.81	19.639	19.774	19.704	19.749	24.188	24.19	24.194	24.196	24.231	0.007556	0.996798	24.155	24.132	19.926	1.077773	4.453133	0.886316	0.252
18	19.775	19.773	19.604	19.752	19.677	19.736	24.172	24.181	24.184	24.186	24.231	0.007555	0.996739	24.157	24.111	19.922	1.077798	4.4713	0.886284	0.247
19	19.736	19.732	19.55	19.722	19.672	19.71	24.149	24.146	24.146	24.177	24.211	0.007554	0.996627	24.096	24.083	19.844	1.077748	4.4788	0.886142	0.245
20	19.778	19.796	19.597	19.73	19.675	19.72	24.143	24.156	24.145	24.18	24.171	0.007555	0.99669	24.08	24.041	19.862	1.077721	4.443	0.886177	0.254
21	19.817	19.801	19.639	19.769	19.711	19.741	24.156	24.174	24.165	24.193	24.22	0.007555	0.996737	24.072	24.041	19.88	1.077775	4.435267	0.886263	0.256
22	19.788	19.817	19.602	19.758	19.682	19.734	24.177	24.174	24.191	24.201	24.217	0.007555	0.996744	24.088	24.052	19.866	1.077755	4.461833	0.886253	0.25
23	19.801	19.807	19.61	19.758	19.693	19.744	24.2	24.19	24.202	24.224	24.241	0.007554	0.996632	24.083	24.049	19.888	1.077651	4.4759	0.886068	0.246
24	19.814	19.828	19.649	19.764	19.706	19.755	24.211	24.206	24.215	24.213	24.243	0.007555	0.996636	24.106	24.07	19.882	1.077633	4.464933	0.886057	0.249
25	19.814	19.828	19.655	19.787	19.732	19.747	24.213	24.2	24.212	24.242	24.261	0.007555	0.996679	24.132	24.109	19.923	1.077663	4.4651	0.88612	0.25
26	19.734	19.776	19.586	19.731	19.681	19.733	24.19	24.178	24.191	24.23	24.267	0.007556	0.996782	24.172	24.133	19.931	1.077676	4.504367	0.886221	0.239
27	19.759	19.776	19.599	19.737	19.68	19.746	24.192	24.172	24.187	24.221	24.247	0.007556	0.996771	24.168	24.147	19.904	1.077671	4.487633	0.886207	0.243
28	19.788	19.807	19.607	19.771	19.698	19.726	24.198	24.185	24.199	24.216	24.233	0.007556	0.996803	24.165	24.163	19.883	1.07768	4.473367	0.886243	0.248
29	19.799	19.827	19.636	19.753	19.706	19.726	24.221	24.185	24.186	24.208	24.235	0.007555	0.996725	24.222	24.21	19.852	1.07768	4.465833	0.886174	0.25
30	19.801	19.827	19.626	19.761	19.706	19.76	24.224	24.213	24.228	24.229	24.266	0.007556	0.996803	24.251	24.225	19.842	1.077665	4.485167	0.886231	0.244
Standard deviation	0.03937	0.038698	0.03777	0.032856	0.032344	0.033689	0.039298	0.041816	0.04	0.04079	0.039171	1.55E-06	0.000204	0.099188	0.098386	0.048464	0.000236	0.055618	0.000371	0.013853
average	19.7861	19.79617	19.6167	19.7522	19.69037	19.73557	24.15787	24.14673	24.15797	24.1759	24.2016	0.007556	0.996891	24.08623	24.05983	19.91467	1.077902	4.438497	0.886505	0.255367
median	19.7935	19.8015	19.6185	19.757	19.688	19.735	24.1535	24.151	24.154	24.183	24.2025	0.007556	0.996805	24.101	24.0765	19.915	1.077828	4.462183	0.886362	0.25

Table C-10: Ethylene Glycol test 2 data.

	glycol test 2																					
1	19.832	19.835	19.654	19.774	19.732	19.759	24.27	24.296	24.287	24.293	24.313	0.00756	0.997322	24.284	24.246	20.012	1.07766	4.527467	0.886689	0.236
2	19.843	19.854	19.688	19.805	19.729	19.78	24.293	24.278	24.305	24.325	24.329	0.00756	0.997333	24.305	24.248	20.014	1.077709	4.522833	0.886739	0.237
3	19.864	19.859	19.686	19.81	19.774	19.801	24.314	24.286	24.305	24.317	24.341	0.007559	0.99727	24.303	24.256	19.993	1.07667	4.5136	0.886647	0.239
4	19.838	19.834	19.656	19.785	19.719	19.778	24.286	24.269	24.28	24.287	24.319	0.007559	0.997229	24.248	24.238	19.96	1.077671	4.519867	0.886615	0.237
5	19.796	19.798	19.623	19.76	19.692	19.738	24.262	24.254	24.269	24.265	24.297	0.007559	0.997227	24.243	24.217	19.935	1.077643	4.5349	0.88659	0.234
6	19.78	19.793	19.625	19.758	19.661	19.712	24.278	24.27	24.261	24.296	24.321	0.007559	0.997187	24.261	24.209	19.926	1.077616	4.5637	0.886532	0.228
7	19.772	19.814	19.594	19.734	19.677	19.72	24.293	24.275	24.292	24.311	24.339	0.007559	0.997181	24.245	24.212	19.908	1.077578	4.5835	0.886496	0.223
8	19.767	19.769	19.586	19.747	19.671	19.709	24.293	24.273	24.305	24.306	24.341	0.007559	0.997181	24.266	24.243	19.914	1.077619	4.595433	0.88653	0.22
9	19.775	19.772	19.596	19.716	19.658	19.709	24.301	24.309	24.305	24.319	24.349	0.007558	0.99711	24.269	24.235	19.922	1.077632	4.612267	0.886477	0.216
10	19.788	19.777	19.583	19.739	19.677	19.723	24.306	24.293	24.295	24.332	24.365	0.007559	0.997166	24.284	24.264	19.935	1.077598	4.6037	0.886499	0.218
11	19.772	19.804	19.594	19.726	19.671	19.725	24.319	24.298	24.32	24.33	24.354	0.007558	0.997053	24.279	24.232	19.931	1.077547	4.608867	0.886357	0.217
12	19.769	19.762	19.594	19.75	19.674	19.709	24.322	24.324	24.336	24.34	24.38	0.007557	0.997031	24.282	24.258	19.908	1.077529	4.630733	0.886322	0.212
13	19.777	19.785	19.589	19.726	19.669	19.709	24.342	24.343	24.336	24.34	24.375	0.007557	0.99702	24.29	24.269	19.945	1.077496	4.638033	0.886285	0.211
14	19.782	19.793	19.607	19.735	19.678	19.696	24.301	24.3	24.297	24.3	24.355	0.007558	0.997034	24.262	24.196	19.865	1.077538	4.595433	0.886332	0.221
15	19.717	19.74	19.544	19.692	19.632	19.665	24.303	24.277	24.31	24.311	24.323	0.007557	0.997028	24.245	24.214	19.874	1.07753	4.6398	0.886321	0.21
16	19.698	19.706	19.536	19.666	19.6	19.667	24.303	24.288	24.305	24.306	24.331	0.007558	0.997038	24.237	24.217	19.878	1.077512	4.6611	0.886314	0.205
17	19.704	19.706	19.523	19.666	19.595	19.652	24.298	24.285	24.3	24.316	24.349	0.007558	0.997135	24.25	24.219	19.915	1.077568	4.6686	0.886447	0.204
18	19.714	19.748	19.541	19.676	19.621	19.662	24.319	24.296	24.31	24.316	24.351	0.007558	0.997089	24.25	24.201	19.905	1.07753	4.658067	0.886375	0.206
19	19.711	19.748	19.552	19.684	19.624	19.68	24.327	24.309	24.315	24.34	24.349	0.007558	0.997105	24.256	24.206	19.913	1.077526	4.6615	0.886385	0.205
20	19.735	19.73	19.57	19.708	19.634	19.678	24.347	24.303	24.32	24.345	24.377	0.007557	0.997008	24.243	24.238	19.96	1.077493	4.662567	0.886272	0.205
21	19.732	19.774	19.565	19.708	19.669	19.673	24.345	24.311	24.344	24.332	24.377	0.007557	0.996997	24.256	24.225	19.911	1.077492	4.654967	0.886261	0.208
22	19.73	19.767	19.565	19.7	19.632	19.68	24.347	24.314	24.323	24.348	24.364	0.007556	0.996879	24.271	24.222	19.909	1.077473	4.6602	0.886141	0.206
23	19.717	19.756	19.567	19.7	19.648	19.67	24.35	24.322	24.338	24.35	24.383	0.007557	0.996969	24.263	24.219	19.927	1.077492	4.672267	0.886236	0.204
24	19.706	19.719	19.539	19.687	19.629	19.672	24.35	24.329	24.331	24.361	24.385	0.007557	0.997028	24.279	24.237	19.905	1.077533	4.692533	0.886323	0.199
25	19.767	19.777	19.598	19.701	19.645	19.672	24.343	24.311	24.337	24.319	24.351	0.007558	0.997056	24.228	24.178	19.846	1.077504	4.638867	0.886324	0.211
26	19.703	19.734	19.532	19.667	19.59	19.633	24.311	24.299	24.301	24.323	24.347	0.007558	0.997038	24.237	24.18	19.842	1.077479	4.673033	0.886288	0.204
27	19.727	19.722	19.538	19.671	19.6	19.643	24.29	24.28	24.32	24.332	24.346	0.007558	0.99704	24.23	24.198	19.86	1.077478	4.663433	0.886288	0.206
28	19.717	19.732	19.541	19.684	19.624	19.672	24.321	24.306	24.299	24.319	24.338	0.007557	0.99698	24.232	24.183	19.866	1.077496	4.654933	0.88625	0.207
29	19.73	19.738	19.552	19.702	19.626	19.654	24.329	24.306	24.307	24.332	24.354	0.007557	0.996979	24.248	24.185	19.877	1.077531	4.6586	0.886277	0.207
30	19.732	19.74	19.565	19.7	19.642	19.654	24.334	24.308	24.315	24.332	24.359	0.007557	0.996987	24.253	24.204	19.862	1.077469	4.657433	0.886233	0.207
Standard deviation	0.045034	0.040852	0.043772	0.039836	0.042451	0.041864	0.024374	0.019691	0.019674	0.02033	0.021429	8.27E-07	0.000109	0.020613	0.024761	0.043686	6.78E-05	0.052469	0.00015	0.011721
average	19.7565	19.76953	19.58343	19.71923	19.65643	19.6965	24.31323	24.29707	24.30893	24.32143	24.34873	0.007558	0.99709	24.25997	24.22163	19.91393	1.077554	4.620941	0.886395	0.214767
median	19.751	19.768	19.5765	19.708	19.653	19.68	24.3125	24.2985	24.306	24.321	24.349	0.007558	0.997047	24.256	24.219	19.912	1.07753	4.639333	0.886328	0.2105

Table C-11: Sample A3 test 1 data.

	sample A3																							
1	19.393	19.468	19.352	19.447	19.424	19.437	23.766	23.749	23.757	23.796	23.81	0.00755	0.996086	23.752	23.744	18.843	1.080822	4.355433	0.888188	0.277
2	19.412	19.463	19.373	19.474	19.419	19.461	23.8	23.796	23.785	23.814	23.828	0.00755	0.996082	23.791	23.778	18.8	1.080828	4.370933	0.88819	0.273
3	19.433	19.463	19.354	19.458	19.424	19.469	23.8	23.785	23.78	23.801	23.834	0.00755	0.996053	23.801	23.788	18.79	1.080832	4.3665	0.888166	0.273
4	19.409	19.476	19.36	19.463	19.429	19.471	23.813	23.806	23.811	23.814	23.852	0.007549	0.99591	23.843	23.806	18.794	1.080819	4.384533	0.888029	0.269
5	19.407	19.463	19.36	19.471	19.437	19.466	23.818	23.811	23.811	23.846	23.846	0.00755	0.995979	23.84	23.814	18.772	1.080739	4.3924	0.888025	0.267
6	19.453	19.48	19.366	19.486	19.436	19.466	23.814	23.809	23.832	23.814	23.881	0.007549	0.995928	23.815	23.795	18.737	1.080713	4.382167	0.887957	0.27
7	19.487	19.503	19.392	19.47	19.425	19.461	23.84	23.803	23.833	23.829	23.857	0.00755	0.996008	23.823	23.805	18.736	1.080781	4.376067	0.888085	0.272
8	19.484	19.51	19.406	19.48	19.438	19.479	23.842	23.819	23.81	23.835	23.878	0.00755	0.996074	23.849	23.818	18.717	1.080747	4.370633	0.888116	0.273
9	19.502	19.5	19.421	19.493	19.465	19.476	23.866	23.814	23.851	23.85	23.89	0.00755	0.996053	23.867	23.846	18.729	1.080783	4.378033	0.888127	0.272
10	19.479	19.521	19.406	19.48	19.459	19.482	23.86	23.84	23.841	23.868	23.901	0.00755	0.996103	23.878	23.872	18.736	1.08074	4.390833	0.888136	0.268
11	19.471	19.51	19.392	19.48	19.441	19.463	23.873	23.858	23.87	23.866	23.911	0.007551	0.996108	23.906	23.891	18.742	1.080743	4.4161	0.888143	0.263
12	19.46	19.521	19.395	19.483	19.433	19.461	23.889	23.876	23.867	23.868	23.898	0.00755	0.996036	23.914	23.893	18.764	1.080767	4.420767	0.888099	0.262
13	19.476	19.497	19.406	19.465	19.441	19.476	23.918	23.879	23.885	23.889	23.942	0.00755	0.996076	23.919	23.909	18.77	1.080691	4.442433	0.888072	0.256
14	19.46	19.505	19.377	19.467	19.415	19.448	23.915	23.886	23.898	23.894	23.937	0.007551	0.996115	23.942	23.914	18.776	1.080697	4.460667	0.888111	0.252
15	19.466	19.518	19.377	19.462	19.423	19.463	23.912	23.892	23.903	23.915	23.958	0.00755	0.996024	23.942	23.929	18.772	1.080699	4.4645	0.888031	0.251
16	19.495	19.497	19.413	19.488	19.444	19.474	23.936	23.905	23.924	23.928	23.95	0.00755	0.996044	23.971	23.945	18.774	1.080678	4.4601	0.888033	0.252
17	19.508	19.521	19.45	19.509	19.475	19.49	23.943	23.915	23.924	23.925	23.976	0.007551	0.996155	23.973	23.953	18.795	1.080703	4.444433	0.888152	0.256
18	19.51	19.544	19.432	19.538	19.491	19.516	23.938	23.933	23.942	23.946	23.986	0.007551	0.996164	23.968	23.955	18.785	1.080713	4.443833	0.888167	0.256
19	19.495	19.558	19.458	19.538	19.48	19.503	23.951	23.962	23.942	23.954	24.005	0.00755	0.996093	23.984	23.953	18.782	1.080681	4.457467	0.888079	0.253
20	19.531	19.55	19.442	19.522	19.483	19.521	23.972	23.98	23.947	23.962	23.999	0.00755	0.995984	23.989	23.984	18.782	1.080651	4.463833	0.887956	0.251
21	19.536	19.579	19.463	19.548	19.493	19.537	23.995	23.962	23.968	23.977	24.005	0.00755	0.996099	23.984	23.984	18.789	1.080673	4.4554	0.888077	0.253
22	19.539	19.568	19.453	19.541	19.514	19.545	23.99	23.969	23.997	23.995	24.015	0.00755	0.996104	23.976	23.955	18.776	1.080676	4.466533	0.888084	0.25
23	19.526	19.558	19.445	19.546	19.509	19.545	23.99	23.982	23.979	24.006	24.028	0.00755	0.996094	23.984	23.971	18.78	1.08067	4.4755	0.88807	0.248
24	19.516	19.565	19.432	19.533	19.47	19.521	24.003	24.011	23.976	24.011	24.036	0.007551	0.996119	23.976	23.966	18.742	1.080653	4.501233	0.888079	0.242
25	19.492	19.544	19.416	19.53	19.491	19.529	24.008	24.006	24.017	24.011	24.033	0.007551	0.996137	23.992	23.966	18.729	1.080636	4.514667	0.888081	0.239
26	19.502	19.539	19.395	19.527	19.459	19.487	24.024	24.024	24.007	24.024	24.036	0.007551	0.996193	23.976	23.976	18.74	1.080611	4.538167	0.88811	0.235
27	19.495	19.523	19.419	19.504	19.465	19.495	24.032	24.019	24.028	24.055	24.069	0.007551	0.996151	23.966	23.989	18.715	1.08063	4.5571	0.888088	0.23
28	19.487	19.539	19.408	19.507	19.472	19.5	24.05	24.019	24.01	24.047	24.064	0.00755	0.9961	23.966	23.979	18.719	1.080571	4.5525	0.887994	0.231
29	19.481	19.516	19.408	19.501	19.459	19.49	24.045	24.026	24.028	24.065	24.082	0.007552	0.99625	23.994	23.963	18.709	1.080587	4.573367	0.88814	0.226
30	19.495	19.526	19.403	19.504	19.465	19.5	24.06	24.047	24.046	24.055	24.067	0.007553	0.996482	23.968	23.966	18.715	1.080907	4.572833	0.888612	0.227
Standard deviation	0.037875	0.03241	0.031455	0.0295	0.027365	0.028265	0.085255	0.088019	0.083882	0.085621	0.081236	7.7E-07	0.000102	0.07162	0.07509	0.031909	7.74E-05	0.06464	0.000111	0.014907
average	19.48	19.5175	19.4058	19.49717	19.45597	19.48773	23.9221	23.9061	23.90897	23.922	23.95247	0.00755	0.996093	23.9183	23.90357	18.76033	1.080715	4.448299	0.888107	0.2549
median	19.487	19.5195	19.406	19.4905	19.459	19.4805	23.927	23.8985	23.9135	23.92	23.954	0.00755	0.996094	23.954	23.937	18.771	1.080701	4.449917	0.888087	0.2545

Table C-12: Sample B3 test 1 data.

	sample B3																							
1	19.852	19.89	19.752	19.849	19.781	19.823	23.551	23.541	23.505	23.552	23.571	0.007552	0.996298	23.668	23.632	18.759	1.077308	3.7195	0.885489	0.456
2	19.865	19.895	19.737	19.834	19.792	19.823	23.525	23.51	23.523	23.567	23.579	0.007552	0.996292	23.583	23.541	18.753	1.077304	3.716467	0.88548	0.457
3	19.82	19.877	19.71	19.826	19.776	19.784	23.523	23.52	23.528	23.557	23.566	0.007551	0.996179	23.492	23.466	18.77	1.077201	3.739967	0.885295	0.45
4	19.844	19.881	19.748	19.814	19.776	19.821	23.528	23.511	23.514	23.551	23.57	0.007552	0.996287	23.406	23.383	18.772	1.077217	3.7208	0.885405	0.455
5	19.857	19.866	19.73	19.851	19.784	19.831	23.532	23.514	23.496	23.555	23.59	0.007552	0.996323	23.392	23.368	18.811	1.077151	3.717567	0.885382	0.455
6	19.862	19.894	19.743	19.849	19.793	19.834	23.532	23.523	23.505	23.546	23.557	0.007553	0.996385	23.374	23.36	18.783	1.077144	3.703433	0.885431	0.461
7	19.875	19.888	19.763	19.86	19.819	19.86	23.515	23.514	23.504	23.529	23.562	0.007553	0.996392	23.377	23.349	18.783	1.077167	3.680633	0.885457	0.468
8	19.87	19.895	19.754	19.864	19.813	19.86	23.501	23.49	23.518	23.546	23.558	0.007553	0.996467	23.384	23.375	18.772	1.077173	3.679933	0.885528	0.468
9	19.845	19.908	19.715	19.868	19.81	19.849	23.532	23.484	23.515	23.531	23.559	0.007554	0.996511	23.403	23.392	18.756	1.077171	3.6917	0.885566	0.464
10	19.824	19.899	19.662	19.836	19.758	19.821	23.515	23.509	23.509	23.543	23.554	0.007552	0.996358	23.431	23.418	18.743	1.077128	3.726	0.885394	0.452
11	19.824	19.905	19.713	19.826	19.789	19.831	23.514	23.492	23.51	23.523	23.562	0.007552	0.996318	23.478	23.452	18.753	1.077093	3.705533	0.88533	0.459
12	19.798	19.852	19.677	19.81	19.765	19.815	23.52	23.475	23.501	23.532	23.552	0.007552	0.99629	23.473	23.455	18.739	1.07714	3.729833	0.885343	0.45
13	19.794	19.877	19.569	19.832	19.725	19.784	23.49	23.459	23.485	23.514	23.535	0.007551	0.99622	23.476	23.448	18.696	1.077061	3.7331	0.885217	0.449
14	19.81	19.844	19.693	19.807	19.78	19.8	23.501	23.489	23.463	23.494	23.52	0.007551	0.996222	23.488	23.443	18.726	1.077073	3.7044	0.885228	0.46
15	19.846	19.853	19.718	19.823	19.773	19.794	23.479	23.463	23.455	23.487	23.514	0.007551	0.996212	23.458	23.458	18.721	1.077071	3.678433	0.885218	0.47
16	19.841	19.881	19.733	19.813	19.775	19.813	23.485	23.468	23.487	23.502	23.51	0.007551	0.996194	23.498	23.482	18.736	1.077065	3.681067	0.885197	0.468
17	19.844	19.883	19.731	19.827	19.775	19.813	23.472	23.462	23.437	23.472	23.494	0.007551	0.996154	23.456	23.45	18.689	1.077069	3.655233	0.885164	0.477
18	19.852	19.881	19.726	19.832	19.759	19.813	23.47	23.472	23.443	23.467	23.481	0.007551	0.996115	23.476	23.435	18.697	1.077056	3.6561	0.88512	0.477
19	19.833	19.857	19.71	19.817	19.754	19.797	23.459	23.433	23.445	23.467	23.481	0.00755	0.996053	23.479	23.44	18.705	1.076954	3.662333	0.88498	0.474
20	19.778	19.814	19.653	19.769	19.722	19.747	23.47	23.441	23.428	23.446	23.488	0.007549	0.995895	23.476	23.445	18.701	1.076947	3.707433	0.884834	0.459
21	19.762	19.79	19.624	19.748	19.693	19.726	23.441	23.431	23.433	23.462	23.485	0.007548	0.995824	23.482	23.456	18.68	1.07695	3.726567	0.884774	0.452
22	19.739	19.772	19.592	19.722	19.662	19.703	23.433	23.433	23.428	23.446	23.472	0.007548	0.995753	23.482	23.45	18.701	1.076968	3.744067	0.884726	0.446
23	19.728	19.761	19.595	19.712	19.654	19.7	23.444	23.402	23.423	23.454	23.47	0.007548	0.995719	23.479	23.469	18.709	1.076928	3.746933	0.884662	0.445
24	19.664	19.71	19.557	19.673	19.618	19.674	23.403	23.415	23.397	23.42	23.471	0.007548	0.995744	23.483	23.452	18.693	1.076925	3.771867	0.884681	0.436
25	19.656	19.714	19.555	19.673	19.608	19.668	23.402	23.393	23.383	23.43	23.468	0.007547	0.995601	23.457	23.46	18.699	1.076916	3.769533	0.884547	0.436
26	19.643	19.684	19.525	19.642	19.597	19.647	23.396	23.374	23.381	23.418	23.448	0.007547	0.995604	23.475	23.444	18.713	1.076911	3.7804	0.884546	0.433
27	19.63	19.678	19.528	19.658	19.608	19.668	23.39	23.387	23.379	23.428	23.443	0.007548	0.995716	23.47	23.46	18.703	1.076949	3.777067	0.884677	0.433
28	19.635	19.684	19.53	19.647	19.616	19.655	23.388	23.355	23.387	23.423	23.432	0.007547	0.995594	23.47	23.447	18.691	1.076933	3.769167	0.884556	0.436
29	19.617	19.676	19.536	19.613	19.597	19.634	23.393	23.384	23.371	23.402	23.458	0.007547	0.995604	23.48	23.465	18.697	1.076878	3.789433	0.884518	0.43
30	19.625	19.671	19.528	19.647	19.605	19.637	23.403	23.374	23.376	23.418	23.461	0.007547	0.995626	23.459	23.47	18.697	1.076872	3.787567	0.884534	0.431
Standard deviation	0.086403	0.082704	0.083493	0.079555	0.075662	0.073302	0.05137	0.051797	0.052018	0.051755	0.047212	2.27E-06	0.000299	0.056648	0.052717	0.034831	0.000122	0.038917	0.000357	0.013803
average	19.7811	19.82267	19.66023	19.77807	19.7259	19.7675	23.47357	23.45727	23.45763	23.4894	23.5137	0.00755	0.996065	23.46683	23.4455	18.72827	1.077057	3.722402	0.885076	0.453567
median	19.822	19.8615	19.7015	19.8155	19.762	19.7985	23.482	23.4655	23.459	23.4905	23.512	0.007551	0.996187	23.4755	23.45	18.717	1.077067	3.72015	0.885207	0.455

Table C-13:Sample B3 test 2 data.

	sample b3 test 2																					
1	19.648	19.686	19.546	19.65	19.616	19.661	23.38	23.35	23.387	23.41	23.445	0.007547	0.995625	23.496	23.457	18.672	1.076886	3.7599	0.884544	0.439
2	19.635	19.673	19.538	19.671	19.6	19.655	23.367	23.371	23.369	23.413	23.448	0.007547	0.99568	23.475	23.465	18.691	1.076857	3.764933	0.884569	0.438
3	19.648	19.686	19.533	19.66	19.608	19.65	23.37	23.358	23.361	23.395	23.43	0.007547	0.995697	23.491	23.465	18.658	1.076855	3.751967	0.884582	0.442
4	19.611	19.652	19.523	19.658	19.59	19.661	23.38	23.392	23.371	23.407	23.437	0.007547	0.99564	23.472	23.467	18.66	1.076851	3.781567	0.884529	0.431
5	19.638	19.663	19.544	19.666	19.603	19.653	23.388	23.379	23.371	23.402	23.437	0.007547	0.995658	23.475	23.462	18.674	1.076879	3.767567	0.884567	0.437
6	19.625	19.697	19.478	19.652	19.611	19.645	23.372	23.381	23.366	23.384	23.445	0.007547	0.995659	23.475	23.47	18.67	1.076844	3.7716	0.88454	0.435
7	19.656	19.711	19.563	19.673	19.645	19.668	23.371	23.346	23.357	23.393	23.427	0.007546	0.995576	23.47	23.444	18.662	1.076864	3.726133	0.884482	0.451
8	19.667	19.703	19.537	19.671	19.637	19.695	23.358	23.344	23.357	23.396	23.414	0.007546	0.995562	23.47	23.449	18.669	1.07685	3.722133	0.884459	0.45
9	19.673	19.73	19.591	19.69	19.647	19.676	23.348	23.342	23.362	23.378	23.428	0.007546	0.995568	23.467	23.476	18.695	1.076819	3.703767	0.884438	0.459
10	19.657	19.735	19.588	19.685	19.637	19.681	23.358	23.355	23.359	23.391	23.426	0.007546	0.995561	23.454	23.448	18.71	1.076846	3.713967	0.884454	0.455
11	19.701	19.751	19.624	19.702	19.687	19.708	23.355	23.349	23.372	23.388	23.419	0.007547	0.995676	23.467	23.459	18.705	1.076808	3.6811	0.884525	0.466
12	19.747	19.765	19.616	19.726	19.701	19.723	23.359	23.332	23.363	23.369	23.383	0.007548	0.995728	23.441	23.422	18.673	1.076855	3.6482	0.88461	0.478
13	19.773	19.797	19.65	19.744	19.709	19.742	23.364	23.33	23.343	23.358	23.411	0.007548	0.995753	23.41	23.409	18.645	1.076835	3.625367	0.884616	0.486
14	19.72	19.786	19.487	19.757	19.641	19.718	23.362	23.335	23.348	23.379	23.409	0.007548	0.995813	23.405	23.404	18.639	1.076884	3.681767	0.884709	0.465
15	19.77	19.787	19.647	19.761	19.709	19.739	23.358	23.34	23.371	23.371	23.397	0.007548	0.995809	23.376	23.367	18.592	1.07685	3.6319	0.884678	0.484
16	19.794	19.823	19.66	19.78	19.727	19.742	23.348	23.317	23.315	23.358	23.357	0.007549	0.995936	23.349	23.321	18.528	1.076842	3.584667	0.884784	0.502
17	19.796	19.812	19.664	19.767	19.708	19.76	23.359	23.335	23.33	23.367	23.385	0.00755	0.995993	23.31	23.302	18.548	1.07688	3.604033	0.884866	0.494
18	19.802	19.817	19.667	19.78	19.725	19.758	23.366	23.35	23.35	23.371	23.4	0.00755	0.996026	23.328	23.292	18.586	1.076866	3.609233	0.884884	0.493
19	19.823	19.812	19.679	19.782	19.735	19.76	23.362	23.337	23.33	23.349	23.401	0.007549	0.995884	23.302	23.29	18.597	1.07685	3.590633	0.884745	0.5
20	19.802	19.841	19.658	19.774	19.719	19.763	23.355	23.345	23.341	23.327	23.396	0.007548	0.995832	23.284	23.266	18.585	1.076874	3.5933	0.884719	0.498
21	19.765	19.802	19.641	19.751	19.71	19.726	23.357	23.317	23.327	23.365	23.388	0.007548	0.995735	23.305	23.29	18.61	1.076828	3.6183	0.884595	0.49
22	19.723	19.777	19.629	19.717	19.677	19.734	23.327	23.319	23.322	23.348	23.379	0.007548	0.995769	23.287	23.282	18.638	1.076826	3.6295	0.884622	0.484
23	19.71	19.752	19.6	19.721	19.683	19.7	23.336	23.314	23.304	23.342	23.38	0.007546	0.995558	23.288	23.269	18.657	1.07679	3.640867	0.884406	0.481
24	19.672	19.716	19.571	19.689	19.645	19.687	23.306	23.294	23.307	23.323	23.354	0.007546	0.995555	23.291	23.283	18.659	1.076761	3.653467	0.884379	0.475
25	19.651	19.705	19.467	19.681	19.603	19.671	23.315	23.278	23.327	23.34	23.378	0.007546	0.995569	23.291	23.283	18.657	1.076749	3.697933	0.884382	0.459
26	19.645	19.707	19.551	19.681	19.634	19.681	23.32	23.28	23.301	23.345	23.375	0.007546	0.99558	23.283	23.28	18.689	1.076731	3.674367	0.884377	0.467
27	19.622	19.689	19.546	19.655	19.618	19.658	23.318	23.306	23.303	23.319	23.362	0.007546	0.995533	23.278	23.257	18.701	1.076681	3.690267	0.884294	0.462
28	19.648	19.681	19.549	19.671	19.629	19.658	23.307	23.296	23.298	23.337	23.375	0.007546	0.995532	23.291	23.262	18.673	1.076718	3.683267	0.884323	0.465
29	19.643	19.676	19.53	19.652	19.613	19.652	23.315	23.298	23.296	23.329	23.367	0.007546	0.995546	23.301	23.275	18.673	1.076746	3.693333	0.884359	0.461
30	19.638	19.686	19.535	19.637	19.603	19.639	23.31	23.267	23.301	23.322	23.349	0.007546	0.995533	23.278	23.291	18.677	1.07669	3.6868	0.884302	0.464
Standard deviation	0.064829	0.055076	0.059842	0.04622	0.045835	0.03976	0.023481	0.030525	0.027191	0.028022	0.029039	1.07E-06	0.000141	0.083655	0.084104	0.044999	5.81E-05	0.058233	0.000158	0.020732
average	19.69677	19.73727	19.5804	19.70347	19.65567	19.69547	23.3497	23.3319	23.3403	23.36587	23.40007	0.007547	0.995686	23.377	23.36357	18.64977	1.07682	3.679394	0.884545	0.467033
median	19.6695	19.723	19.567	19.687	19.643	19.684	23.358	23.336	23.3455	23.368	23.3985	0.007547	0.995658	23.3625	23.344	18.661	1.076845	3.682517	0.884542	0.465

APPENDIX D: Arduino Code

Final code:

```
#include <SPI.h>
#include <Wire.h>
#include <LiquidCrystal_I2C.h>
LiquidCrystal_I2C lcd(0x27, 16, 2);
#include <max6675.h>
#include <PID_v1.h>

#include <ADS1115.h>

ADS1115 ads; // declare new ADS1115 instance
/*************Prototypes*************************/
float read_voltage(void); // this function read differential voltage (A0_P, A1_N)
float read_current(void); // this function read current (A2_P, A3_N)

/*************Globale Variable*************************/
const float Vref = 4.096; // this is imternal reference of ADS1115

const uint8_t GAIN_0 = 0; // gain is 2/3
const uint8_t GAIN_1 = 1; // gain is 1 etc...
const uint8_t GAIN_2 = 2;
const uint8_t GAIN_4 = 3;
const uint8_t GAIN_8 = 4;
const uint8_t GAIN_16 = 7;
```

```
const uint8_t SPS_8 = 0; // 8 samples (readings) per second : the more accurate but the slowest

const uint8_t SPS_16 = 1; // 16 samples (readings) per second

const uint8_t SPS_32 = 2; // 32 samples (readings) per second

const uint8_t SPS_64 = 3; // 32 samples (readings) per second

const uint8_t SPS_128 = 4; // 32 samples (readings) per second

const uint8_t SPS_250 = 5; // 32 samples (readings) per second

const uint8_t SPS_475 = 6; // 32 samples (readings) per second

const uint8_t SPS_860 = 7; // 32 samples (readings) per second


float Voltage; //Declaration of values

float Current;


double P;

float value;


int clk = 8;

int data = 9;


int clk_State;

int Last_State;

bool dt_State;


//Variables

double   set_temperature_hot = 0;


double Num_read = 4;


float elapsedTime, Time, timePrev;
```

```
int button_pressed = 0;

int menu_activated = 0;

float last_set_temperature_hot = 0;

const int Hot =1;

const int Cold =0;


double read_temp(int,double);


//PID constants


double Setpoint_hot, Input_hot=0, Output_hot;

double Setpoint_cold, Input_cold=0, Output_cold;


//aggressive PID values for when the results fed back to the PI are severly out
of range of the predefined value.

double aggKp_hot=50, aggKi_hot=0, aggKd_hot=0;

double consKp_hot=25, consKi_hot=5, consKd_hot=0;


double aggKp_cold=0, aggKi_cold=0, aggKd_cold=0;

double consKp_cold=40, consKi_cold=50, consKd_cold=0;


//defining what each pin does.

int PID_values_fixed = 0;


int PWM_pin_cold = 3;

int PWM_pin_hot = 5;

int PWM_pin_guard = 6;
```

```
int thermoDO = 12;

int thermoCS1 = 2;

int thermoCS2 = 4;

int thermoCS3 = 7;

int thermoCLK = 13;


    MAX6675 thermocouple1(thermoCLK, thermoCS1, thermoDO);

    MAX6675 thermocouple2(thermoCLK, thermoCS2, thermoDO);

    MAX6675 thermocouple3(thermoCLK, thermoCS3, thermoDO);

double temperature_read_guard;

    PID myPID_hot(&Input_hot, &Output_hot, &Setpoint_hot, consKp_hot,
consKi_hot, consKd_hot, DIRECT);

    PID myPID_cold(&Input_cold, &Output_cold, &Setpoint_cold,
consKp_cold, consKi_cold, consKd_cold, REVERSE);


void setup() {

  Serial.begin(9600);


  delay(2500);

  lcd.init();

  lcd.backlight();

  pinMode(PWM_pin_cold, OUTPUT);

  pinMode(PWM_pin_hot, OUTPUT);

  pinMode(PWM_pin_guard, OUTPUT);


  TCCR0B = TCCR0B & B11111000 | B00000011 | 0x03;


  TCCR2B = TCCR2B & B11111000 | B00000011  | 0x05;

  Time = millis();
```

```
  Last_State = (PINB & B00000001);

  PCICR |= (1 << PCIE0);
  PCMSK0 |= (1 << PCINT0);
  PCMSK0 |= (1 << PCINT1);
  PCMSK0 |= (1 << PCINT3);

  pinMode(11, INPUT);
  pinMode(9, INPUT);
  pinMode(8, INPUT);

  Input_hot = (thermocouple2.readCelsius());
  Input_cold = (thermocouple1.readCelsius());
  Setpoint_hot = 25;
  Setpoint_cold = 22.75;

  myPID_hot.SetMode(AUTOMATIC);
  myPID_cold.SetMode(AUTOMATIC);

   ads.begin(0x4A); // initialize and set adress

 ads.setFullScaleRange(GAIN_0); // setting the gain of the ads
  ads.setSamplingRate(SPS_64); // Here the the reading speed is 64 samples per second

}

void loop() {
```

```
 {



//CURRENT,VOLTAGE AND POWER CALCULTIONS


  Voltage = read_voltage();
  Current = read_current();


P=Voltage*Current*3;
 // PID CALCULATIONS


Input_hot=read_temp(1,Num_read);//sampling of the hot tempretures


  double gap_hot = abs(Setpoint_hot-Input_hot); //deviation from the set point
  if (gap_hot < 10)
  { //the PID values used when close to the set point
    myPID_hot.SetTunings(consKp_hot, consKi_hot, consKd_hot);
  }
  else
  {
     //the PID values used when far to the set point
     myPID_hot.SetTunings(aggKp_hot, aggKi_hot, aggKd_hot);
  }
  myPID_hot.Compute();//output of the hot PWM value
  analogWrite(PWM_pin_hot, Output_hot);
```

```
Input_cold=read_temp(0,Num_read);//sampling of the cold tempretures



  double gap_cold = abs(Setpoint_cold-Input_cold); //deviation from the set
point

  if (gap_cold < 10)

  { //the PID values used when close to the set point

    myPID_cold.SetTunings(consKp_cold, consKi_cold, consKd_cold);

  }

  else

  {//the PID values used when far to the set point


     myPID_cold.SetTunings(aggKp_cold, aggKi_cold, aggKd_cold);

  }

  myPID_cold.Compute();//output of the cold PWM value

  analogWrite(PWM_pin_cold, Output_cold);


    temperature_read_guard = (thermocouple3.readCelsius());    //This section
uses the hot plate as an input for the bang bang controller of the guard heater

    if (temperature_read_guard<Setpoint_hot-0.8) {

          digitalWrite(PWM_pin_guard,HIGH);

    }

    else {

          digitalWrite(PWM_pin_guard,LOW);

    }


//SERIAL COMMANDS

{

//serial commands to laptop
```

```
    Serial.print(thermocouple1.readCelsius());
    Serial.print(",");
    Serial.print(thermocouple2.readCelsius());
    Serial.print(",");
    Serial.print(Current);
    Serial.print(",");
    Serial.print(Voltage);
    Serial.println("");
    }



//LCD COMMANDS
  lcd.clear();
  lcd.setCursor(0,0);
    lcd.print("TESTING");
  lcd.setCursor(0,1);
    lcd.print("C=");
  lcd.setCursor(2,1);
    lcd.print(thermocouple1.readCelsius(),1);
  lcd.setCursor(8,1);
    lcd.print("H=");
  lcd.setCursor(10,1);
    lcd.print(thermocouple2.readCelsius(),1);
  lcd.setCursor(9,0);
    lcd.print("G=");
  lcd.setCursor(11,0);
    lcd.print(thermocouple3.readCelsius(),1);}
```

APPENDIX E: Drawings

OVERVIEW DRAWING

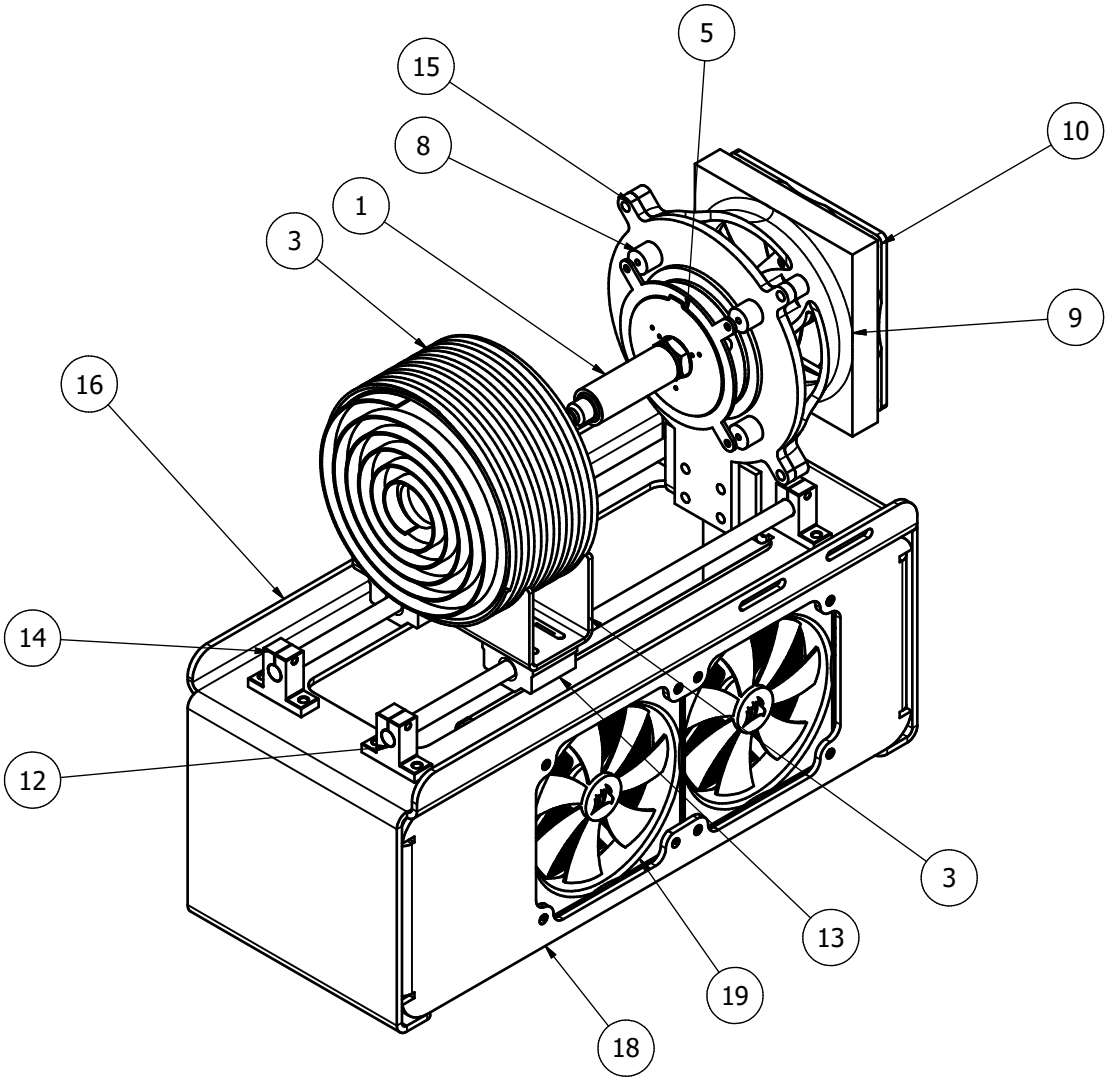

PARTS LIST			
ITEM	QTY	PART NUMBER	DESCRIPTION
1	1	OMEGA PX409 HIGH ACCURACY PRESSURE TRANSDUCER	STEP AP214
3	1	GUARD HEATER ASSEMBLY	
5	1	CORE ASSEMBLY	
8	4	STAND OFFS	
9	1	Fan cowel	
10	1	case_fan_120mm	
12	2	RAIL SHAT	
13	2	SCS10UU	STEP AP214
14	4	SK10	
15	1	COLD PLATE MOUNT	
16	1	BASE PLATE	
17	1	Insulating Ring	
18	1	radiator mount	
19	1	dual radiator	

Designed by	QTY:1 OFF	MATERIAL:	SCALE:1:2	Date	
Laptop				2022/11/21	

Cape Peninsula University of Technology

GUARDED HOT PLATE ASSEMBLY

MECHENG-001 | Edition 5 | Sheet 1 / 13

FRONT VIEW (1 : 4)

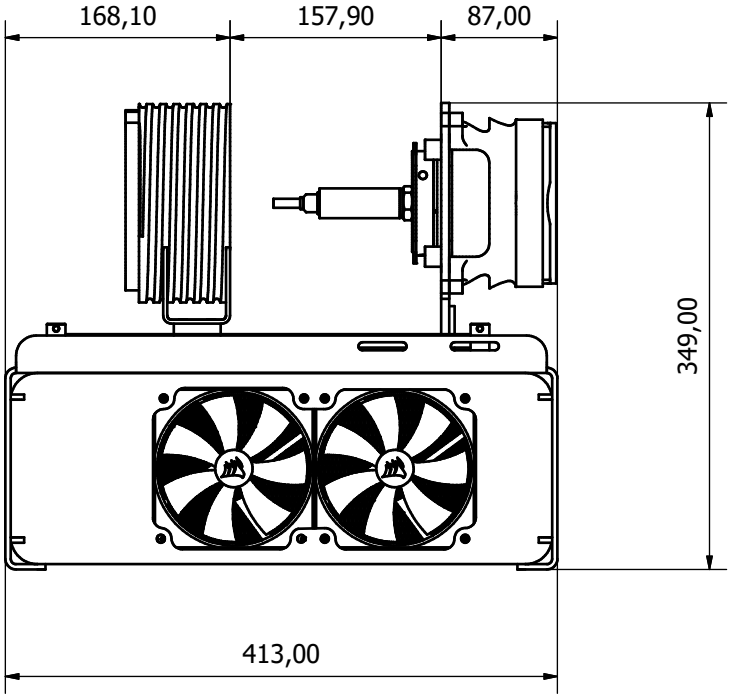

SIDE VIEW (1 : 4)

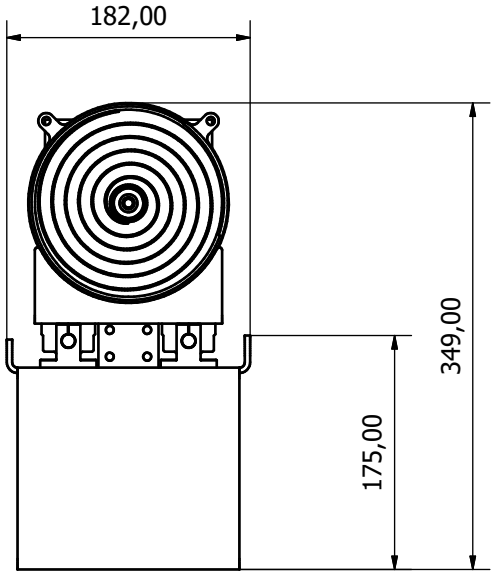

TOP VIEW (1 : 4)

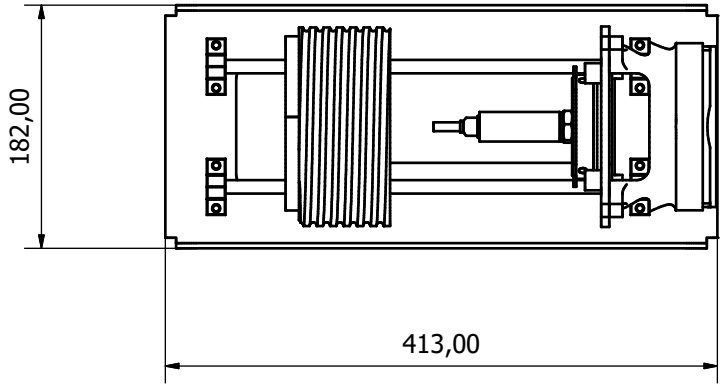

Designed by	QTY:1 OFF	MATERIAL:	SCALE:1:2	Date	
Laptop				2022/11/21	

Cape Peninsula University of Technology

GAURDED HOT PLATE ASSEMBLY

MECHENG-001	Edition 5	Sheet 2 / 13

A-A (1 : 2)

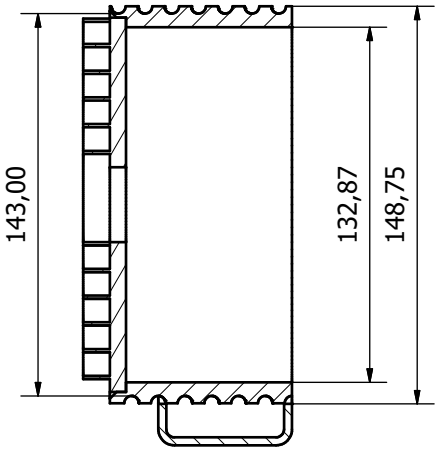

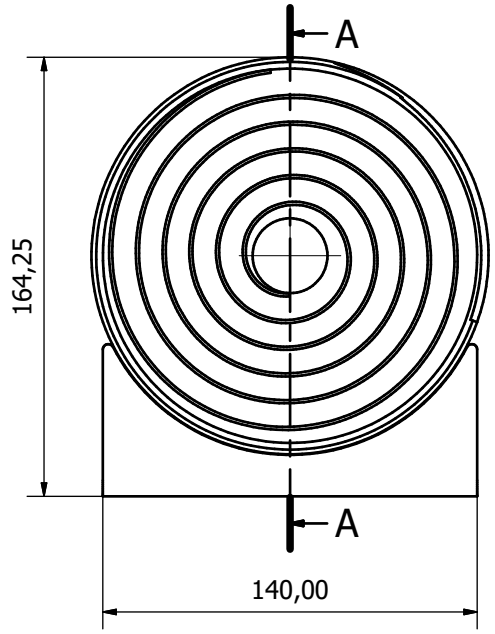

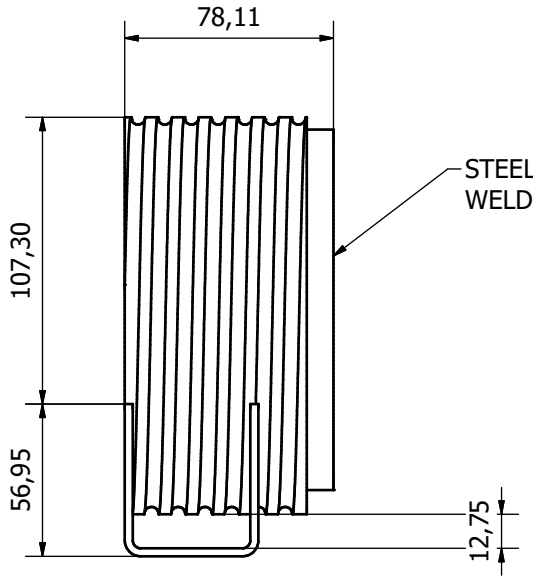

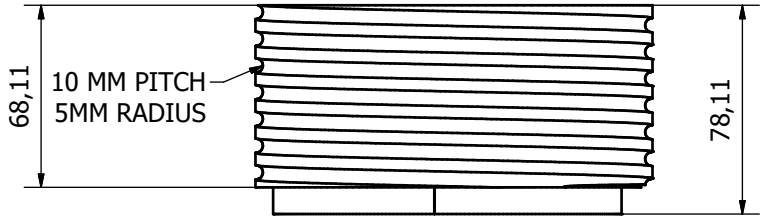

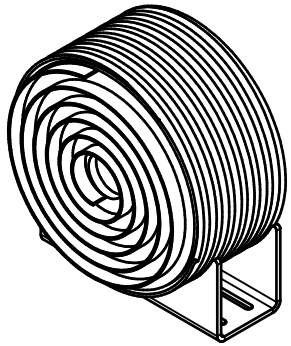

Designed by Laptop	QTY:1 OFF	MATERIAL: MILD STEEL	SCALE:1:2	Date 2022/11/21	
Cape Peninsula University of Technology	GUARD HEATER				
	MECHENG-001-001		Edition 3	Sheet 3 / 13	

CORE/STACK ASSEMBLY

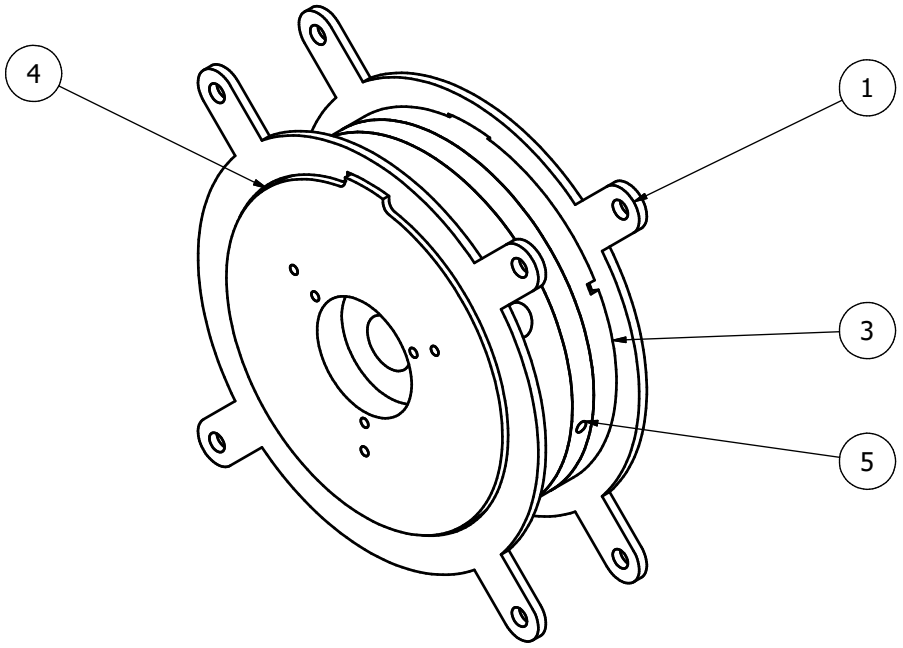

PARTS LIST			
ITEM	QTY	PART NUMBER	DESCRIPTION
1	2	MOUNT PLATES	
3	1	COLD PLATE final prototype	
4	1	HOT PLATE final prototype	
5	1	7.5ml ring	

Designed by Laptop	QTY:1 OFF	MATERIAL:	SCALE:1:2	Date 2022/11/21	

Cape Peninsula University of Technology

CORE/STACK ASSEMBLY

MECHENG-001-002 | Edition 5 | Sheet 4 / 13

FRONT VIEW (1 : 1)

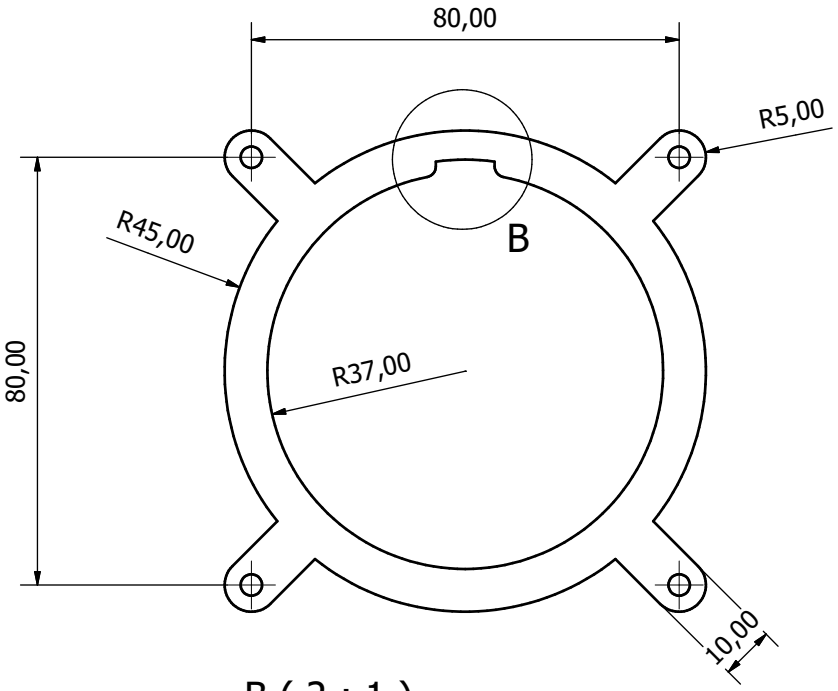

SIDE VIEW (1 : 1)

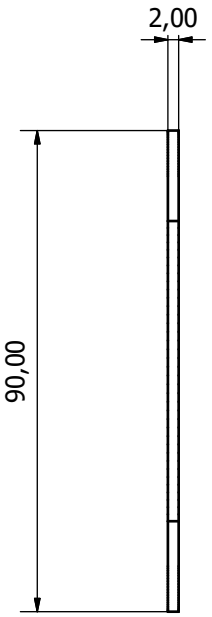

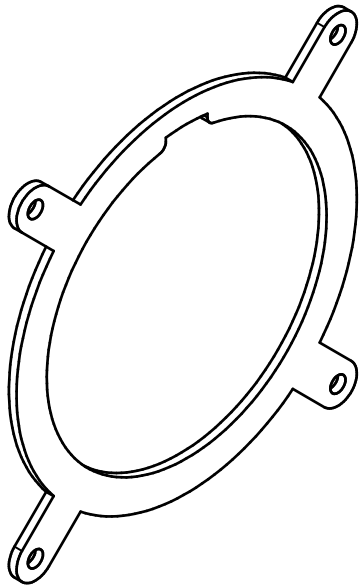

B (2 : 1)

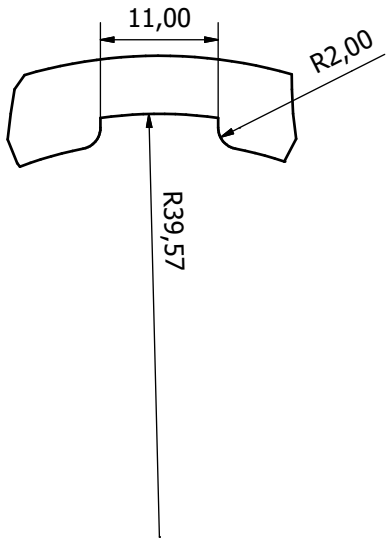

Designed by Laptop	QTY:1 OFF	MATERIAL: SS304	SCALE:1:2	Date 2022/11/21	
Cape Peninsula University of Technology	MOUNT PLATES				
	MECHENG-001-002-001		Edition 1	Sheet 5 / 13	

FRONT VIEW (1 : 1)

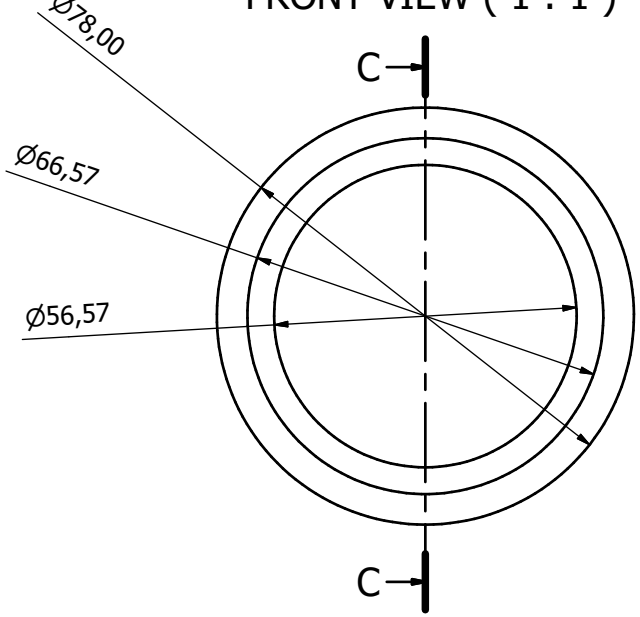

C-C (1 : 1)

SIDE VIEW (1 : 1)

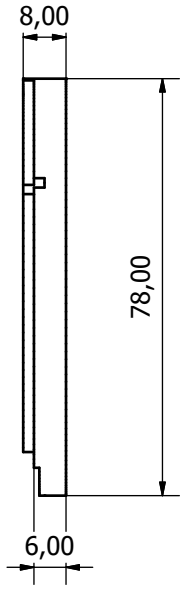

REAR VIEW (1 : 1)

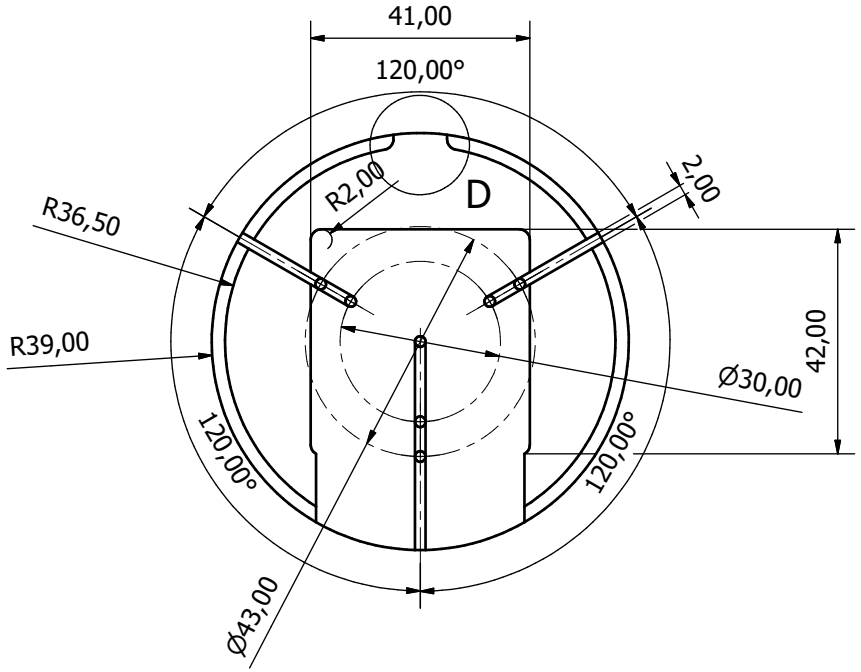

D (2 : 1)

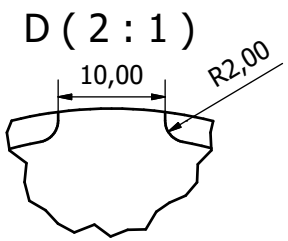

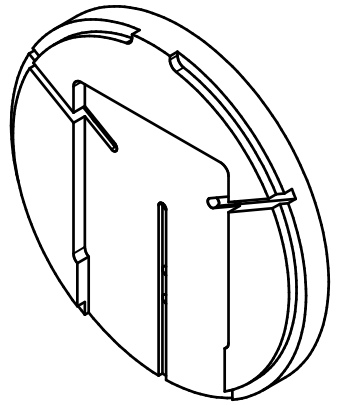

Designed by Laptop	QTY:1 OFF	MATERIAL: COPPER	SCALE:1:2	Date 2022/11/21	
Cape Peninsula University of Technology	COLD PLATE				
	MECHENG-001-002-002		Edition 3	Sheet 6 / 13	

FRONT VIEW (1 : 1)

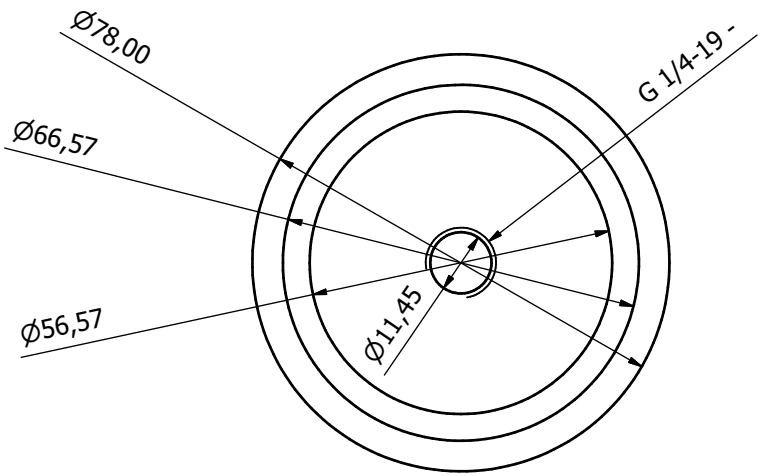

SIDE VIEW (1 : 1)

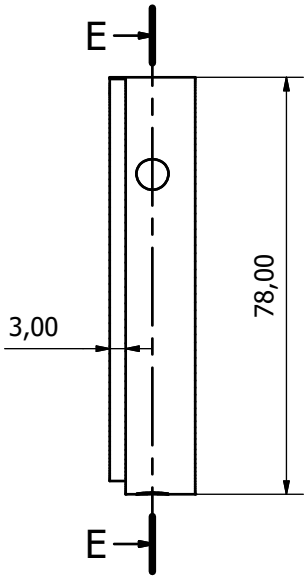

E-E (1 : 1)

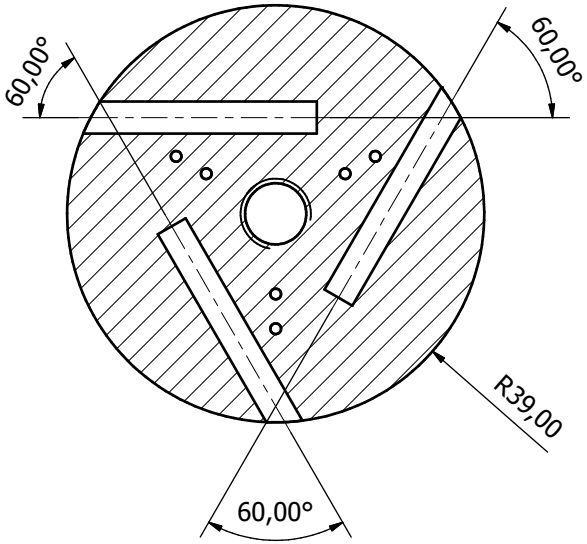

REAR VIEW (1 : 1)

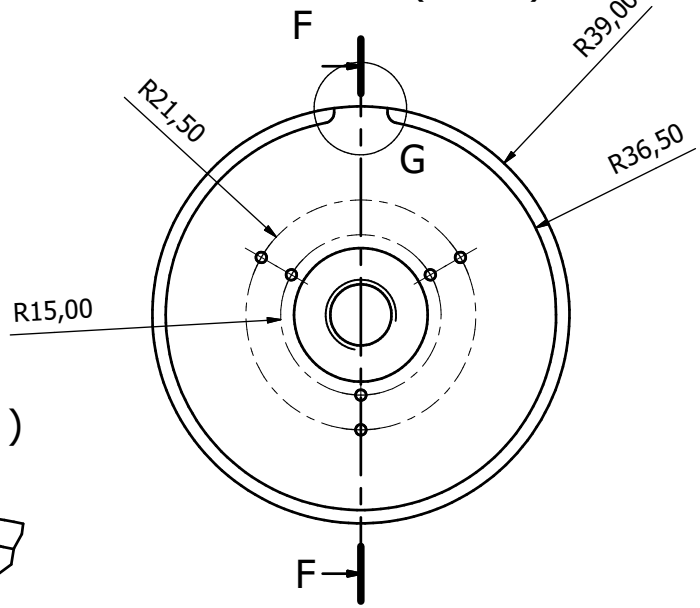

F-F (1 : 1)

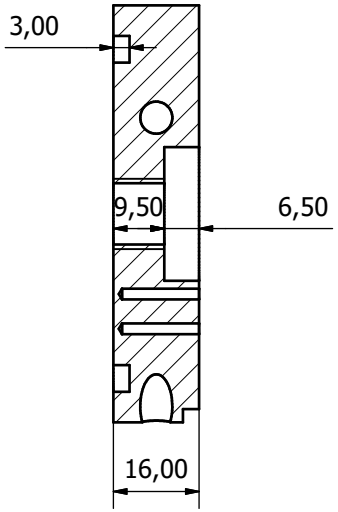

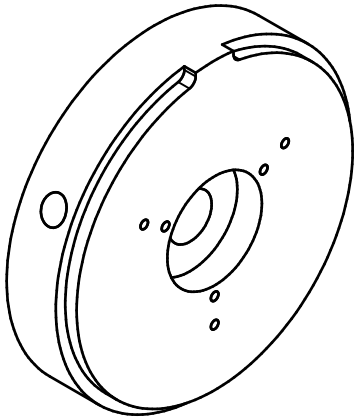

G (2 : 1)

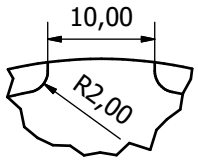

Designed by Laptop	QTY:1 OFF	MATERIAL: COPPER	SCALE:1:2	Date 2022/11/21	
Cape Peninsula University of Technology	HOT PLATE				
	MECHENG-001-002-003		Edition 3	Sheet 7 / 13	

FRONT VIEW (1 : 1)

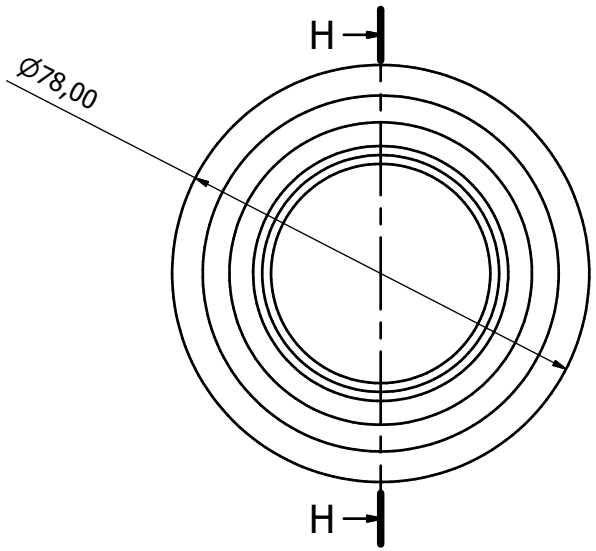

H-H (1 : 1)

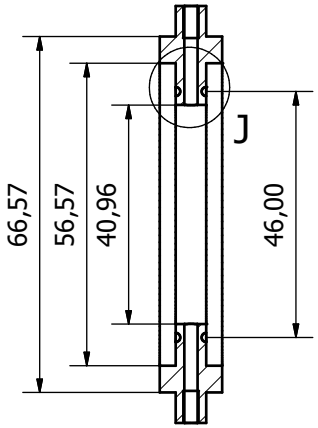

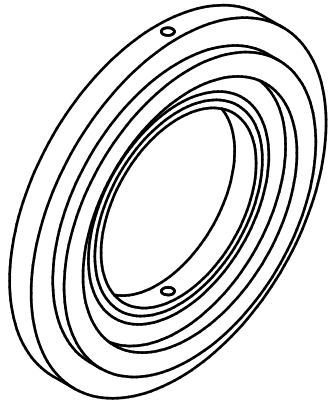

TOP VIEW (1 : 1)

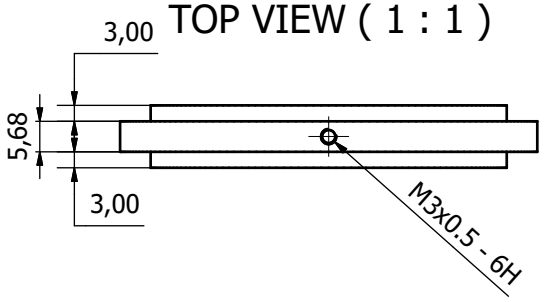

J (2 : 1)

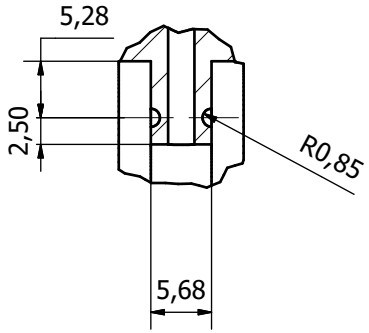

Designed by Laptop	QTY:1 OFF	MATERIAL: VESCONITE	SCALE:1:2	Date 2022/11/21	
Cape Peninsula University of Technology	7.5 ml SEPERATION RING				
	MECHENG-001-002-004		Edition 2	Sheet 8 / 13	

FRONT VIEW (5 : 1)

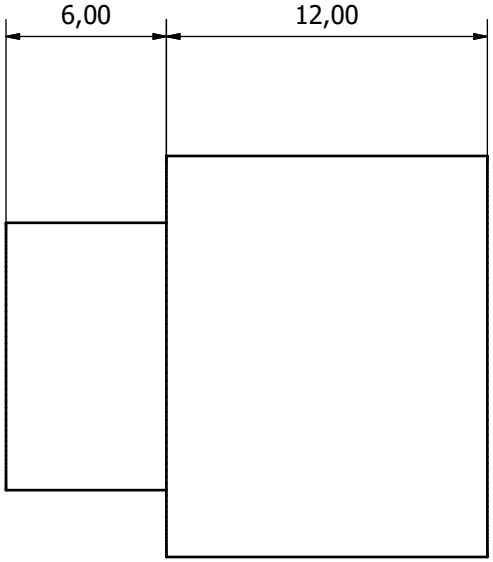

SIDE VIEW (5 : 1)

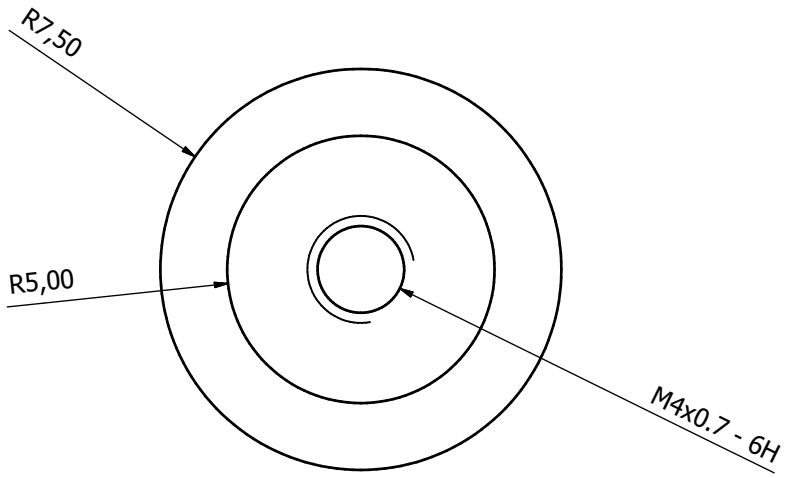

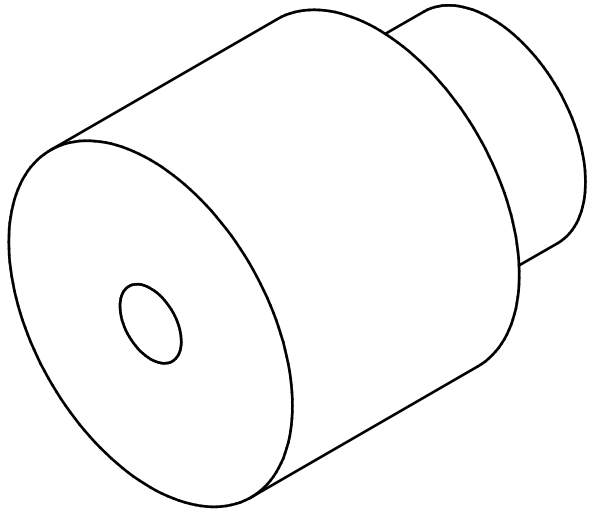

Designed by Laptop	QTY:1 OFF	MATERIAL: NYLON	SCALE:1:2	Date 2022/11/21	
Cape Peninsula University of Technology	STAND OFFS				
	MECHENG-001-003		Edition 1	Sheet 9 / 13	

FRONT VIEW (1 : 1.5)

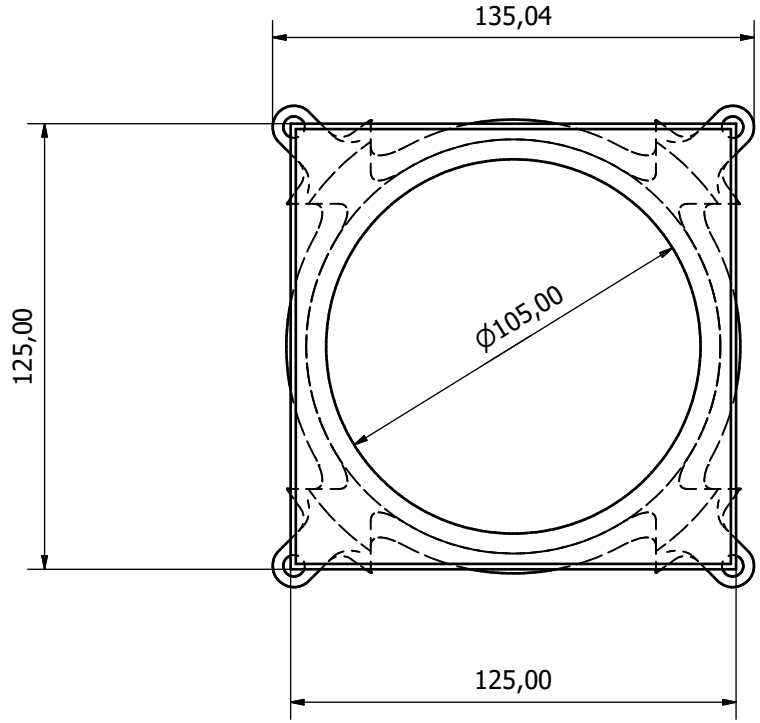

SIDE VIEW (1 : 1.5)

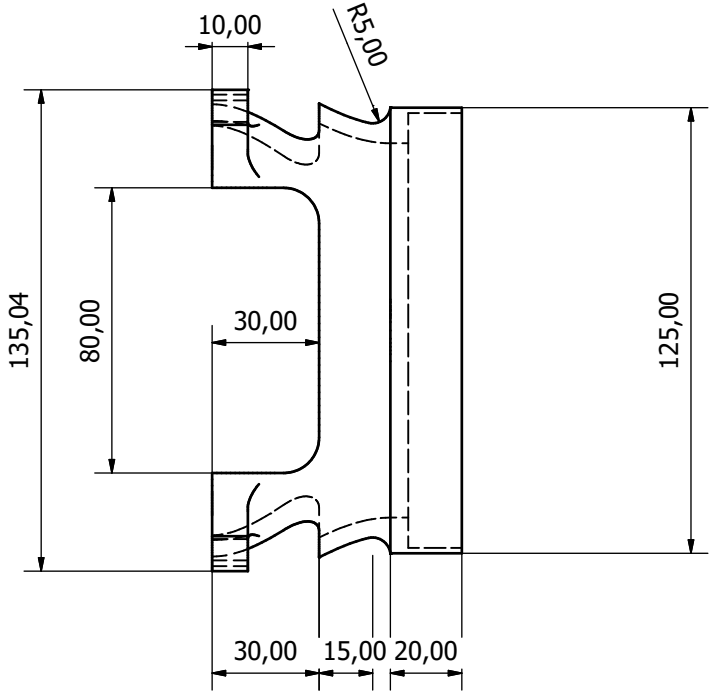

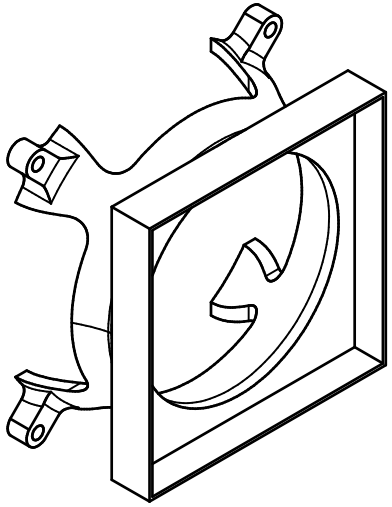

Designed by Laptop	QTY:1 OFF	MATERIAL: PLA	SCALE:1:2	Date 2022/11/21	
Cape Peninsula University of Technology	FAN COWEL				
	MECHENG-001-004		Edition 1	Sheet 10 / 13	

FRONT VIEW (1 : 2)

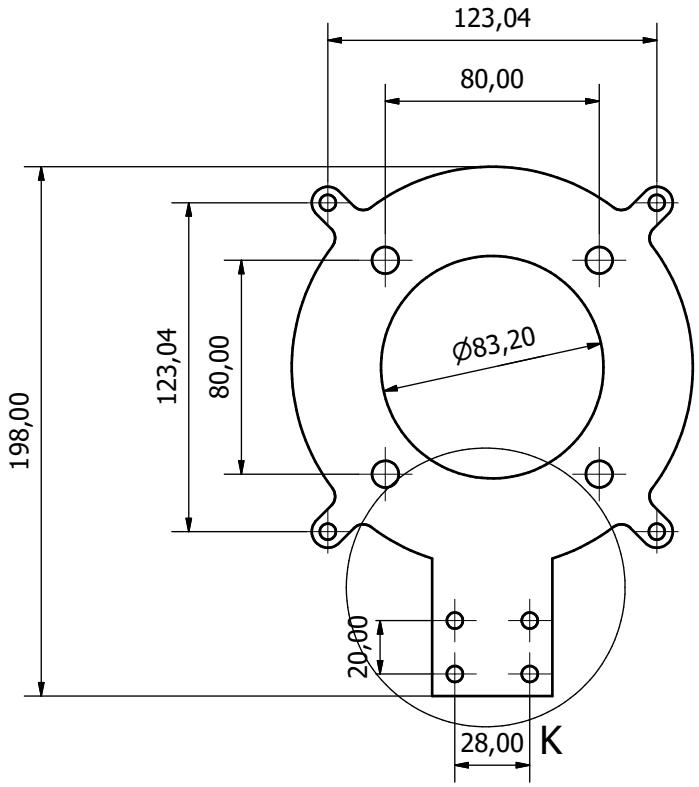

SIDE VIEW (1 : 2)

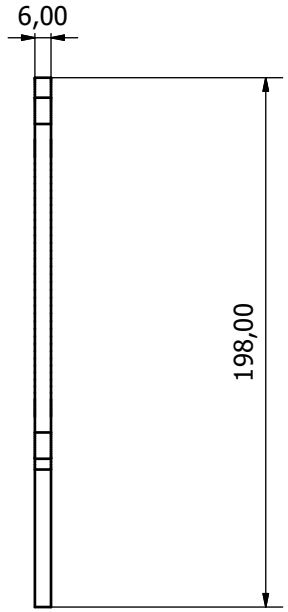

K (1 : 1)

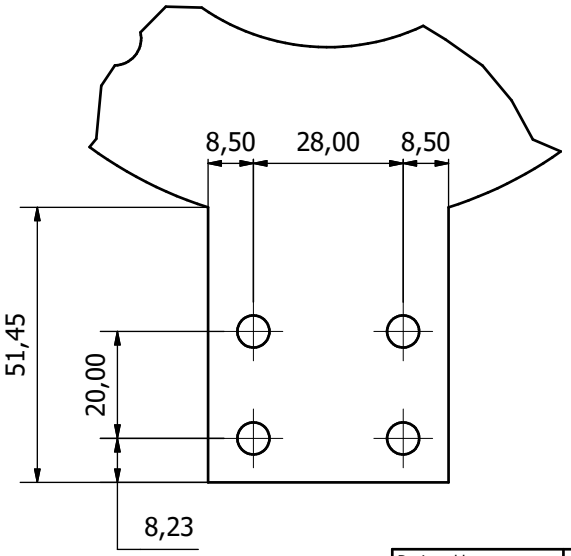

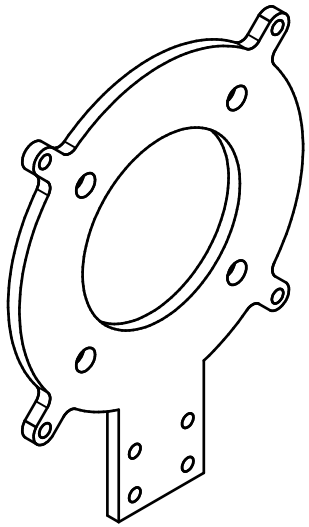

Designed by Laptop	QTY:1 OFF	MATERIAL: ALUMINIUM	SCALE:1:2	Date 2022/11/21	
Cape Peninsula University of Technology	COLD PLATE MOUNT				
	MECHENG-001-005		Edition 4	Sheet 11 / 13	

FRONT VIEW (1 : 4)

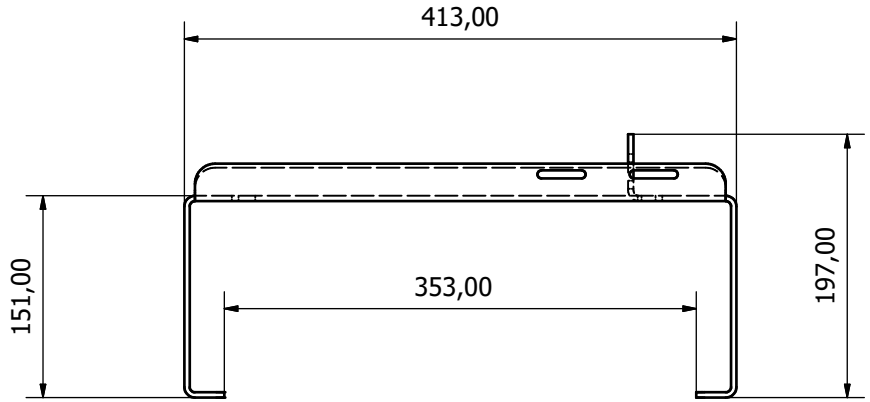

SIDE VIEW (1 : 4)

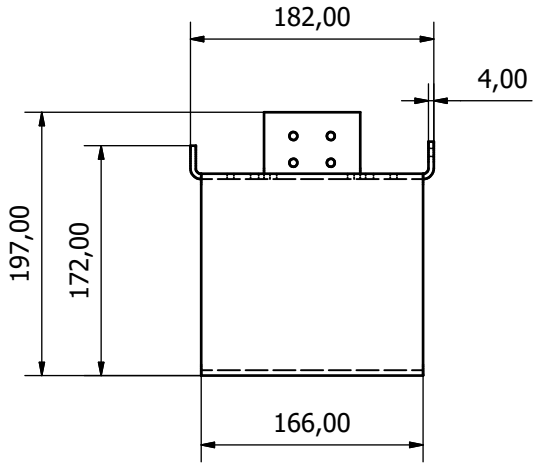

TOP VIEW (1 : 4)

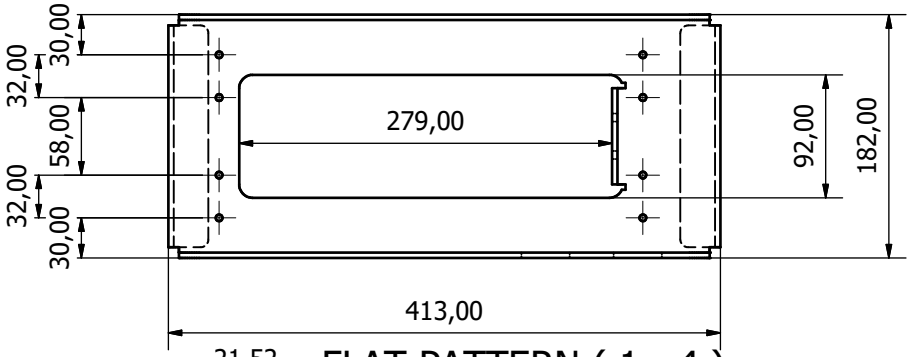

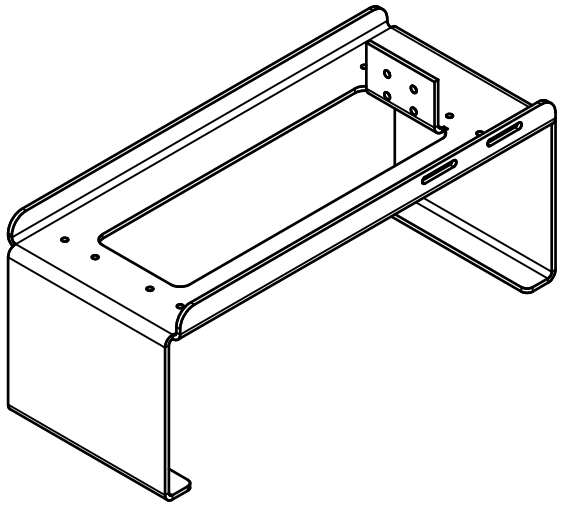

FLAT PATTERN (1 : 4)

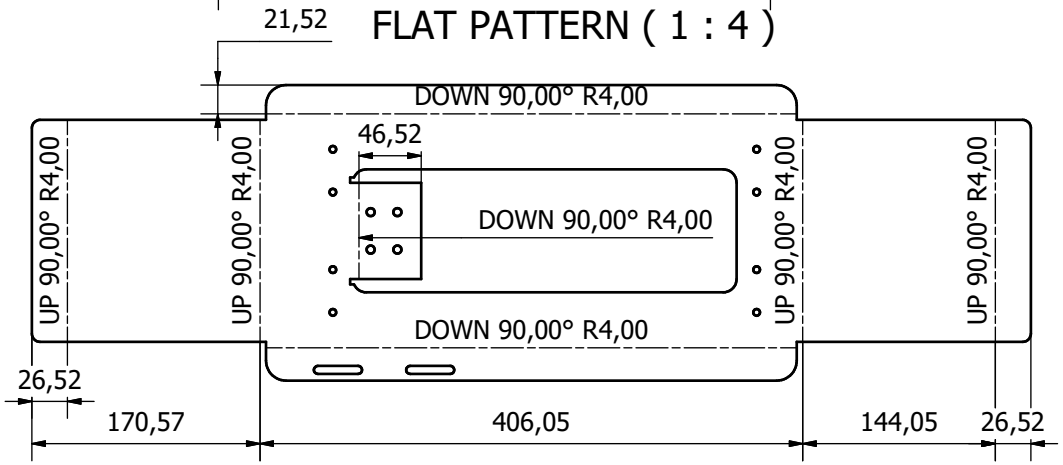

Designed by: Laptop	QTY:1 OFF	MATERIAL: SS304	SCALE:1:2	Date: 2022/11/21	
Cape Peninsula University of Technology	BASE PLATE				
	MECHENG-001-006		Edition: 3	Sheet: 12 / 13	

FRONT VIEW (1 : 3)

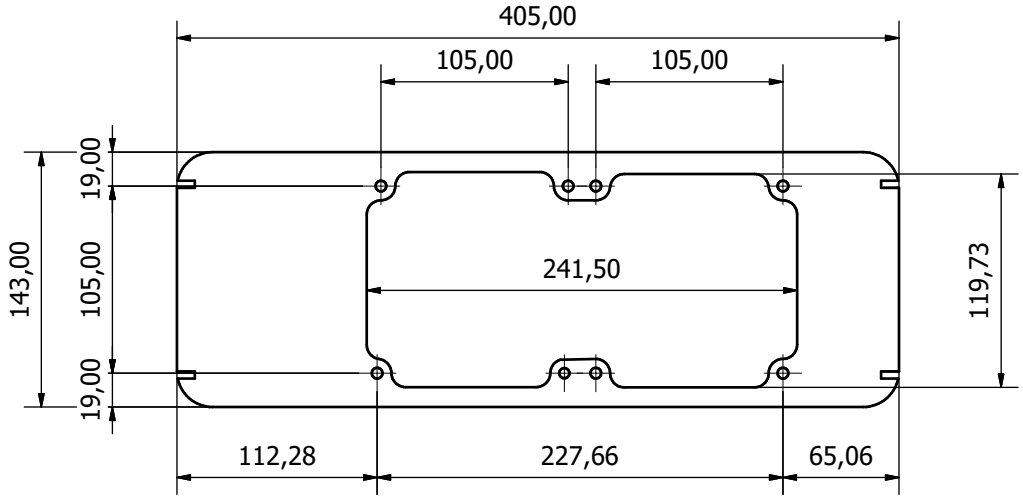

SIDE VIEW (1 : 3)

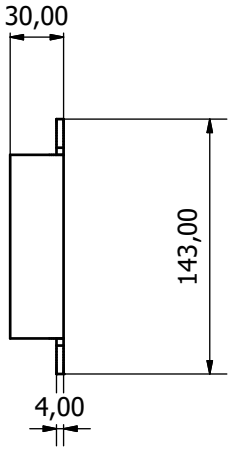

TOP VIEW (1 : 3)

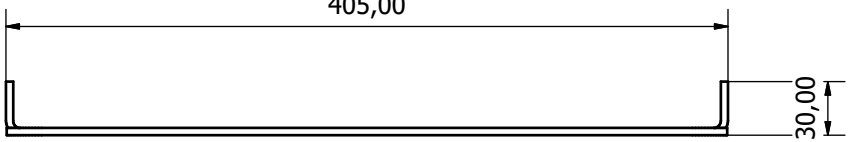

FLAT PATTERN VIEW (1 : 2)

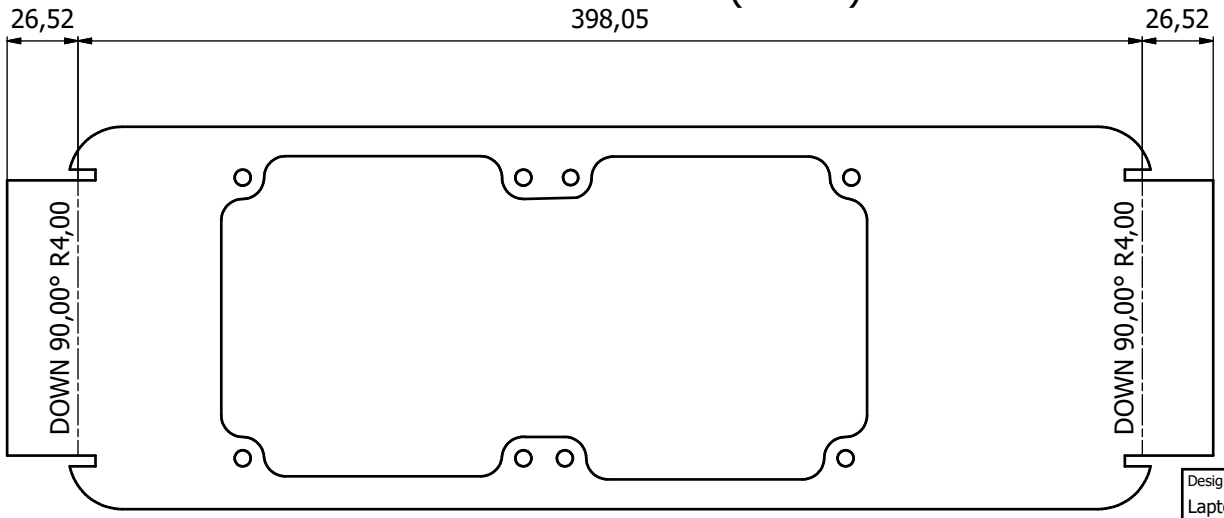

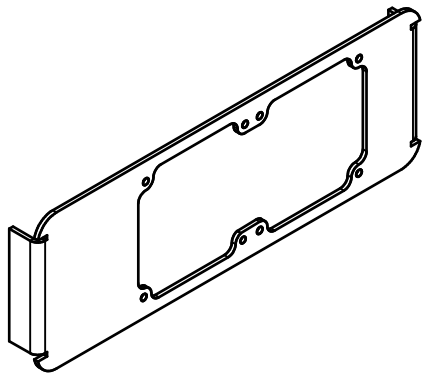

Designed by: Laptop	QTY:1 OFF	MATERIAL: SS304	SCALE:1:2	Date: 2022/11/21	
Cape Peninsula University of Technology	RADIATOR MOUNT PLATE				
	MECHENG-001-007		Edition: 2	Sheet: 13 / 13	